Triboelectric Nanogenerator Device Development, Analysis and Prediction for Energy Harvesting

Submitted in partial fulfilment of the requirements
for the award of the degree of

Doctor of Philosophy

by

RAVI SANKAR PUPPALA
(Roll No: 719067)

Under the supervision of

Prof. Prakash Kodali

(Assistant Professor)

Department of Electronics & Communication Engineering
National Institute of Technology Warangal
Telangana, India - 506004

2024

Dedicated

To

Amma & Nanna,

Nagasri , Sasi Manvith & Sagnika

Approval Sheet

This thesis entitled **Triboelectric Nanogenerator Device Development, Analysis and Prediction for Energy Harvesting** by **RAVI SANKAR PUPPALA** is approved for the degree of **Doctor of Philosophy**.

Examiners

Research Supervisor

Prof. Prakash Kodali
Department of ECE,
NIT Warangal, India-506004

Head of the Department

Prof. D. Vakula
Department of ECE,
NIT Warangal, India-506004

Place: Warangal
Date: 19.01.2024

Declaration

This is to certify that the work presented in the thesis entitled "Triboelectric Nanogenerator Device Development, Analysis and Prediction for Energy Harvesting" is a bonafide work done by me under the supervision of Prof. Prakash Kodali, Department of Electronics and Communication Engineering, National Institute of Technology Warangal, and was not submitted elsewhere for the award of any degree.

I declare that this written submission represents my ideas in my own words and where others' ideas or words have been included, I have adequately cited and referenced the original sources. I also declare that I have adhered to all principles of academic honesty and integrity and have not misrepresented or fabricated or falsified any idea/date/fact/source in my submission. I understand that any violation of the above will be cause for disciplinary action by the institute and can also evoke penal action from the sources which have thus not been properly cited or from whom proper permission has not been taken when needed

Place:Warangal
Date:19.01.2024

Ravi Sankar Puppala
Research Scholar
Roll No.: 719067

NATIONAL INSTITUTE OF TECHNOLOGY

WARANGAL, INDIA-506004

Department of Electronics and Communication Engineering

CERTIFICATE

This is to certify that the dissertation work entitled "Triboelectric Nanogenerator Device Development, Analysis and Prediction for Energy Harvesting", which is being submitted by Mr. RAVI SANKAR PUPPALA (Roll No. 719067), is a bonafide work submitted to National Institute of Technology Warangal in partial fulfilment of the requirement for the award of the degree of Doctor of Philosophy in Electronics and Communication Engineering.

To the best of our knowledge, the work incorporated in this thesis has not been submitted elsewhere for the award of any degree.

Prof. Prakash Kodali

Research Supervisor,

Department of ECE,

NIT Warangal,

India-506004.

Place:Warangal

Date:19.01.2024

Acknowledgements

First and foremost, I would like to express my sincere gratitude to my supervisor Prof. Prakash Kodali for continuous support of my research, for his patience, motivation, and guidance. My sincere thanks to him for providing me with an opportunity to join the institute as a research scholar and giving me access to research facilities. I find words inadequate to thank him for enabling me to complete this work in spite of all obstacles. The thesis would not have seen the light of day without his continued support and cooperation. Sir, I think you deserve an extra note of thanks for your ongoing leadership and support. Finally, I just wanted to thank you for being such a great advisor in my personal life. I have enjoyed working with you so much over the past few years. My special word of thanks should also go to Prof. D. Vakula, Professor, Head of the department, of Electronics and Communication Engineering Department, NIT Warangal for her valuable suggestions and support that he offered during my research. Here, I also would like to take this privilege to thank my DSC members, Prof. T. V. K. Hanumantha Rao, Professor, Department of Electronics and Communication Engineering, NIT Warangal, Prof. S. Anuradha, Professor, Department of Electronics and Communication Engineering, NIT Warangal and Prof. P. Syam Prasad, Professor, Department of Physics, NIT Warangal for their continuous support, suggestions and advice during my research period whenever required. I am grateful to the former Heads of the ECE department Prof. P. Sree Hari Rao, Prof. L. Anjaneyelu and Prof. N. Bheema Rao for their continuous support and encouragement. I would also appreciate the encouragement from teaching, non-teaching members and fraternity of Dept. of E.C.E. of N.I.T. Warangal. They have always been encouraging and supportive.I would like to extend my sincere and special gratitude to **Dr. R. Rakesh Kumar** for his invaluable guidance, unwavering support, and profound insights throughout the course of my research. His mentorship has been instrumental

in shaping the trajectory of my academic journey. I am also thankful to Dr. K. Uday Kumar,Prof. D. Haranath and Dr. Cheruku Ramalinga swamy for their continuous support and encouragement throught my research work. I am also thankful to Dr. M. Raja Vishwanathan provided much help in proofreading my research papers. It is my pleasure to show my indebtedness to my co-scholars at NITW Mr. M. Praveen, Mr. P. Raveendra, Mr. V. Venkata Narayana, Mr. D. Ramesh Reddy, Ms. P. Supraja, Mr. Siju Mishra, Mr. Lakshakoti, Mr. M. Navaneeth, Mrs. T. Ragini, Mrs. B. Vijaya Sree, Mrs. B. Kranthi, and friends for their help during this work. Their timely help and friendship shall always be remembered during my stay. I owe my deepest gratitude towards my better half (Nagasri Puppala) for her continuous support, love and understanding of my goals and aspirations. Her patience and sacrifice will remain my inspiration throughout my life, without her help, I would not have been able to complete much of what I have done and become who I am. Also, I love my Children (Sasi Manvith & Sagnika) for giving me happiness and support during my research. I appreciate my Children for the patience they showed during my research. I consider myself the luckiest in the world to have such a lovely and caring family, standing beside me with their love and unconditional support. My heartfelt thanks to my family members (parents Puppala Suri Babu, and Rama Devi Sisters' family (Sudheer- Ramya - Chethan) for supporting me spiritually throughout my life in general. Their unconditional love, support, self-sacrifices and patience have always been the source of my strength. I shall be grateful forever because of their kindness and love. Finally, I thank God, for filling me every day with new hopes, strength, purpose, and faith.

Ravi Sankar Puppala

Abstract

As the global need for renewable energy sources grows, research into clean and cost-effective harvesting of energy devices has become vital. The purpose of this thesis is to explore the design, production, and optimizing of Triboelectric Nanogenerator (TENG) technologies using reusable waste materials. The goal is to limit waste accumulation and boost sustainable energy generation by reusing materials. The current thesis focuses on the use of reusable material aluminium foil as an electrode in a device. As a dielectric material, the gadget used a laboratory film known as Parafilm, which the researchers compared to other low-cost materials such as OHP, PET, and PMMA. created several Triboelectric Nanogenerator (TENG) architectures and observed that the output response improved significantly from 4 V to 200 V. This enabled the TENG to power tiny devices such as digital watches, calculators, thermometers, and even LEDs containing up to 85 LEDs. To validate the practical results, with the help ofsimulation platform called COMSOL tool, by considering various parameters for simulation, such as the hardware design materials, their thickness, and properties, keeping them consistent with the practical setup. The simulation results closely matched the practical findings, reinforcing the accuracy of their experiments. To further improve the prediction of output power for unknown load conditions, incorporated algorithms for to reduce the loss in the accuracy prediction used deep learning and machine learning algorithms. In Machine learning random forest regression and in deep learning Adamdelta is giving less loss compared to existing algorithms. The outcome of this research lead to reduce the waste materials and helpful to the society in terms of air, water, and soil pollution. The proposed research offers the design of TENG device with less cost, validate the practical results with simulation results with scaling factor and for the complex designs to predict the output power for unknown load conditions using AI.

Contents

List of Figures

List of Tables

List of Abbreviations

TENG	Triboelectric Nanogenerators
CS Mode	Contact Separation Mode
LS Mode	Lateral Sliding Mode
FS Mode	Free Standing Mode
PDMS	Polydimethylsiloxane
PMMA	Polymethyl Methacrylate
OHP	Overhead Projector
PTFE	Polytetrafluoroethylene
PET	Polyethylene Terephthalate
DFACF	Discarded Food Packaging Aluminium Cover Foils
AI	Artificial Intelligence
KNN	K Nearest Neighbor
NN	Neural Network
DNN	Deep Neural Network
TP	True Positive
FP	False Positive
TN	True Negative
FN	False Negative
GPU	Graphics Processing Unit
MSE	Mean Square Error
RMSE	Root Mean Square Error
MAE	Mean Absolute Error
DC	Direct Current

List of Abbreviations

VB	Valence Band
CB	Conduction Band
FTIR	Fourier Transform Infrared spectroscopy
Voc	Open Circuit Output Voltage
PD	Power Density
APA	Aluminium Foil Parafilm Aluminium Foil
SEM	Scanning Electron Microscopy
EDAX	Energy Dispersive X-ray Analysis
XRD	X-ray Diffraction
FEA	Finite Element Analysis
Q_{SC}	Short Circuit Charge
SGD	Stochastic Gradient Descent
AI	Artificial Intelligence

Chapter 1

Introduction

The rapid progress in the field of electronics observes an obvious trend of functionality, miniaturization, and portability. This is evident from the development of handheld mobile phones which are one of the most popular and widely used examples of portable electronics which come with large functionalities. The current and upcoming focus will be on enhancing the existing functionalities of electronics by the application of a wide range of sensors including but not limited to gas, chemical, biological, motion, and navigation sensors [2, 3, 4, 5, 6]. A lot of efforts are being made to develop electronics that are much smaller than the size of a mobile phone so that every individual on average can have multiple electronic devices catering to different requirements of humans. These small-sized electronics are in general operated on ultralow- power levels which provides us with an opportunity to power them by harvesting energy from our living environment [7, 8, 9] With the application of nanomaterials and nanotechnology for harvesting energy for powering micro/nano-power systems, new technologies capable of harvesting energy from the environment thereby acting as sustainable and self-sufficient small- scale power sources are constantly emerging and being worked in the field of nano energy. With the growing popularity of portable electronics, the challenge remains to develop energy storage-related technologies as most of them are still running on batteries. As sensors are employed in different electronics, it will become more and more impossible to power such a tremendous network consisting of trillions of sensors around the world. One cannot opt for batteries due to the drawbacks they offer such as replacing them, checking their orientation, and inspecting them from time to time. A sustainable power source capable of

harvesting energy from the environment can be seen as one of the possible solutions to the problem mentioned. Thus, there is a need for nano energy and dependent power sources which are available, efficient, and stable [10, 11]. Triboelectric Nanogenerator (TENG) is a new type of technology, first demonstrated in 2012 by Prof.Zhong Lin Wang's group at the Georgia Institute of Technology [12, 13, 14, 15]. Working in conjunction with the triboelectric effect and electrostatic induction, it is an energy harvesting device that converts small-scale produced mechanical energy into electricity. TENG has a wide range of applications due to its ability to produce a scale of output. Few of the applications and the corresponding level of power is depicted in figure 1.1.

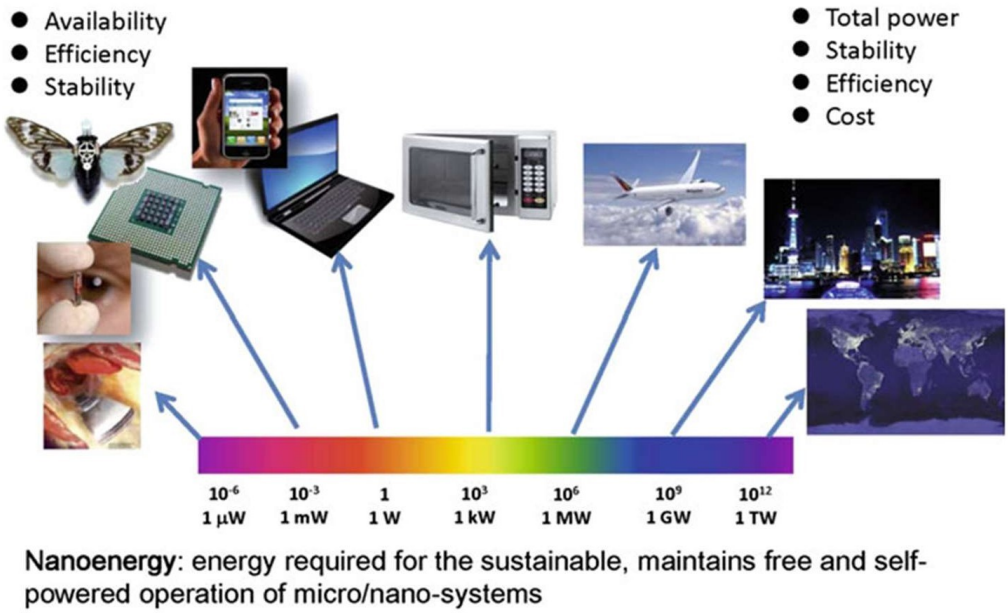

Figure 1.1: Magnitude of Power and its corresponding applications Reproduced from [2].

1.1 Triboelectric effect

It is a contact-induced electrification phenomenon where the material becomes electrically charged once it is contacted with another material through friction. The sign of charges carried by the material depends on its relative polarity in comparison with the material it's brought into contact with.The effect can be generally understood as the consequence of the flow of charges from one material to another material via a chemical bond formed between some parts of the two surfaces, often referred to as adhesion, when brought into contact by the application of mechanical force. The transferred charges can

be either electrons or ions/molecules. When separated, few of the bonded atoms can keep extra electrons while others can give them away, resulting in the possible development of triboelectric charges on surfaces

1.2 Motivation

Climate change and environmental degradation have been at an alarming rate pressing mankind to take immediate action. Innovative and sustainable solutions are the need of the hour for forever increasing energy needs. In this context, the concept of transforming reusable materials into sustainable energy sources has gained significant attention. This energy need and the possibility of waste reduction by transforming waste materials into energy sources is the motivation for this thesis.This paradigm shift holds tremendous promise for promoting a more sustainable and resource-efficient future. Building and promoting a circular economy, waste reduction, recycling are an added advantage in this method of using waste material for energy generation. By reimagining waste as a valuable input, we can foster a more sustainable and resilient society. Moreover, transforming reusable materials into sustainable energy holds the potential to drive economic growth in terms of new industries and job opportunities. This will enable nations to become energy secure.Some of the still active challenges in this field are technological advancements for efficient energy conversion, optimized waste management processes, and the establishment of appropriate policy frameworks and regulations.This thesis aims to contribute to the existing body of knowledge by exploring the potential of transforming reusable materials into sustainable energy and providing insights into the technical, economic, and environmental aspects of this innovative approach. In summary, the motivation behind this thesis lies in the urgent need to transition towards sustainable energy systems and adopt circular economy principles. By investigating the transformation of reusable materials into sustainable energy sources, we aim to contribute to the development of practical solutions that address both environmental and energy challenges. Through this research, we aspire to inspire and guide policymakers, industry stakeholders, and researchers towards a more sustainable and resilient future.

1.3 Problem Statement

The problem statement for triboelectric nanogenerators (TENGs) revolves around addressing the existing challenges and limitations associated with their design, performance, and practical implementation. Some key problem areas include: The objective of this thesis is to develop sustainable Triboelectric Nanogenerator (TENG) devices by incorporating waste materials, with the aim of reducing waste and promoting clean energy generation. The thesis will focus on validating simulation results using the COMSOL tool and leveraging machine learning and deep learning optimizers for accurate power output prediction. Specifically, the project aims to:

- Design and fabricate TENG devices that utilize waste materials, contributing to waste reduction and promoting sustainable energy generation.
- Validate the simulation results of the TENG devices using the COMSOL tool, ensuring the accuracy and reliability of the simulation model.
- Employ machine learning and deep learning optimizers to predict the power output of the TENG devices, enabling accurate performance estimation.
- Compare and evaluate the effectiveness of different machine learning and deep learning techniques for power output prediction in TENG devices.
- Optimize the design parameters of the TENG devices using the selected optimizer, maximizing power generation efficiency.
- Assess the impact of the optimized design parameters on the power output and overall performance of the TENG devices.

1.4 Research Objectives

The research objectives are formed based on the identified gaps in the literature. The summary of the research objectives are given as follows.

- Design a novel Triboelectric Nanogenerator (TENG) device capable of driving small electronic gadgets.

- Incorporate reusable materials in the design of the TENG device to reduce environmental pollution.
- Perform simulation and validation of the TENG device using the COMSOL tool.
- Evaluate and compare the predictive capabilities of different machine learning and deep learning techniques.

Contribute to reducing environmental pollution by promoting the use of reusable materials in TENG devices and optimizing their performance for sustainable energy generation.

1.5 Thesis Contributions

The research work present in ensuing chapters of this thesis makes original contribution to the field of tribo electric nano generators and comparison of different device designs and materials, analysis with COMSOL platform and predicting the output power using AI for unknown load resistances.

1.5.1 A triboelectric nanogenerator based on food packaging Aluminium foil and Parafilm for self-powered electronics

In this contribution a novel TENG is fabricated based on WFPAC foil and parafilm for mechanical energy harvesting for the first time and studied its performance. Further, fabricated TENG has been demonstrated to power up portable electronic devices and a group of LEDs. A new TENG has been demonstrated based on the waste food packaging Aluminium covers foil and the parafilm to power portable electronic devices. In our design, the parafilm and conducting side of WFPAC foil serve as the triboelectric pair. TENG's open-circuit voltage can reach ~ 4 V and the maximum power density 11.8 nW/cm^2. The prepared TENG was demonstrated to power up portable electronic devices and LEDs. The present work opens up a new triboelectric pair for energy harvesting. This new parafilm tribo-layer can form new triboelectric pairs with other materials for enhanced mechanical energy harvesting as shown in figure 1.2. Furthermore, the idea of using WFPAC foil reduces environmental pollution to a certain extent.

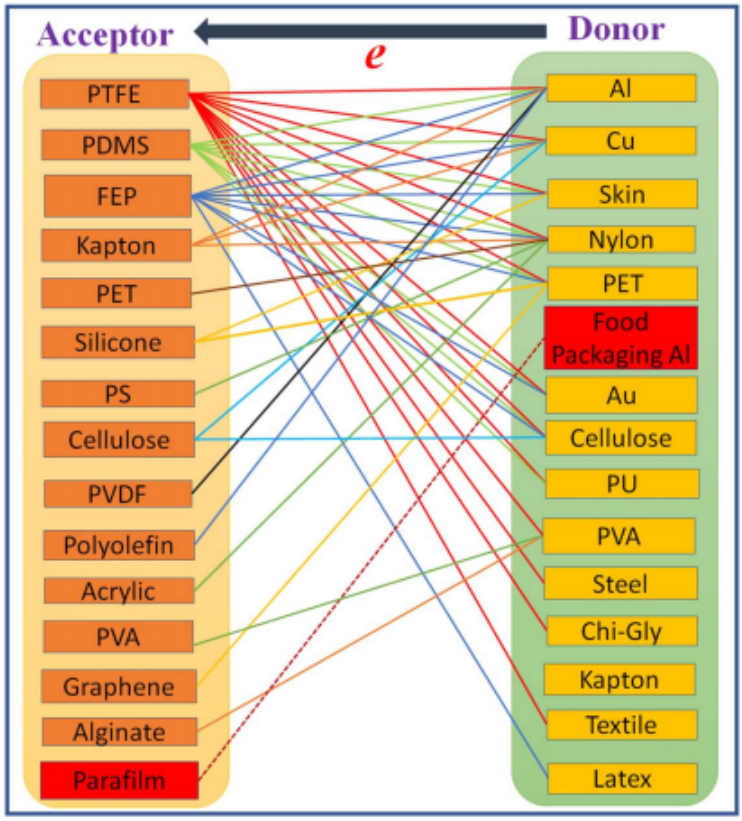

Figure 1.2: List of Triboelectric pairs reported in the Literature and our Current work highlighted in dotted line.

1.5.2 A Novel Triboelectric Nanogenerator based on only Food Packaging Aluminium Foils

The rapid increase of food packaging waste is a significant cause of air, water, and land pollution. Therefore, a triboelectric nanogenerator (TENG) has been developed using only food packaging aluminium covers. The demonstrated TENG helps in reducing environmental pollution as well as harvesting mechanical energy. In the demonstrated TENG, electroplated aluminum surface and PET surface of food packaging cover act as tribo-layers. The fabricated TENG generates voltage and instantaneous power density of $\sim$ 4 V and 40 nW/cm^2. The TENG stability was tested over 4000 cycles and found highly stable. The demonstrated TENG output power can be increased by using other tribo layer materials such as PDMS, PVDF, and PVC films. Therefore, it can be utilized to power up portable electronic devices in the future.

TENG was fabricated using only discarded food packaging aluminium foils and demon-

strated to turn on 3 LEDs directly. The TENG's open-circuit voltage can reach up to ∼ 4 V and the maximum power density achieved is 40 nW/cm^2 . The power density of TENG can be further improved by attaching other tribo-layers to the top electrode. Thus, this study presents a novel way to utilize food packaging waste foil alone for energy harvesting applications. The structure and its SEM and EDAX as shown in Figure 1.3.

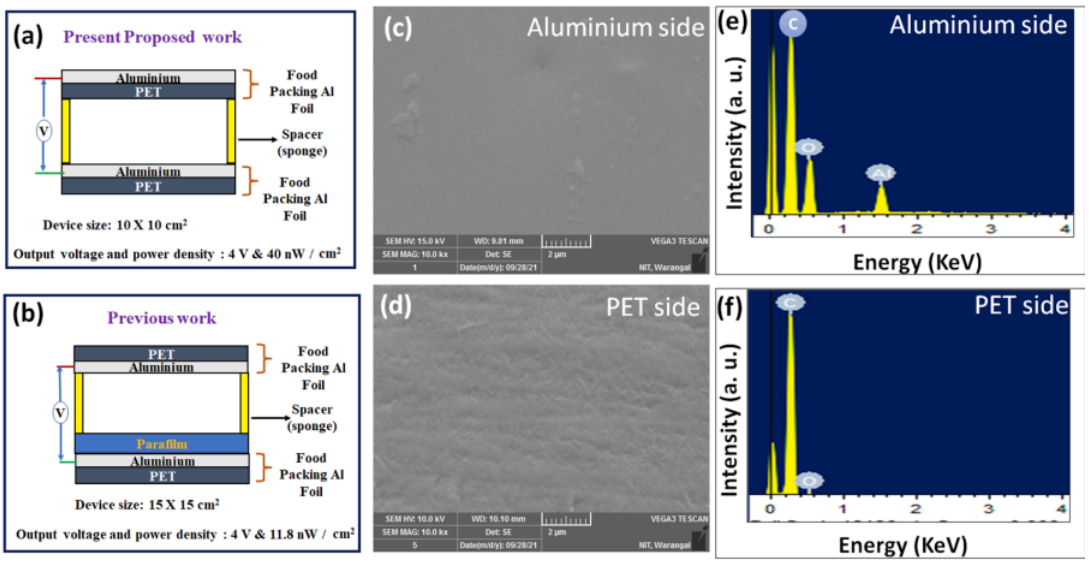

Figure 1.3: (a) Structure of demonstrated TENG device, (b) Previous work structure with parafilm as a tribo-layer, (c) - (d) SEM images of the Aluminum side & PET side, (e) - (f) EDX spectrum of Aluminum side and PET side.

1.5.3 A Triboelectric Nanogenerator Based on PDMS and Parafilm for Biomechanical Energy Harvesting

In this report, a triboelectric nanogenerator is fabricated using parafilm, polydimethylsiloxane (PDMS) films for the first time as shown depicted in Figure 1.4. The fabricated TENG has been used for low frequency mechanical energy harvesting to drive wearable and low-power electronic gadgets.The parafilm and PDMS layers act as triboelectric layers, and packaging aluminium foil acts as conducting electrodes. A flexible TENG with a dimension of 5 x 5 cm^2 generated an output voltage ∼ 8 V and output power of 20.25 µW at the applied load of 1 MΩ. Further, TENG was explored for switching on several LEDs. The current report presents a simple and cost-effective method for fabricating TENG and can be used for self-powered device applications.

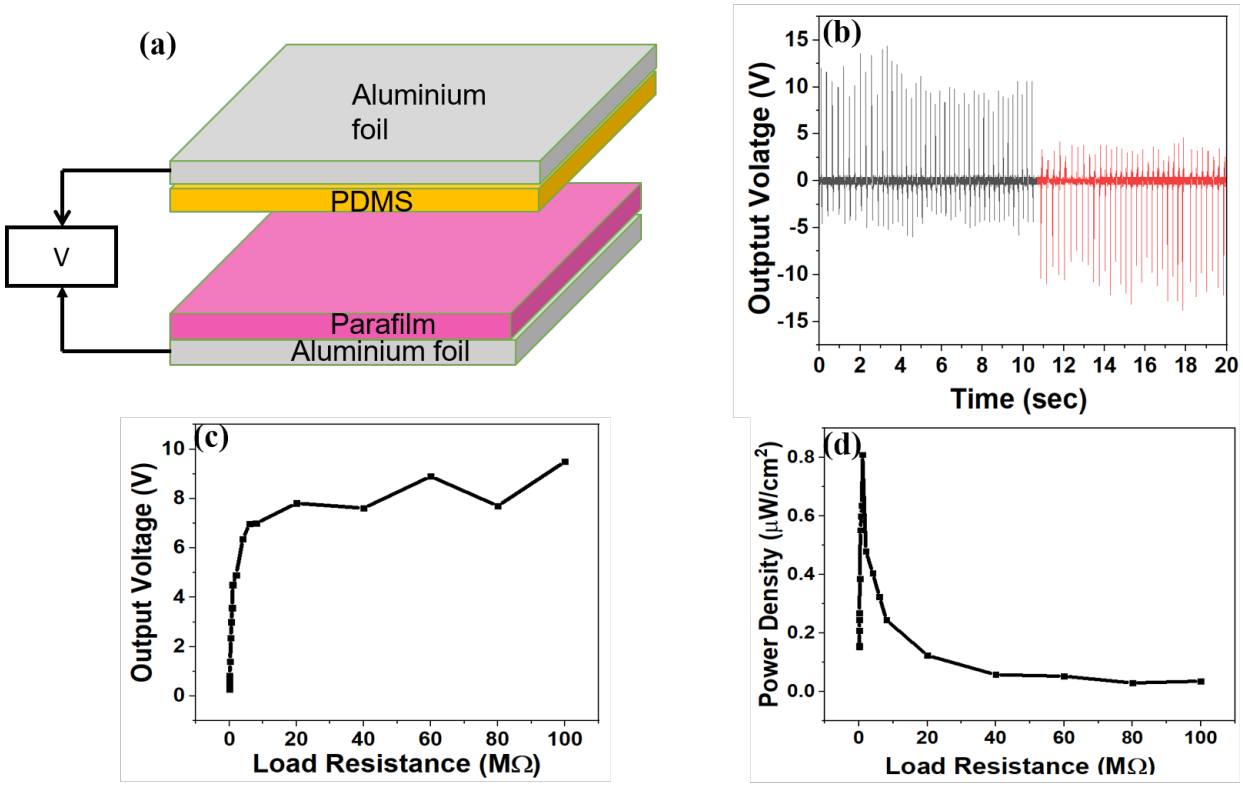

Figure 1.4: (a) Illustrative of TENG device (b) TENG output voltage in open circuit under forward and reverse connections, (c) Load Characterization of TENG, (d) Power Density of TENG.

1.5.4 Triboelectric Nanogenerator Based on Different Polymers: Experimental and Simulation Study

In this study, triboelectric nanogenerators are fabricated using a variety of polymers, including PET, PMMA, and OHP sheets. Packaging aluminum foil functions as conducting electrode, while the PET, OHP, and PMMA act as triboelectric layers in the design represented in Figure 1.5. A flexible TENG with a 5 x 5 cm^2 surface area produced an output voltage between 6 V(AOA), 5 V (APA) and 25 V (APMA). The current work provides a simple and cost-effective method for creating TENG structure, which may be employed for applications involving self-powered devices. By using FEM analysis also for the three TENG structures obtained output response is higher for PMMA used as the dielectric in the TENG i.e. (APPMA), in the same way in practical designed TENG structures also APPMA structure is giving higher response compared to remaining to structures. Furthermore, the built APMA structured TENG was capable of turning on

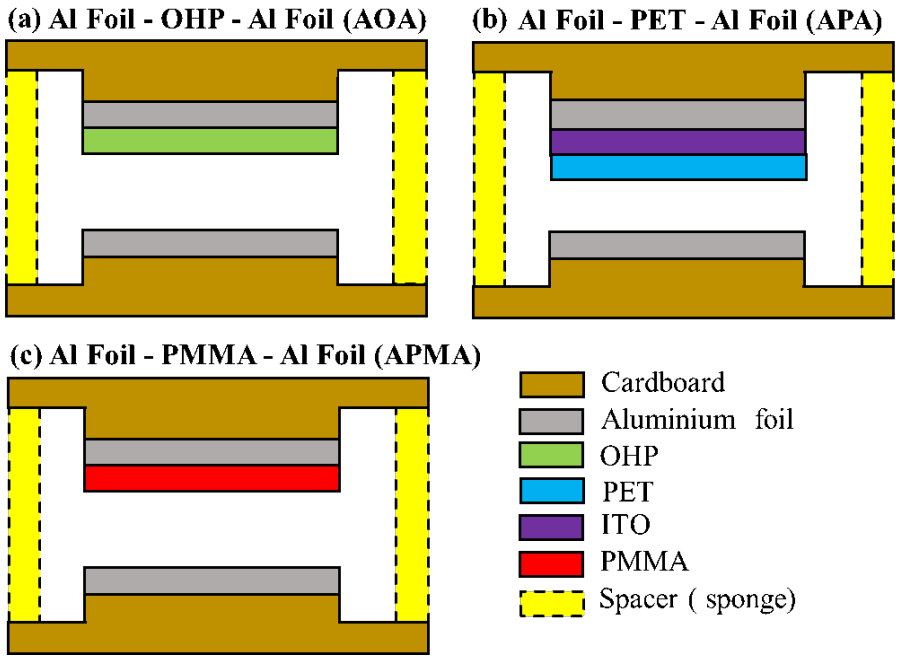

Figure 1.5: TENG Structures (AOA, APA, APMA) using the OHP, ITO coated PET and PMMA dielectrics.

the 19 commercial LEDs.

1.5.5 Performance Prediction of Contact Separation Mode Triboelectric Nanogenerators using Machine Learning Models

The use of Artificial Intelligence (AI) algorithms for analyzing practical data has increased with the advent of AI models. Combining physics and engineering has garnered a lot of interest so much so that the triboelectric Nano-generators (TENG) industry may also use AI technologies.In this work, the classifiers suitable for predicting the system accuracy for TENG are analyzed with the help of experimental data when training and testing, and two of the Machine Learning (ML) classifiers provide promising results: **K** Nearest Neighbor (KNN) and Neural Network (NN). Different ML parameters are generated such as precision, recall and F1 with the help of Confusion matrix for KNN and NN. Additionally, we assess the TENG's output quality in CS mode under various load factors using ML model.

1.5.6 Accurate Output Power Prediction in TENG Devices using Artificial Intelligence: A Comparative Analysis.

The utilization of AI algorithms in the application of processing the experimental data obtained manually relevant to engineering and physics has gained significant attention in the emergence of the field of artificial intelligence (AI). Consequently, in the area of triboelectric nanogenerators (TENG) may also adopt AI technology. The analysis of how structural characteristics impact output performance in physical tests can present occasional challenges and limitations.TENGs' structure varies over a narrow range, which makes experiment control challenging. However, it is impractical to conduct experiments encompassing all possible parameter combinations to establish definitive experimental guidelines. For anticipating the performance of triboelectric nanogenerators' output across numerous structures, configurations. This study introduces a novel AI algorithm model based on deep neural networks specifically designed for TENGs.The results reveal that the DNN model accurately predicts the expected output power levels for TENGs with the CS mode structure, aligning with the physical experimental data and represented the experimental setup in figure 1.6. Subsequently, the DNN model is utilized to predict the

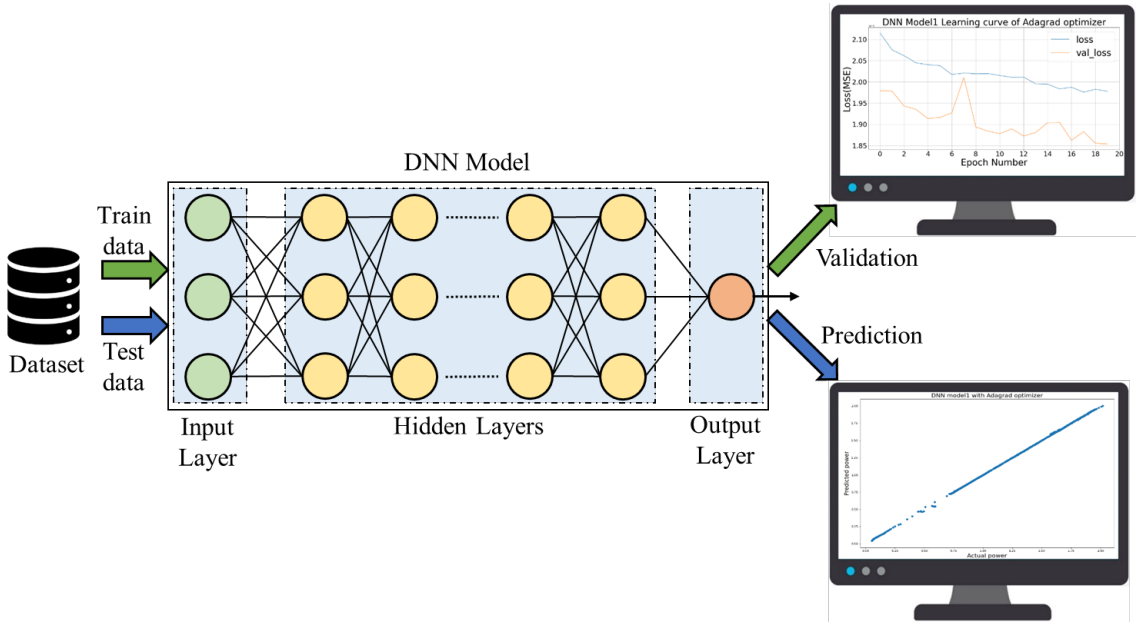

Figure 1.6: Experimental Setup.

output power of TENGs within the parameter range that was not tested in the CS mode structure. This will undoubtedly aid researchers in their analysis of the data's law over

a larger range of parameter values, leading to a more accurate experimental law. The utilization of AI algorithms in the fields of engineering and physics has experienced a substantial growth in recent years. AI technology can be helpful in analyzing experimental data, predicting outcomes, and discovering patterns in complex systems.

1.6 Thesis Organization

The thesis is organized as follows.

Chapter 1: Introduction

This chapter presents an introduction to the research work, Motivation, Problem statement, and outline of the thesis contributions.

Chapter 2: Preliminaries

The chapter begins with an overview of the literature review, providing a context for the subsequent discussions. Key themes and concepts identified from the literature are then presented, highlighting the current understanding of the research topic. Notable studies and research findings are discussed, showcasing the advancements made in the field. Additionally, the chapter examines the current state of knowledge, identifying any gaps and limitations in the existing literature that motivate the need for the present study.

Chapter 3: Material Selection and Performance Comparison

An overview of type of materials are present in the triboelectric series and finding of new materials to enhance the output response and other performance characterizations of nanogenerator.

Chapter 4: TENG Device Designs and Small Gadgets Applications

This chapter discusses about the new material concept as electrode and dielectric and its device making in vertical contact separation mode due to its easy to process the design and device characterizations and small electronic gadgets applications are mentioned.

Chapter 5: Assessing the Accuracy of COMSOL Simulation Results through Comparison with Practical Measurements in TENG

This chapter provides a structure for discussing the design procedure of TENG devices in COMSOL, comparison of different polymers in the software tool, and validation of simulation results with practical data, further expand each section and incorporate specific

parameters, procedures, and findings relevant to our research.

Chapter 6: Power Prediction using AI

This chapter introduces a novel method to predict the output performance for an unknown load resistance using machine learning (ML) and deep learning (DL) techniques. Experimented with various ML algorithms on the dataset and found that the Random Forest Regression algorithm achieved a lower error rate. Moreover, when employing DL techniques, they observed that the Adamdelta optimization algorithm yielded a lower loss compared to the other five regression methods. These findings highlight the effectiveness of Random Forest Regression in ML and the Adamdelta optimization algorithm in DL for accurately predicting the output performance of unknown load resistances.

Chapter 7: Conclusions and Future Scope

Finally, this chapter summarizes the thesis conclusions from the contributions and provides a brief discussion on the direction for future work.

Chapter 2

Literature Survey

This chapter is devoted to the review of research work reported in the literature in the area of Nanogenerators. The consolidated findings and results of various researchers for different methods and techniques are discussed. The literature review was carried out in four parts. In the first part Energy, review of along its pros and cons was discussed. In the second part, review Types of Nanogenerators along its pros and cons was discussed. In the third part, a review of Triboelectric Nanogenerator (TENG) for Energy Harvesting and Modes of Operating TENG was, along its pros and cons was done. At last, deployment of Response Boosters of TENG discussed.

Energy transformation has now firmly established itself as a major component and accelerating force in environmental and human development, caused by scientific advancement and innovation. It is a major source of public benefits. In modern society, fossil fuels such as coal, petroleum, and natural gas have historically dominated the energy landscape, accounting for the bulk of energy use. Since 1950, fossil fuel usage has increased eightfold, raising worries about energy crises and environmental implications from an overreliance on conventional fossil fuels. Furthermore, current energy trends are propelling the Fourth Industrial Revolution. With the Internet of Things (IoT) interconnecting over 30 billion devices in the future.The era of sensor networks, big data, robots, and AI is these days. Realizing the promise of the emergence of the fourth industrial revolution offers a big challenge: supplying enough electricity to run these breakthroughs effectively while enhancing our energy consumption.

A number of energy-harvesting technologies have been researched to produce electrical energy from sustainable energy sources and enable sustainable operation in real-world applications. These technologies include thermoelectric generators (TEGs), photovoltaic (PV) cells, piezoelectric generators (PEGs), and triboelectric nanogenerators (TENGs). Mechanical energy sources, which include wind, human motion, vibration, and so forth, are among the many sustainable energy sources that can be used to provide enough energy for various Internet of Things sensors. These sources are ubiquitous and can be used at any time to realise self-powered portable electronic devices. It has been extensively studied how to produce electricity from mechanical energy found in our surroundings using a variety of energy-harvesting methods based on well-established scientific phenomena like piezoelectric, electrostatic, and electromagnetic effects have been extensively researched in order to generate electricity from mechanical energy in our surrounding environment.

2.1 Energy

Energy is a fundamental concept in physics that refers to the ability of a system to do work or cause a change. It is a scalar quantity, meaning it is described by magnitude alone, and it exists in various forms. The most common forms of energy include:

2.1.1 Kinetic Energy

This is the energy possessed by an object due to its motion. The kinetic energy of an object depends on its mass and velocity. For example, a moving car or a flowing river possess kinetic energy.

2.1.2 Potential Energy

Potential energy is stored energy that an object possesses due to its position or condition. There are several types of potential energy, including:

a. Gravitational Potential Energy: It is associated with an object's height in a gravitational field. The higher an object is lifted, the greater its gravitational potential energy.

For instance, a raised weight or a stretched spring have gravitational potential energy.

b. Elastic Potential Energy: This form of potential energy is stored in objects that can be compressed or stretched, such as a compressed spring or a stretched rubber band.

c. Chemical Potential Energy: It is the energy stored in chemical bonds between atoms and molecules. When chemical reactions occur, this energy can be released or absorbed.

2.1.3 Thermal Energy

Also known as heat energy, thermal energy refers to the energy associated with the motion of particles within a substance. The higher the temperature, the greater the thermal energy. Thermal energy flows from a higher-temperature object to a lower-temperature object, resulting in heat transfer.

2.1.4 Electrical Energy

Electrical energy is associated with the flow of electric charges, such as electrons through a conductor. It is the energy that powers electrical devices and is commonly generated from sources like power plants or batteries.

2.1.5 Light (Radiant) Energy

Light energy is a form of electromagnetic radiation that can be detected by the human eye. It travels in the form of waves or particles called photons. Light energy is responsible for vision, photosynthesis in plants, and various technological applications.

2.1.6 Nuclear Energy

Nuclear energy is released during nuclear reactions, such as nuclear fission (splitting atoms) or fusion (combining atoms). It is the energy source of the sun and other stars, as well as nuclear power plants. Energy can be converted from one form to another. The law of conservation of energy states that energy cannot be created or destroyed, but it

can only be transformed or transferred from one form to another. This principle is often summarized as "energy is conserved."

2.2 Types of Energy Sources

There are various types of energy sources used in the world, which can be classified into two main categories: renewable energy sources and non-renewable energy sources.

2.2.1 Renewable Energy Sources

Renewable energy sources are derived from natural processes that are constantly replenished and do not deplete over time. They are considered environmentally friendly and sustainable. Some common renewable energy sources include:[16]

a. Solar Energy: Solar power harnesses energy from the sun using photovoltaic (PV) panels or solar thermal collectors to convert sunlight into electricity or heat. In the Figure 2.1

b. Wind Energy: Wind turbines capture the kinetic energy of the wind and convert it into electricity.

c. Hydroelectric Power: Hydroelectric power is generated by harnessing the energy of flowing or falling water, typically through the use of dams.

d. Geothermal Energy: Geothermal power utilizes heat from the Earth's interior to generate electricity or provide heating and cooling.

e. Biomass Energy: Biomass energy is derived from organic matter, such as wood, crop residues, and agricultural byproducts, which can be burned or converted into biogas for energy production.

f. Tidal Energy: Tidal energy exploits the gravitational pull of the moon and the sun on the Earth's oceans to generate electricity using tidal turbines or barrages.

Figure 2.1: Renewable and non Renewable resources.

2.2.2 Non-Renewable Energy Sources

Non-renewable energy sources are finite and deplete over time as they are extracted and used. They are formed over millions of years and cannot be readily replaced within a human lifetime. The main non-renewable energy sources include:

a. Fossil Fuels: Fossil fuels, including coal, oil, and natural gas, are formed from the remains of ancient plants and animals. They are burned to release energy, but their combustion releases carbon dioxide and other pollutants, contributing to climate change and air pollution [17].

b. Nuclear Energy: Nuclear power is generated through controlled nuclear reactions, such as nuclear fission or fusion, which release large amounts of energy. It is considered non-renewable because the fuel used in nuclear reactors, such as uranium or plutonium, is finite.

c. Natural Gas Liquids (NGLs): NGLs are hydrocarbons extracted from natural gas, including propane, butane, and ethane. They are primarily used as feedstocks for various industrial processes.

d. Coal Seam Gas: Coal seam gas, also known as coal bed methane, is natural gas trapped

in coal deposits. It is extracted through drilling and can be used as a source of energy.

e. Shale Gas: Shale gas is natural gas trapped in shale rock formations. Its extraction requires hydraulic fracturing to release the gas. It is worth noting that the global energy landscape is evolving, with increasing efforts to transition towards a greater reliance on renewable energy sources to mitigate climate change and reduce dependence on finite resources.

2.3 Types of Nanogenerators

Nanogenerators are an energy-harvesting technology that produces electricity from thrown-away ambient mechanical energy [18, 19]. Through a variety of processes, they harness and transform energy using nanoscale structures or materials. There are several kinds of nanogenerators: Types of Nanogenerators are Listed below in Figure 2.2

2.3.1 Piezoelectric Nanogenerators

The devices run on the concept of the piezoelectric effect. When put under pressure or mechanical stress, piezoelectric materials produce an electric charge. A piezoelectric nanogenerator uses thin films or nanoscale piezoelectric devices to transform mechanical resonances and deformations to generate electrical energy. Both current and voltage are produced whenever the piezoelectric substance is subjected to mechanical strain, such as pressure or bending. This kind of nanogenerator could be utilized to generate power from vibrations in the surrounding environment, human movements, or both.

2.3.2 Triboelectric Nanogenerators

The triboelectric effect is the basis for triboelectric nanogenerators' operation when two different substances come into contact with one another and rub or encounter friction, a phenomenon develops. When this occurs, one substance has a tendency to pick up electrons and become charged negatively, while the other substance loses electrons and becomes positively charged. Nanoscale structures or thin films with various triboelectric

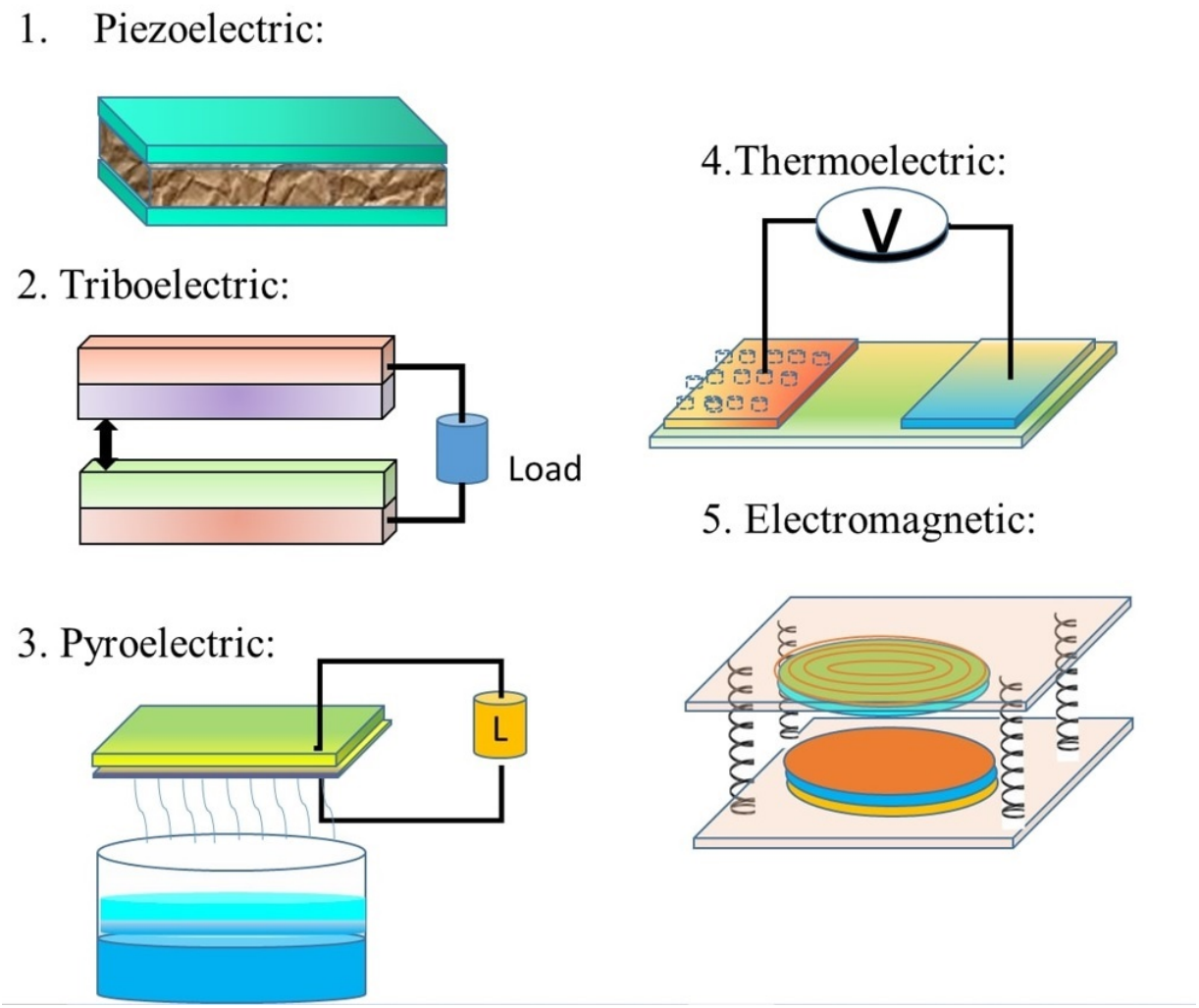

Figure 2.2: Types of Nano generators. Reproduced from [35]

characteristics are used in triboelectric nanogenerators. These materials produce an electric charge as a result of the redistributing of electrons when they come into contact and are later separated. Electricity can be produced by repeatedly pressing or rubbing the materials together. This type of nanogenerator is able to harvest power from a variety of sources like mechanical vibrations, human motion, and flowing fluids.

2.3.3 Thermoelectric Nanogenerators

Using Seebeck's phenomenon, thermoelectric nanogenerators transform variations in temperature into electrical energy. A temperature gradient can be transferred transfer through by using thermoelectric materials that are thermoelectric. High heat conductivity as well as low electrical conductivity micron-sized substances or nanostructures are used

in thermoelectric nanogenerators. The flow of electrons from the hot end to the cold side that results from the temperature variation across the device produces an electric current. This type of nanogenerator can be used to capture waste heat from a variety of sources, including human metabolism, electronic devices, and industrial operations.

2.3.4 Pyroelectric Nanogenerators

These devices generate power from temperature variations. The pyroelectric effect is the term used to describe the phenomena wherein some materials produce an electric charge in response to temperature fluctuations. Electrical charges are produced as a result of the pyroelectric material's polarization shifting when its temperature varies. In pyroelectric nanogenerators, the heat energy from the surrounding atmosphere is captured using very thin films or nanostructured substances with pyroelectric characteristics. Differences in the surrounding temperature or even human body heat may be to blame for temperature differences. These generators are appropriate for powering tiny machines and sensors.

2.3.5 Electromagnetic Generators

Devices built using coils and magnets are a legitimately developed approach. Based on Faraday's law of induction, the electromagnetic force is created by the mutual vibration movement between an electric circuit as well as a magnetic field, resulting in current flowing across the electric load. Under diverse vibration conditions, electromagnetic transducers that have low impedance can deliver large current output. However, a small voltage output as well as a small electromechanical coupling coefficient limit output power. These particular nanogenerators have special benefits due to their compact size, adaptability, and suitability for nanoscale applications. Smaller gadgets like wearable technology, sensors, and other applications that require little power may be powered by them. In order to increase their effectiveness, scalability, and ability to be integrated into other energy-harvesting systems, the application of nanogenerators is constantly evolving and investigating new materials, architectures, and device designs.

2.4 Triboelectric Nanogenerator

It works on two different principles, the triboelectric effect is used by this particular type of nanogenerator to produce Electrical Energy by using power when two dissimilar materials rub or contact against one another, the triboelectric effect takes place, which causes electrons to move between the materials and Electrostatic Induction it would re-distributing the electrons among the one electrode to another electrode In a TENG, different materials with differing triboelectric characteristics are brought into touch and subsequently separated that is when two materials come into contact, an interchange of electrons and ions results in one substance gaining the electrons (negative charge), as well as the other to lose electrons (positive charge). Due to the redistributed charges, a voltage difference between the materials is produced during separation, which results in an electric current shown in Figure 2.3. The repeating contact as well as separation between the materials made possible by mechanical force or bodily forces acting on the TENG, for instance rubbing, pushing, or vibration, results in a continual creation of electrical miniature electronic devices, sensors, and battery-powered gadgets that can all be powered by this electrical energy, which can be collected and used in a variety of ways. TENGs have benefits including flexibility in extracting energy from different mechanical resources, energy efficiency during conversion, cost-effectiveness, and potential application into self-powered systems. They have been used in wireless sensors, electronic devices for environmental surveillance, and other uses when there is access to a mechanical energy source in the ambient environment. TENGs lessen reliance on outside power sources by assisting in the development of self-sufficient, sustainable energy solutions.

2.4.1 Triboelectric Nanogenerator Operating Modes

Different working Modes: TENGs have a number of working modes, including single-electrode, lateral sliding, vertical contact-separation and free-standing modes shown in figure 2.4 (ii), enabling design flexibility and adjusting depending on the material used and applications.

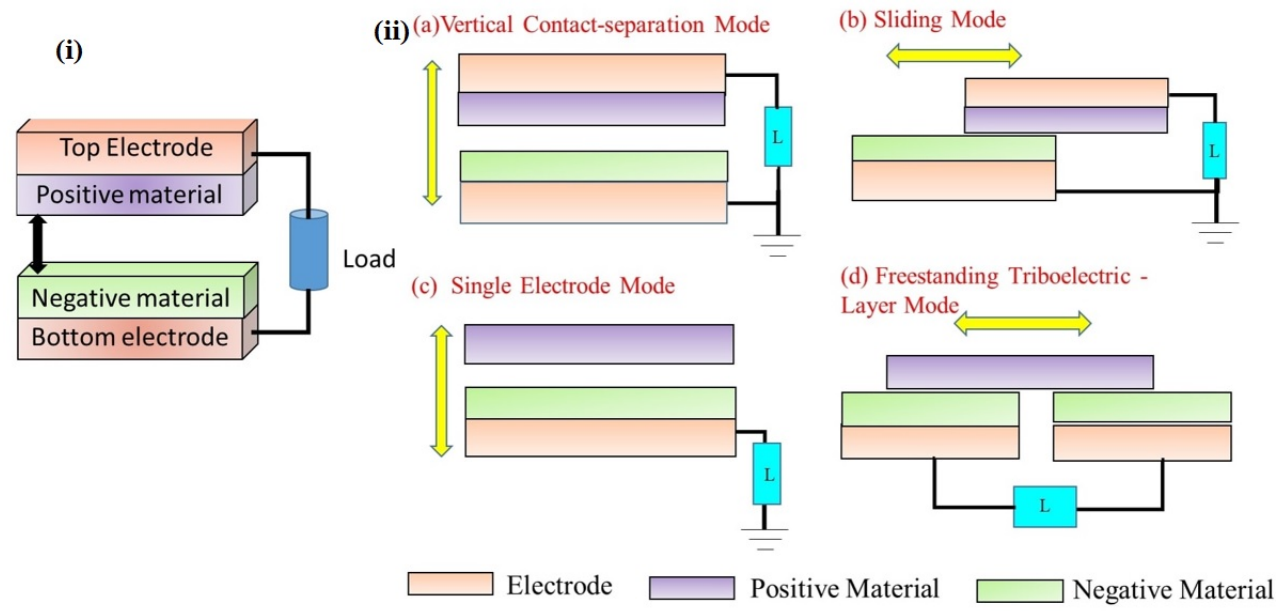

Figure 2.3: (i) Current flow in TENG. (ii) The Four Fundamental modes of Triboelectric nanogenerators: a) vertical contact-separation mode; b) in-plane contact-sliding mode; c) single-electrode mode; and d) freestanding triboelectric-layer mode.

2.4.2 Vertical Contact-Separation Mode

The contact-separation mode is the simplest TENG as shown in Figure 2.3(ii)(a). In this configuration, two dissimilar dielectric films are stacked as triboelectric pair, facing each other. Due to the difference in triboelectric polarity, charges are transferred between the interfaces when these two films come into direct contact. This transfer results in the formation of opposite charges on the two tribo-layers. When a mechanical motion triggers the vertically separated layers, a potential drop occurs between the two back electrodes coated on the dielectric films. This potential drop allows electrons to pass through the external circuit. The potential formed by the triboelectric charges tends to decrease as the two layers approach each other, and electrons flow back to restore the original electrical equilibrium. This contact-separation mode is ideal for TENG operation because it enables high output generation, minimal structural damage, and practical applications [20, 21].

2.4.3 Lateral Sliding Mode

The contact-separation mode has the same configuration as the sliding mode as shown in Figure 2.3 (ii)(b). When two dielectric films come into full contact, triboelectric charges are generated on the interfaces due to relative sliding motion in the in-plane direction. A lateral polarization emerges along the sliding direction as the two tribo-layers slide outward. This polarization creates an interfacial potential, which drives electron flow on the rear electrodes and attempts to equalize the electric field generated by the triboelectric charges. The periodic motion of sliding in and out produces an alternating current (AC) output, which represents the Triboelectric Nanogenerators (TENG) fundamental sliding mode. Planar motions, cylinder rotations, and disc rotations are all methods for achieving sliding motion. This sliding mode generates charges between the two tribo-layers more efficiently than the pure contact mode. The in-plane charge separation in the sliding mode can be significantly improved by using a grating design, outperforming the vertical contact-separation mode by multiple orders of magnitude. This enhanced charge transfer capability results in a significant increase in power output [22].

2.4.4 Single-Electrode Mode

In both modes, the moving tribe-layers are covered with two back electrodes. In real-world situations, however, moving dielectric materials frequently collect charges when they come into contact with the surrounding air or other constituents. This makes establishing an electrical connection between the TENG and the load difficult, especially when a person is walking or jogging on the floor. This problem can be solved with a single-electrode TENG setup as shown in Figure 2.3 (ii)(c). One electrode is connected to one tribo-layer while the other is grounded in this design. The local distribution of the electrical field changes when the bottom object moves away from or towards the single electrode, resulting in electron exchange between the electrodes as well as the ground, which keeps the overall potential equilibrium. This is true as long as the TENG is of limited size. The single-electrode Triboelectric Nanogenerator (TENG) arrangement allows for relative movement between the tribo-layers or between the tribo-layer and the electrode by employing various modes such as vertical contact-separation, sliding, and

hybrid modes. This adaptable design is ideal for harvesting energy from moving charged objects while also acting as an independent sensor to accurately track their motion [22] [23]

2.4.5 Freestanding Triangle-Layer Mode

A TENG, consisting of two fixed electrodes, is introduced in this development with the goal of harnessing kinetic energy from a free-moving object via triboelectric effect as shown in Figure 2.3 (ii)(d). Because of the symmetric design, a freestanding triboelectric layer approaches one of the two electrodes alternately, resulting in a periodic change in the induced polarization potential difference between the electrodes. For this mode to work properly, the electrode sizes and spacing must match those of the moving freestanding triboelectric layer. To balance the local potential distribution, electrons flow between the two electrodes, resulting in AC output generation by the periodic movement of electrons between the electrode pair. The electrodes top dielectric layer does not need to come into physical contact with the moving layer. This feature allows unrestricted rotation without direct mechanical contact, reducing stress on the triboelectric interfaces significantly. As a result, this technique improves the toughness and dependability of TENGs. Extensive demonstrations have shown that this freestanding layer structure can harvest energy from moving vehicles and humans, highlighting its significant potential for capturing energy from unconnected free-moving objects. [22, 23, 24]. This is accomplished by putting a set of symmetrical electrodes below a dielectric layer, arranging their sizes and the gap between each of them in precisely the same order in the size of a moving object. As the object moves toward or away from the electrodes, the asymmetrical charge distribution is created. This model's capacity to increase TENG durability is a bonus feature. Although an object needs not even contact the top a dielectric layer in this case, free rotations without touch can take place, greatly reducing the amount of wear on the surfaces. TENG's main benefits include its high power density, stability, adaptability, sustainability, and efficiency, variety of working modes, material options, and simplicity of application.

2.4.6 Additional Features of TENG

TENGs have the capacity to produce a substantial quantity of electrical energy per surface area or volume, which is known as high power density. They are therefore appropriate for applications that call for efficient and portable power generation.

2.4.7 Stability

TENGs show good performance stability over time. They may continue to generate electricity without suffering appreciable degradation, ensuring dependable and long-lasting operation.

2.4.8 Flexibility

TENGs are capable of being made flexible and conformable, which enables them to be integrated into a variety of curved or oddly shaped surfaces. Due to their adaptability, they can be used in flexible electronics, wearable technology, and various other applications that call for conformable power generation. TENGs are regarded as sustainable energy harvesting technologies because they can without wasting natural resources, create power from mechanical energy in the environment. They provide a clean, renewable energy alternative.

2.4.9 High Efficiency

TENGs have the capacity to transform mechanical power into electrical energy with high energy conversion efficiency. This great efficiency makes it possible to efficiently capture energy from different mechanical sources. TENGs have the ability to function at low frequencies, which enables them to absorb and transform energy from slowly occurring or low-frequency mechanical vibrations. As a result, there are now more possible sources of energy that can be used.

2.4.10 High Output Voltage

Because TENGs can produce relatively large outputs the voltages they are appropriate for applications that call for higher voltages to transmit power or charge energy storage devices. Cost-effectiveness: TENGs could be made from inexpensive materials and production techniques. Compared with a few other energy harvesting devices, they are comparatively affordable thanks to certain approaches. This increases their likelihood of being widely used and commercialized.

2.4.11 Operating Principles of TENG

A wide variety of materials with various triboelectric characteristics can be used to design TENGs. This wide range of material options makes it possible to optimize device performance and ensure compatibility with particular application requirements.

Maxwell's equations:

$$\nabla \cdot \mathbf{D} = \rho \tag{2.1}$$

$$\nabla \cdot \mathbf{B} = 0 \tag{2.2}$$

$$\nabla \times \mathbf{E} = -\frac{\partial \mathbf{B}}{\partial t} \tag{2.3}$$

$$\nabla \times \mathbf{H} = \mathbf{J}' \tag{2.4}$$

$$\mathbf{J}' = \mathbf{J} + \frac{\partial \mathbf{P}_S}{\partial t} \tag{2.5}$$

Where:

$\mathbf{E}$ is the electric field

$\mathbf{B}$ is the magnetic flux density (magnetic induction)

$\mathbf{D}$ is the electric displacement field

ρ is the charge density

$\mathbf{H}$ is the magnetic field intensity

$\mathbf{J}$ is the current density

$\mathbf{J}'$ is the modified current density

$\mathbf{P}_S$ is the polarization density of the material

t is time

The above equations are useful to understand the Displacement current of TENGs, Equation highlights the significance of two key terms: (1) (E/t), representing Maxwell's displacement current, crucial at high frequencies, and (Ps/t), denoting surface charge-induced displacement current, more relevant at low frequencies. These terms play varying roles in energy generation, emphasizing the importance of understanding their interplay for analyzing nanogenerators' performance across different frequency ranges

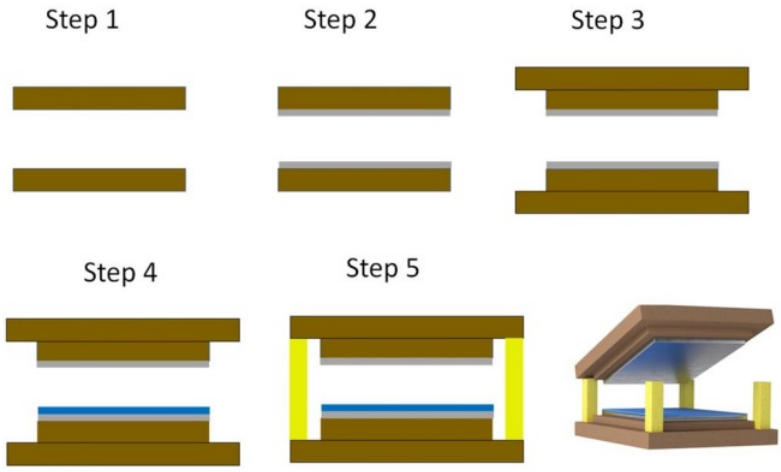

Figure 2.4: Steps for TENG Preparation.

Simple Architecture and Operation Principles TENGs can be relatively simple to implement and incorporate with existing systems or devices. This makes it easier to deploy and integrate TENGs into different applications.TENGs can be made to take up the least

amount of space possible, which makes them ideal for applications with constrained space or tiny devices. TENGs are often lightweight, making it simple to include them in wearable or portable devices without significantly adding to their weight.

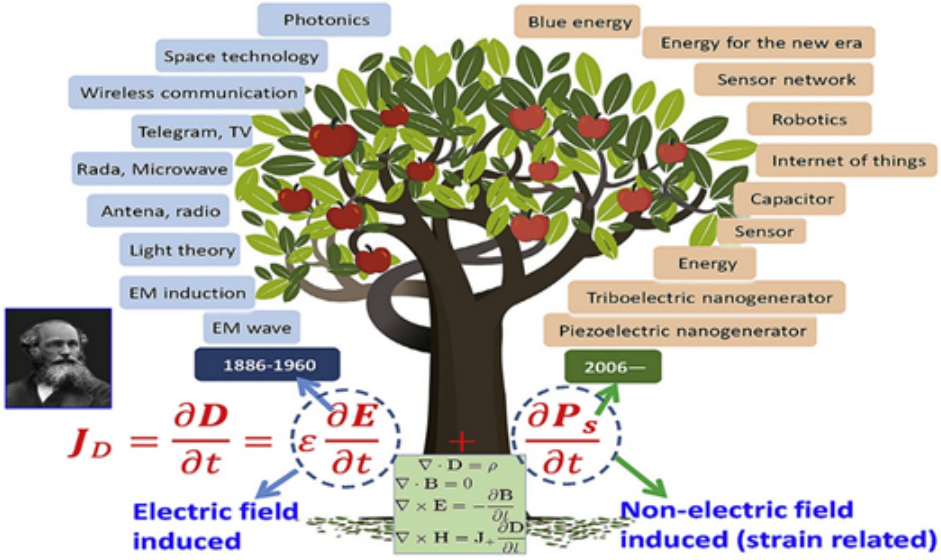

Figure 2.5: A displacement current comparison using Maxwell's and Wang's extended equations. Maxwell gave the first term $\frac{\partial E}{\partial t}$ in J_D induced by the electric field in 1861, while Wang demonstrated the second term $\frac{\partial Ps}{\partial t}$ in 2017. The governing principle of mechanical energy harvesters based on piezoelectricity, electrostatics, and triboelectricity is the displacement current density J_D. Reproduced from [1].

The total voltage (V), which is across a circuit is defined by the contributions of various voltage sources as well as the voltage drop caused by air.

$$V = E_1 \cdot d_1 + E_2 \cdot d_2 + E_{\text{air}} \cdot a \tag{2.6}$$

The entire voltage or potential difference across the circuit is denoted by V. E_1 and E_2 are constants that indicate Electric fields due to uneven distribuition of Electrons, d_1 and d_2 are thickness of dielectric Electricfield over an air a represents the area (units vary depending on the context).

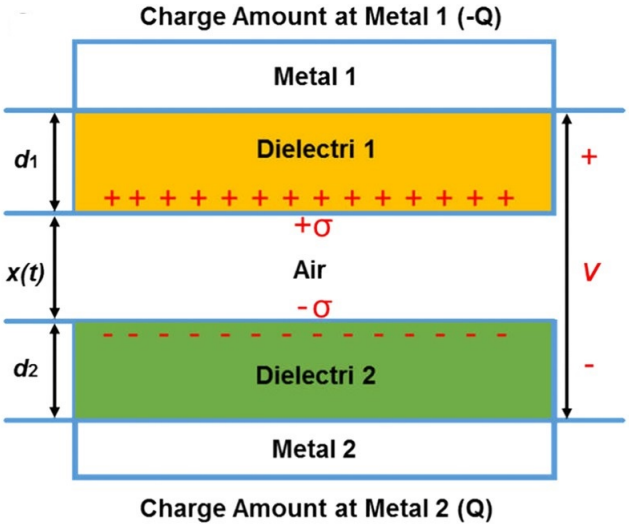

Figure 2.6: Electron Flow.Reproduced from[35]

$$E_1 = -\frac{-Q}{A\varepsilon_0\varepsilon_1} \tag{2.7}$$

$$E_2 = -\frac{-Q}{A\varepsilon_0\varepsilon_2} \tag{2.8}$$

$$E_{\text{air}} = \frac{-\left(\frac{Q}{A}\right) + \sigma}{A\varepsilon_0\varepsilon_1} \tag{2.9}$$

E_1 ,E_2 ,E_{air} denotes the electric field produced by an electric charge distribution exhibiting total charge -Q (a negative charge) across area A, separated by a material with a permittivity ε_0 (such as vacuum permittivity) and material permittivities ε_1 and ε_2. ε_0 = 8.8 x $10^{-12} F/mpermittivity$.

When the TENG device is in open circuit condition, we have:

$$V_{\text{out}} = \frac{-Q}{A\varepsilon_0\varepsilon_1}\left(\frac{d_1}{\varepsilon_1} + \frac{d_2}{\varepsilon_2} + x\right) + \frac{\sigma x}{\varepsilon_0} \tag{2.10}$$

$$V_{\text{oc}} = \frac{\sigma x}{\varepsilon_0} \tag{2.11}$$

2.5 TENG Performance Analysis

TENGs are appealing because of these characteristics for a variety of applications, such as wearable electronics, sensors that can run on their own power, wireless commu-

nication systems, and harvesting energy in varied situations. Ongoing TENG technology research and development continue to look for methods to improve these capabilities and maximize their effectiveness for application specifications. A Triboelectric Nanogenerator (TENG) can be built to optimize energy conversion efficiency and numerous strategies can be used to increase current output.

2.5.1 Surface Alteration

Charge transport can be improved and the triboelectric effect can be strengthened by altering the material's surface characteristics of the triboelectric materials. Increased surface roughness, encouraged charge separation, and improved triboelectric charging efficiency can all be achieved through surface treatments such as coatings, or Nano Structuring

$$Q_{\mathrm{sc}} = \frac{A\sigma x}{d_0 + \Delta x} \tag{2.12}$$

the charge density (x), area (A), and distance ($d_0 + \Delta x$) to another point relative to the surface charge density (Q_{sc}) associated with a charged object. According to this, the surface's charge density rises with surface area, charge density, and proximity to the object of interest. The formula expresses the physical properties of the distribution of charges on surfaces by saying that the surface's charge density is influenced by the charge density distributed over an area. Understanding how charges are dispersed on objects and how they effect neighbouring spots depending on proximity and surface area is crucial in electrostatics.

2.5.2 Material Selection

It's essential to select triboelectric materials with the best possible triboelectric properties [25]. The current output of the TENG can be increased by using material with a high charge density, severe triboelectric polarization, and a broad contact area.Configuration of the electrodes: Improving the electrodes' layout and design can improve the effectiveness of charge collection. In order to do this, the right electrode materials must be chosen, their arrangement and placement have to be optimized, and the parasitic capacitance or resistance in the electronic system must be kept to a minimum.

2.5.3 TENG's Structural Design

Performance may be affected by the size, shape, and placement of the electrodes and triboelectric layers. Increasing the optimal contact area, promoting charge separation, and enhancing overall performance can all be accomplished by designing the right patterns, forms, or surface characteristics.

2.5.4 Mechanical Amplification

The displacement and strain delivered to the TENG can be improved by including mechanical amplification methods. This can entail amplifying the mechanical action to increase the output current by employing levers, springs, and or other mechanical components.

2.5.5 Frequency Matching

The effectiveness of energy harvesting can be increased by aligning the frequency of operation of the TENG to that of its external mechanical source. Because of the efficient power transfer between the sources of energy to the TENG made possible by this, the current output is boosted.

2.5.6 Multiple TENG Units

Multiple TENG devices could be used in a stacked configuration to increase the total current output. The captured charges and voltages from individual TENG units can be combined by connecting additional TENG devices in parallel, increasing the output of the total current.

2.5.7 Matching the External Load's Resistance

Load Resistance within the electric system that is linked to the TENG can enhance current output and increase power transfer efficiency, by ensuring that the external load

resistance matches the internal impedance of the TENG, effective power transfer is made possible. It's critical to remember that the exact methods used to boost a TENG device's output response. TENG will vary according to the application's needs, the obtainable mechanical energy source, and the desired performance traits. To determine the most productive TENG system, experiment, and optimization may be required.

2.6 Characterizations of Triboelectric Nanogenerators

2.6.1 Changing the Polarity

Triboelectric Nanogenerator (TENG) device's capacity to change the path of the generated electric current is referred to as switching its polarity. To do this, the TENG must be built in a fashion that permits charge transfer to be reversed after the contact-separation process [26]. The fundamental TENG setup uses two triboelectric materials to further elucidate the idea: In both Materials A and B, Charge transfer takes place between these materials when they come into contact after which they separate, creating a difference in electrical potential and a corresponding current flow. One typical method for changing the polarity is to move the materials inside the TENG device while the contact is being separated [27]. This implies that Material A and Material B come into touch during one cycle, and Material B and Material A interact during the following cycle. The electrostatic attraction of the current that is produced is likewise flipped as a result of the materials' location, which also flips the direction of charge transfer. consider the equation below, which connects a TENG's current output (I) to its charge flow rate (Q) and charge time at which charges transfer (t):

$$I = Q/t. \tag{2.13}$$

The quantity of charge transported per unit of time, or the charge rate of transfer (Q/t), determines the present output in this equation. The direction of charge transfer is reversed when the polarity is changed, which leads to a change of the sign of Q. As a result, the current output's (I) polarity likewise alters. For instance, reversing the polarity will

produce a negative current output (the opposite side of conventional current flow) if the initial polarization is positive. The polarity change is made possible by the TENG device's architecture, which may techniques that enable a reverse of charge transfer, such as changing the arrangement or positioning within the triboelectric materials, adding extra electrodes, or using switching circuits. It is important to keep in mind that the precise design and implementation specifications for polarities switching in a TENG can change based on the device layout, the materials utilized, and the required operational requirements. For polarity altering in TENG devices to be effective and dependable, experiment and optimization may be required.

2.6.2 Contact Area

A Triboelectric Nanogenerator's (TENG) output and current output are greatly influenced by the contact area. The area on the surface on which triboelectric material comes into contact and goes through friction or rubbing is referred to as the contact area. A deeper connection in general results in improved current generation and increased charge transfer. The following equation describes the relationship between a TENG's current output (I) and contact area (A) [28] I = α * A

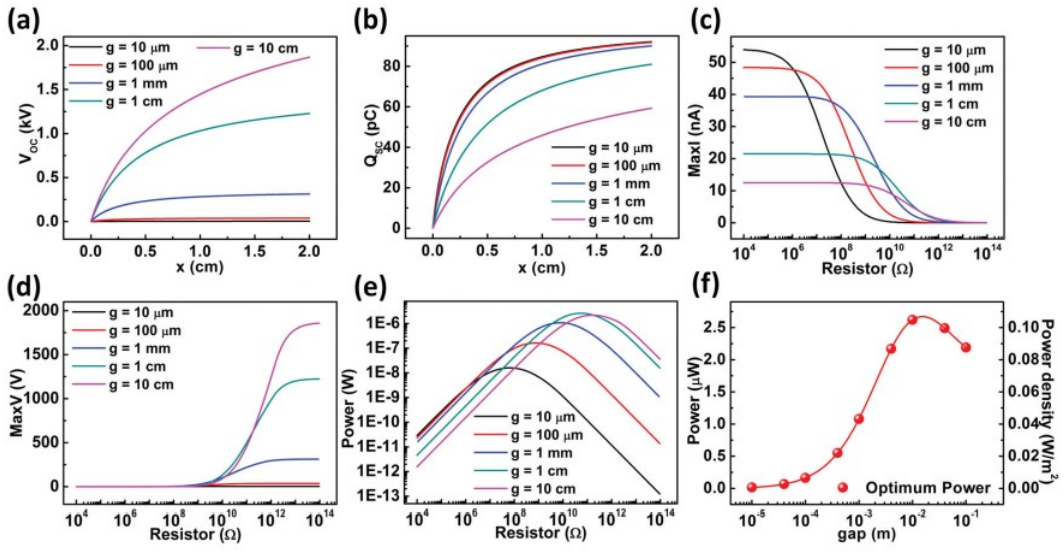

Figure 2.7: (a) Contact Area vs voltage (b) Contact Area vs Short Circuit Current (c-e) Different Resistances vs Voltage, Power and Current. Reproduced from [25]

Where the α current density, or amount of current produced for each area throughout

the contact region, is shown by the symbol. The value is influenced by a number of variables, including the type of triboelectric material employed, the effectiveness of charge exchange, as well as the mechanical motion utilized to move the TENG. The TENG's with more area of contact in the region enable more thorough contact and a higher coefficient of friction among the materials when it is affected by mechanical forces, like rubbing or pushing. Because more charge is transferred as a result, the output of current is higher relative to contact with another region. The effective surface that is accessible for the transfer of charge is increased by expanding the contact area, which maximizes charge creation and improves the current generation of the TENG. There's a suitable range of the contact area depending on the particular substances, and operating circumstances of the TENG, although a greater contact area typically results in a higher current output. To get the best performance, it is critical to balance the area of contact, the friction transfer of charge efficiency, along with other design factors. The contact area increases with a smaller spacer height while decreasing with a greater spacer height shown in a and b of Figure 2.7.

2.6.3 Output Voltage and Load Resistance

The load resistance with Triboelectric Nanogenerator (TENG) devices is the external resistance linked to the TENG's output to remove the electrical energy produced. The resulting voltage generated by TENG is greatly influenced by the load resistance. The generated current passes through a closed circuit if the resistance of the load is attached to the TENG. The output voltages (V) of the TENG are precisely proportionate to the current (I) passing through the load resistance (R), in accordance with Ohm's Law (V = I R). Fluctuations in the voltage that is output occur from changes in the flow of charges through the circuit as a result of fluctuations in the load resistance value depict in Figure 2.8. In general, a greater output voltage results from a decrease in output current as load resistance rises. In contrast, as the load resistance falls, the output current rises, and lower output voltage results.

There is, however, a load resistance setting that maximizes the TENG's power output. By locating the resistance of the load that maximizes the product of the voltage that is generated and the current, the maximum power point, or MPP, may be calculated.

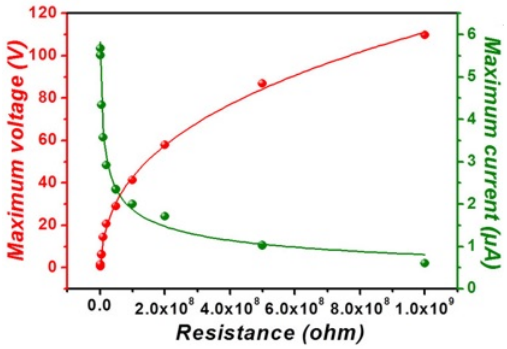

Figure 2.8: Output Voltage vs Load Resistance Reproduced from [26]

Effective power extraction from a TENG depends on choosing the right load resistance. It requires finding a balance between the necessity to optimize power output and increased output voltage. The efficient transfer and use of the electrical energy generated in the various TENG-powered applications and systems depends on the selection of the load resistance.

2.6.4 Power Density and Resistance to Load

The power density of the TENG device determines the amount of power produced per unit area or volume. The power density is significantly impacted by the TENG's output voltage. A TENG's power density is inversely proportional to the sum of its output voltage and current. TENG improves the electrical power density, grows along with [27] [29] the output voltage at a constant current. This is due to the fact that power is computed as a product of voltage and current (P = V I). To attain the greatest power density, it is necessary to take into account the ideal working circumstances. TENG power density can be maximized at an ideal output voltage, which is usual. Reduced power density may be experienced when operating at or below this optimum voltage.Power density and output voltage must be balanced shown in Figure 2.9, and this is critical. P = J * E

P refers to power density, which is expressed as watts per cubic metre, or W/m^3. J is the current density, expressed as A/m^2 (amperes per square metre). E is the amplitude of the electric field, expressed in volts per metre, or V/m

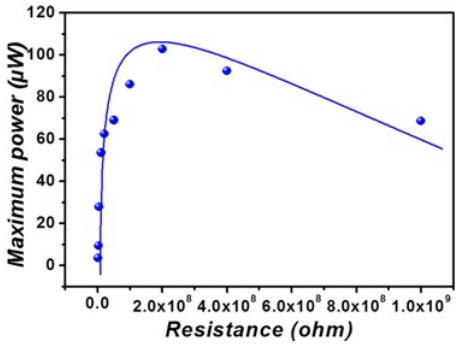

Figure 2.9: Power vs Load Resistance Reproduced from [32]

$$J_D = \sigma T \left[\frac{dx}{dt}\right] \left[\frac{\frac{d\varepsilon_0}{\varepsilon_1} + \frac{d\varepsilon_0}{\varepsilon_2}}{\left(\frac{d\varepsilon_0}{\varepsilon_1} + \frac{d\varepsilon_0}{\varepsilon_2} + X\right)^2}\right] \tag{2.14}$$

(s_T) is the charge density, x is displacement w.r.t time, εr_1,εr_2 relative permittivity, and x gap between to materials [30, 31, 32]. P1 - Triboelectric effect, P2 - Device contact separation function , P3 - Electrostatic induction. Changing rate of the applied strain is proportional to the output current density. The current density (J_D) affected by different parameters like Transfer charge density (s_T), separation speed (dx/dt), permittivity variations of two dielectric materials ($d_o/ \varepsilon_1 + d_o/ \varepsilon_2$), and distance all The equation is denotes that how the electric currents behave in electrical systems that contain dielectric components like capacitors or insulating materials. Increasing the output voltage can increase power density, but it should be balanced against other elements like the resistance of the load and the forces that are being applied towards the TENG. The optimum power density of output for a particular TENG device can be attained by optimizing these parameters. This is due to the fact that power is computed as a product of voltage and current (P = V I). To attain the greatest power density, it is necessary to take into account the ideal working circumstances. TENG the power density of a TENG is a crucial factor since it establishes the energy production per area or size, which is essential in a variety of applications where size and space restrictions are taken into account. Higher power density makes it possible to capture energy from mechanical sources more effectively and compactly, which helps to make self-sufficient powered devices and sustainable energy options.

2.6.5 Rectified Output Voltage

The rectified output voltage of a TENG is the voltage that results from the rectification and filter of the AC (alternating current) signal produced by the TENG. On the other side, the load resistance is the external resistance linked to the TENG to remove the electrical energy generated [22]. This is due to the fact that power is computed as a product of voltage and current (P = V I). To attain the greatest power density, it is necessary to take into account the ideal working circumstances. In a TENG, the rectified outcome voltage and load resistance have the following relationships shown in Figure 2.10:

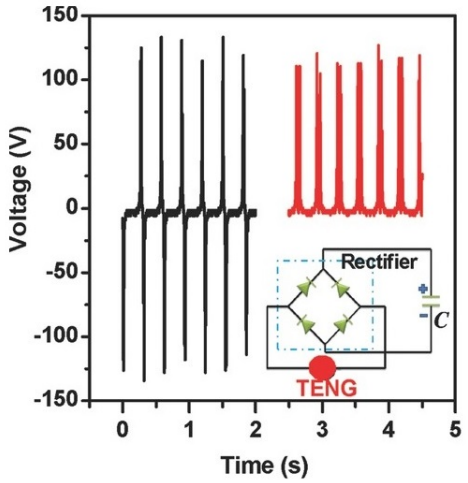

Figure 2.10: Load Resistance vs Rectified Output Voltage, Reproduced from [45]

In order to create a direct current, or DC, signal, the AC signal produced by the TENG is normally rectified. In the TENG circuit, diodes of other rectification components are used to achieve this rectification [33]. The DC voltage obtained following this rectification process is represented by the rectified output voltage.

2.6.6 Load Resistance

In order to extract and use the electrical energy created by the TENG, a load resistance is linked to the resultant power of the device. It controls the electrical voltage from the load and influences the current flow.In a TENG, Ohm's Law governs the connection among the rectified voltage as well as the load resistance. This is due to the fact that power is computed as a product of voltage and current (P = V I). To attain the greatest

power density, it is necessary to take into account the ideal working circumstances. The resultant voltage (V) over a load resistance has directly in proportion towards current (I) going through the load, with regard to Ohm's Law (V = I R). The circuit's current flow reduces as the load resistance is raised, [34] resulting in a greater rectified output voltage. In contrast, when the load resistance reduces, the current increases, and the rectified output voltage decreases. it's critical to choose the load resistance that optimizes power production or produces the required voltage level. The internal impedance of the TENG, the characteristics of its maximum power point (MPP), and the desired power transfer efficiency can all be taken into account when determining the ideal load resistance. This is due to the fact that power is computed as a product of voltage and current (P = V I). Toget higher power density, it is necessary to take into account the ideal working circumstances. The rectified voltage generated can be tuned to meet application requirements by modifying the load resistance, balancing energy extraction effectiveness, and the intended voltage level.

2.6.7 Voltage Output vs Frequency

Charge transfer occurs between triboelectric layers come in contact throughout the contacting process of the TENG process. The total amount of the transferred charge is influenced by the contact area. More charge can transfer when there is a bigger contact area than when there is a smaller contact area. Voltage and current at the output: The charge transfer affects a TENG's output voltage and current. Increased charge transfer is made possible by a bigger contact area, which is attained with a reduced spacer height, leading to increases in voltage and current. A higher spacer height, on the other hand, decreases the contact area and restricts the charge transfer, resulting in reduced voltages and current.

2.6.8 Effect on Capacitance

The amount of capacitance that exists among the triboelectric layers is likewise impacted by the height of the spacer. shorter spacer height reduces the separation between the layers, increasing capacitance. The capacitance affects how the TENG accumulates

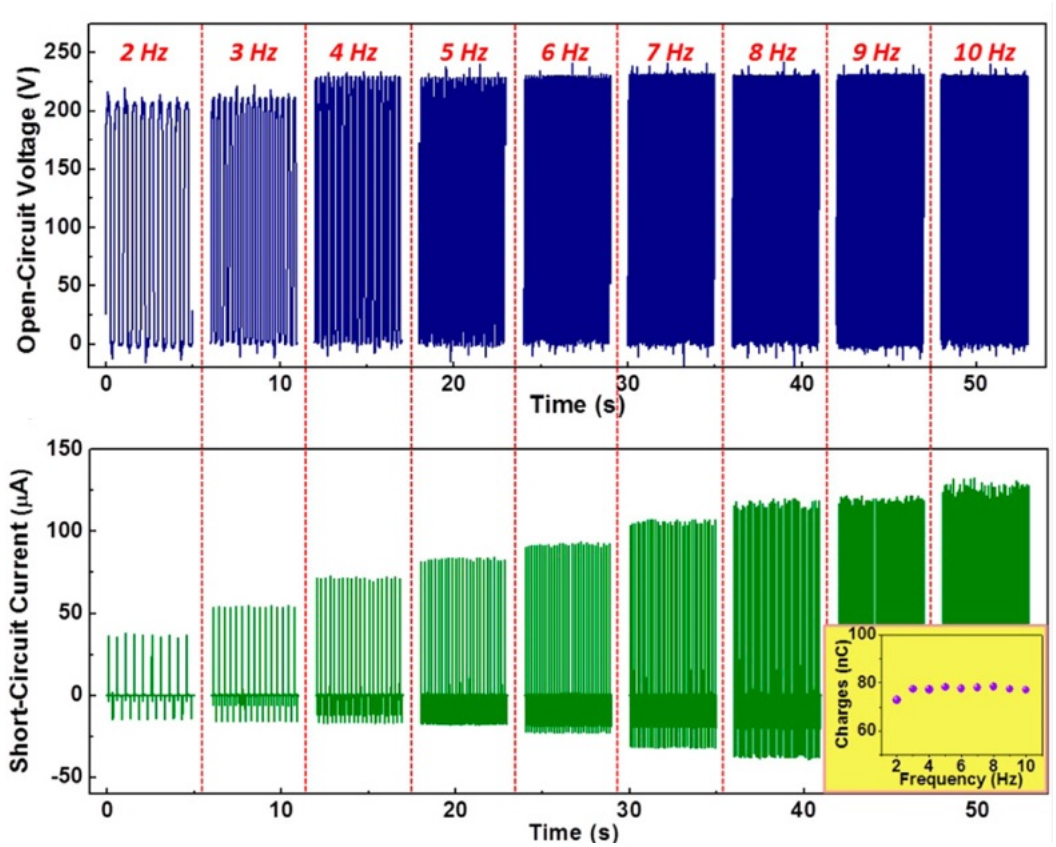

Figure 2.11: (a) Open Circuit Voltage , Short Circuit Current vs vs Frequency variation. Reproduced from [27]

charges and responds to voltage.

$$C = \frac{S\varepsilon_0}{d_0 + x} \tag{2.15}$$

capacitance (C), S is the surface area , vacuum permittivity ε_0, d_0 thickness of the dielectric Interial capacitance of the TENG device could effect by the the Surface area and thickness of the dielectric and air medium shown in Figure 2.12.

2.6.9 Resonance

The height of the spacer may have an impact on the TENG's resonance behaviour. You can change the spacing The TENG's essential frequency can be modified by varying the height of the spacer, which enhances impact responses at particular frequencies. Voltage and current responses at the output are boosted by repetition. These models take

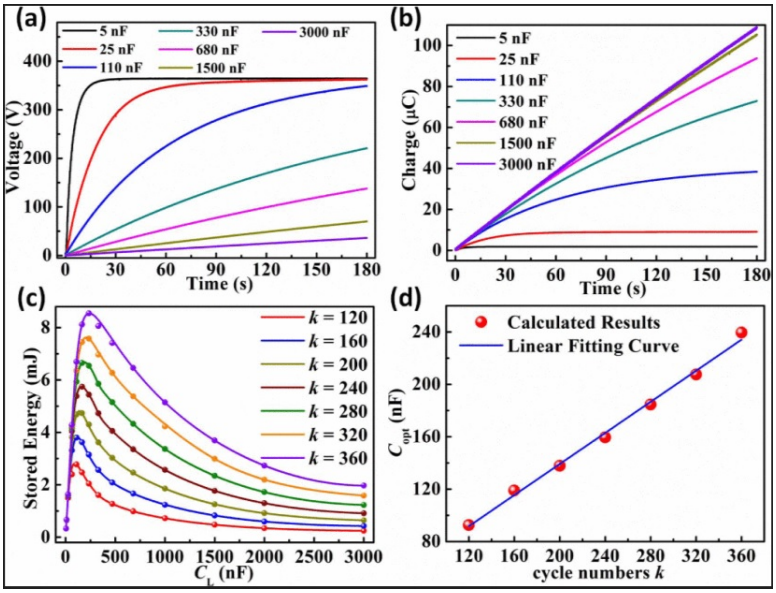

Figure 2.12: (a - d) Capacitance Graphs Reproduced from [31]

into account elements including the triboelectric characteristics, system dynamics, and the mechanical characteristics of the spacer material.

2.6.10 Optimizing the Spacer Height

In a TENG design is critical to achieving the intended performance, such as maximizing power generation, improving energy conversion efficiency, or tuning the responsiveness to certain operating conditions. It is important to remember that the spacer height's effect on the output response may differ according to the specific TENG design, the materials utilized, and the operating conditions. The ideal spacer height for a specific TENG design and application is often determined through experimentation and optimisation.

2.6.11 Different Tests in TENG

Triboelectric Nanogenerators (TENGs) undergo stability testing by analysing their performance and behaviour over a lengthy period of time to ascertain their subsequent stability and reliability. These tests aid in assessing the TENG's capacity to sustain constant output characteristics and endure a range of operational and environmental circumstances.

During this test, the TENG is operated continuously for a long period of time while output parameters including power, voltage, and current are tracked. To ensure stability during continuous operation, it is important to monitor any modifications or fluctuations in output performance over time

The TENG is put through numerous cycles of operations, including alternate contact and separation motions, in a cycling test. In order to guarantee constant performance over numerous cycles, the TENG's durability and stability against repetitive mechanical stress are being evaluated displayed in Figure 2.13.

2.6.12 Stability Test

During operating, TENGs are subjected to a range of temperatures [35]. The TENG will be exposed to a variety of temperatures as part of the temperature stability test, and its output response will be tracked. This test aids in determining how stable the TENG is under various heat conditions. Humidity has an impact on the efficiency and

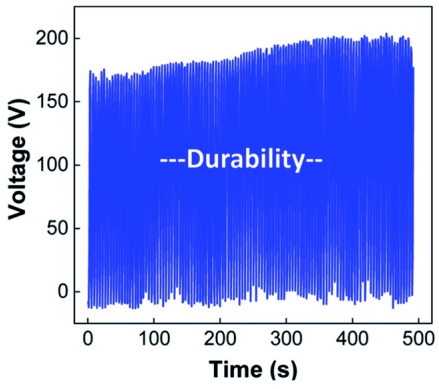

Figure 2.13: Stability Test.Reproduced from [37]

dependability of TENGs. The TENG is subjected to various amounts of humidity as part of the humidity stability test, and its output behaviour is evaluated. This test aids in determining the TENG's performance and stability under various moisture conditions [36].

2.6.13 Environmental Stress Testing

During environmental stress testing, the stability and dependability of the TENG are evaluated in the context of extreme environmental circumstances. These tests could involve putting the TENG through temperature changes, humidity changes, mechanical vibrations, or chemical exposure. The objective is to assess the stability of the TENG under plausible environmental situations.

2.6.14 Temperature Stability

TENG (Triboelectric Nanogenerator) devices entails subjecting TENG devices to controlled temperature fluctuations in order to evaluate their performance and dependability. The test is critical for understanding how TENG systems operate in various heat settings and assuring their efficacy and endurance in actual applications. Researchers and engineers may analyze how temperature affects the efficiency and stability of TENG devices by measuring electrical output and other key metrics during temperature cycling or steady-state circumstances. The findings of these tests are used to better design and deploy thermal management techniques to optimize TENGs for real-world conditions.

2.6.15 Performance Monitoring

It is essential to continuously check the TENG's performance metrics, including current, voltage, power, as well as frequency response, throughout the stability testing process. This enables measurement of stability by allowing for the recognition of a change or performance decline. Researchers can assess a TENG's long-term performance, pinpoint any flaws or failure mechanisms, and suggest design upgrades or optimization techniques to increase stability and dependability by carrying out these stability studies. To make inferences regarding the stability and longevity of TENG devices, it is crucial to carry out these tests methodically and record through data.

Below table 2.1 represents the comparison for the characterization of TENG in literature survey.

Table 2.1: Table of Waste Materials and Their Triboelectric Properties

S. no	Waste material	Opposite triboelectric layer	Voltage, Current, Power Density	Applications	Stability cycles	Ref
1	Polyvinyl chloride (PVC)	Nylon	31, 3.1 μA, 11.9 mW m^{-2}	Self-powered Morse code generator	10,000	[37]
2	Waste plastic bags	Polytetrafluoroethylene (PTFE)	251, 34.1 μA, 1.74 W m^{-2}	Self-powered pencil-on-paper strain sensor	—	[38]
3	Waste tea leaves and packaging bags	Polytetrafluoroethylene (PTFE)	792, 42.8 μA, 4.88 W m^{-2}	Powering electronic office supplies	10,000	[39]
4	Aloe vera	Polydimethylsiloxane (PDMS)	32, 0.11 μA, 1.9 mW m^{-2}	Self-powered finger monitoring sensor	2,500	[40]
5	Biowaste peanut shell	Polyethylene terephthalate (PET)	910, 104.5 μA, 5.33 W m^{-2}	Self-powered devices	—	[41]
6	Bio-waste sunflower husks	Polyethylene terephthalate (PET)	488, 28.5 μA, 0.48 W m^{-2}	Self-powered devices	—	[42]
7	Eggshell	Polytetrafluoroethylene (PTFE)	924, 1.3 μA, 0.25 W m^{-2}	Self-powered wristwatch	—	[43]
8	Bacterial cellulose	Teflon	57.6, 5.78 μA, 43 mW m^{-2}	—	1,000	[42]
9	Fish bladder film	Fluorinated ethylene propylene (FEP)	106, 7.3 μA, 200 mW m^{-2}	Smart electronic skin-based wearable electronics	850	[44]
10	Rice husks	Polytetrafluoroethylene (PTFE)	190, 1 μA, 0.12 W m^{-2}	Power source for LEDs	—	[45]
11	Rice paper	Polyvinyl chloride (PVC)	244, 6 μA, 376.4 mW m^{-2}	Power source for LEDs	10,000	[46]

Continued on the next page

S. no	Waste material	Opposite triboelectric layer	Voltage, Current, Power Density	Applications	Stability cycles	Ref
12	Aluminum recyclable paper (ARP) for electrodes	Pt/PET	3.12, 82.8 nA, 3.54 mW m^{-2}	—	—	[47]
13	Waste rubber powder	Aluminum	100, 5.5 mA m^{-2}, 68 mW m^{-2}	Self-powered electronics	5,000	[48]]
14	Fluorinated wasted rubber powder (WRP)	Aluminum	265, 75 mA m^{-2}, 4.6 W m^{-2}	Self-powered electronics	—	[48]
15	Recycled plastic bags	Nylon	35.7, 1.56 μA, 152.6 mW m^{-2}	Integration with supercapacitors for powering LEDs	—	[38]
16	Plastic waste and carbon-coated paper wipes	Polytetrafluoroethylene (PTFE)	3.5 μA, 0.24 W m^{-2}	9-Segment keyboard	1,000	[49]
17	Waste milk carton	Polyethylene (PE)	600, 40 μA, 55.9 mW m^{-2}	Power wireless sensor for environmental monitoring	65,000	[50]
18	Waste polystyrene	PTFE	250, 52 μA, 4.05 W m^{-2}	Vehicle speed monitoring sensor	20,000	[51]
19	Recycled plastic and electronic wastes	Chart paper	83.88, 101 μA, 265 mW m^{-2}	Self-powered portable electronics	5,000	[33]
20	Aseptic carton package	Oxidized low-density polyethylene	200, 400 nA, —	Power source for LEDs	97,000	[52]
21	Discarded plastic waste	PTFE	3.5 μA, 0.61 W m^{-2}	Self-powered keyboard and wearable electronics	—	[53]

Continued on the next page

S. no	Waste material	Opposite triboelectric layer	Voltage, Current, Power Density	Applications	Stability cycles	Ref
22	Surgical face mask	Waste Mylar	200, 0.29 mA m^{-2}, 71.16 mW m^{-2}	Self-powered watches and calculators	10,000	[54]
23	Nylon (polyamides)	PMMA	35.7, 5.85 μA, 152.6 mW m^{-2}	Antitheft warning device	3,000	[55]
24	Household plastic waste	PU foam	44, 289 nA, —	Self-powered LED display	3,000	[35]
25	Scrap paper	PTFE	205, 18 μA, —	Human physiological monitoring	1,100	[56]
26	X-ray sheets	Silicone	201, 62.8 μA, 1.39 W m^{-2}	Self-powered devices, force sensors, LEDs, and smart buildings	10,000	[57]

Chapter 3

Material Selection and Performance Comparison

This chapter focuses on the material selection for the TENG (Triboelectric Nanogenerator) device, with a focus on reusability and cost-effectiveness. It also includes measurements of voltage, current, stability, and other essential characteristics for nanogenerators within the TENG device. In addition, the chapter includes a description of the simulation procedure for the TENG device. The discussion provides basic knowledge on these subjects. This chapter divided into two contributions one is discussing with APPA (Al foil parafilm PDMS Al foil) and second one is discussing with comparison of different dielectric materials like OHP, PET and PMMA based on their surface roughness and compare those materials with COMSOL simulation study also.

3.1 Introduction

Materials having high positive and negative triboelectric characteristics are those with an increased capacity to gain as well as lose electrons when coming into contact other materials. Here are some materials that are often used in TENGs that have high positive and negative triboelectric properties [25].Choosing the right materials for the TENGs becomes crucial for maximizing their effectiveness and performance. Consideration of a number of elements and criteria is part of the material selection process. Consider the

following factors while choosing materials for TENGs:

Choosing materials with different triboelectric characteristics will maximize the creation of charge between contact and separation.Triboelectric effects typically manifest themselves more effectively in materials with drastically varying electronegativities or electron affinities. PTFE (polytetrafluoroethylene (PI) polyimide, PDMS(Polydimethylsiloxane), along with other metals are some examples of frequently used materials.

Charge and ion transfer, as well as material transfer, are critical processes in the operation of a Triboelectric Nanogenerator (TENG). TENGs generate electricity by using the triboelectric effect, which involves the transfer of charges between two materials due to their relative motion and contact.

Charge Transfer: Charge transfer is the primary mechanism in TENGs. Electrons transfer from one triboelectric material to the other when they come into contact and then separate. The first material becomes negatively charged (electron excess), while the second material becomes positively charged (electron deficiency). This charge separation results in an electric potential difference or voltage difference between the two materials, which can be used to generate electricity.

Ion Transfer: Like charge transfer, ion transfer can occur in TENGs. This is especially true in environments with high humidity or moisture present. Ion movement between materials can be caused by humidity, which contributes to the charge transfer process. TENG performance can be affected by ionic conductivity.

Material Transfer: Material particles can be transferred between two surfaces in a TENG due to physical contact and separation of materials. These material transfers may affect the triboelectric properties of the materials, thereby affecting the overall efficiency and durability of the TENG. Material transfer control is critical for maintaining consistent and dependable TENG performance.

$$V = -\frac{Q}{s}\,(d_0 + x(t) + \frac{\sigma x(t)}{\varepsilon_0} \tag{3.1}$$

3.1.1 Mechanical Flexibility

TENGs frequently need to be flexible in order to adapt to various materials or mechanical deformations. For continuous repetitive motion without significantly degrading performance, choose components that are mechanically flexible, stretchy, and resilient.Because of their flexibility, polymer-based materials like elastomers and thin films are frequently used.

3.1.2 Electrical Conductivity

Take into account the materials' electrical conductivity, particularly for the conductive electrode layers within TENGs. The electrodes should have minimal resistance and effectively transfer charges. Because of their high conductivity, the metals and conductive polymers like graphene, indium tin oxide (ITO), and silver nanowires are frequently used.

3.1.3 Surface Characteristics Materials

Triboelectric properties are influenced by their surface features. Contact area, surface friction, and charge transfer efficiency can be impacted by surface texture, topography, and chemical composition. To improve triboelectric performance, optimize material surfaces using processes like tiny structures, surface layers, or modification procedures. Consideration would give to the materials' long-term toughness and stability during use [25]. Analyze their resistance to chemical exposure, mechanical wear, deterioration, and environmental issues including humidity and temperature. High levels of stability and durability in materials guarantee dependable functioning over an extended length of time.

3.1.4 Cost and Availability

Take into account the materials' affordability and accessibility. For large-scale manufacture or the widespread use of TENG technology, pick materials that are readily available on the market, accessible, and economical.

Consider the compatibility of the chosen materials with the other TENG system

components, such as the surfaces, encapsulation materials, or linkages. To create a dependable and functioning TENG device, ensure adequate attachment, electrical insulation, and compatibility.

The choice of materials must take into account theoretical factors, experimental characterization, and optimization, it is crucial to emphasize. To validate and optimize material selections, it is imperative to conduct material compatibility studies, characterize their triboelectric properties, and assess their performance in TENG prototypes.

1.Charge producing layer: creates charge via triboelectric effects and electrostatic induction.

2. Charge acquiring layer: collects the charges created by the charge developing layer and transfers those into the external circuit.

3.Charge trapping layer: This layer prevents the charge from leakage or dissipate while they can be captured through the charge acquiring layer. PDMS has deeper charge traps. It boosted TENG's power density which by 178 times.

4.Charge storage layer: This stores the created charges till they are required by the external circuit.

3.2 Types of Materials

Material selection to improve TENG efficiency and effectiveness are described.

3.2.1 Metal Materials

Metal materials including silver (Ag) copper (Cu),as well as gold (Au), aluminum (Al), are often employed in TENG devices as triboelectric layers and electrodes. These metals have a wide range of triboelectric properties, electrical conductivities, along with mechanical strengths. Aluminum, for example, is recognized because of its lightweight and low cost, making it suited for certain a TENG applications, whereas gold has greater conductivity than other metals, making it a good choice of electrodes in outstanding

performance [58].

3.2.2 Organic Materials

Table 3.1: Dielectric Constants of Various Materials

Material	**Dielectric Constant (ε)**
Graphene	1 (low)
MoS_2 (Molybdenum Disulphide)	4-7
WS_2 (Tungsten Disulphide)	4-7
MXenes	10-20
PEG (Polyethylene Glycol)	47-60
PLA (Polylactic Acid)	3.2
PVA (Polyvinyl Alcohol)	1.3-1.7
PVC (Polyvinyl Chloride)	3.1-3.4
PMMA (Polymethyl Methacrylate)	2.9-3.4
FEP (Fluorinated Ethylene Propylene)	2.1-2.3
PVDF (Polyvinylidene Fluoride)	7.2-15.2
PU (Polyurethane)	3.1-3.4
Polycarbonate	2.8-3.1
Polyethylene	2.25-2.3
Polypropylene (PP)	2.2-2.3
PZT (Potassium Zirconate Titanate)	900
$BaTiO_3$ (Barium Titanate)	1200
$LiNbO_3$ (Lithium Niobate)	33
Al_2O_3 (Aluminum Oxide)	8.5
SiC (Silicon Carbide)	9.7-10.6
BN (Boron Nitride)	4

Nanocellulose

Cellulose nanofibrils (CNFs), as well as bacterial cellulose nanocrystals (BCNCs),cellulose nanocrystals (CNCs), Large surface area, excellent mechanical strength, as well as one-of-a-kind optical characteristics [59].

Microcellulose

MCC (microcrystalline cellulose) Cellulose that has been regenerated by dissolving cellulose fibers in a solvent, such as N-methylmorpholine N-oxide (NMMO), cellulose fibers made from carboxymethyl cellulose (CMC), hydroxyethyl cellulose, also known as (HEC), and methyl cellulose (MC). In food additives, medicines, and construction materials, to promote water retention and adhesion. Organic substances utilized in TENG as charge trapping and charge storage layers [60].

3.2.3 Inorganic 2D Materials

These have been attracting a lot attention in recent times because of their distinctive features and prospective uses in a variety of industries. the most commonly used inorganic 2D materials:

Graphene

Graphene comprises a single layer made of carbon atoms organized in a two-dimensional honeycomb lattice. It is well-known for its outstanding hardness, high electric and thermal conductive properties, and good optical characteristics [61]. Graphene is used throughout electronic devices, storing energy, sensors that are and composite materials and it's Dielectric Constant value is given in 3.1.

MoS_2 (Molybdenum Disulphide)

MoS2 represents a stacked materials having a structure that's similar to graphene, from the molybdenum and sulfur atoms. It has fascinating electrical along with opti-

cal characteristics along with is employed in electronics, optoelectronics, catalyst. WS2 (Tungsten Disulphide): WS2 is another transition metallic dichalcogenide (TMD) member. It, like MoS2, has a layered structure and unique features that make it useful for a wide range of applications such as lubricants, and sensors, and transistors [62].

MXenes

These are metal carbide particles, nitrides, or carbonitrides MXenes are a class of two-dimensional materials formed by selectively removing the "A" part of the layer of MAX phases (wherein M is a metal of transition, A represents a chemical element such as aluminum or silicon, which is and X contains carbon or nitrogen). Because of their programmable electronic properties, MXenes are interesting possibilities to supercapacitors with catalysts, as well as water purification [63]. Inorganic two-dimensional substances have changed nanomaterials and materials science. Researchers are constantly investigating their characteristics and developing novel synthesis processes in order to realize their full potential in a wide range of technical applications, including electronics and energy storage, as well as environmental cleanup and biomedical devices. We should expect even more intriguing discoveries and uses in the future when the area of 2D materials expands.

3.2.4 Polymer Materials

Because of their adaptability and customized features, chemically engineered polymers play an important role in a variety of sectors. Some of the most frequently utilized chemically modified polymers with their applications [64].

PEG

It is a type of water-soluble, biocompatible polymer that is widely utilized in medications, cosmetics, and food goods. It is an useful excipient for drug delivery systems because to its potential for improving drug solubility, rigidity, and lower toxicity [2].

PLA

comprises a biodegradable polymer made from renewable resources such as cornstarch or sugarcane. Because of its eco-friendliness, it is appropriate for a wide range of uses, such packaging materials, medical equipment, and biodegradable plastic [65].

PVA

(Polyvinyl Alcohol), PVA belongs to a water-soluble polymer with outstanding film-forming and adhesive characteristics It is utilized in a variety of sectors as an adhesive, coating, and releasing agent. It is utilized in a variety of sectors as an adhesive, coating, and releasing agent. PVC (Polyvinyl Chloride), it is a popular polymer that is noted by its robustness, chemical resistance, and adaptability. It is used to construct (pipes, window frames), the automobile sector, and a variety of consumer products [40].

Polymethyl Methacrylate (PMMA)

It serves as a transparent polymer with outstanding optical characteristics. It is also referred to as acrylic or plexiglass [66]. It's popular as lenses for visual, signage, medical gadgets, and architectural applications

Fluorinated Ethylene Propylene (FEP)

FEP is a fluoropolymer with excellent chemical resistance as well as low friction, and nonstick characteristics. It is utilized in wire the insulation, tubing, and nonstick cookware coatings [67].

Including the PVDF, PVA,PU, Polycarbonate, Polydime thylsiloxane, Polytetrafluoroethylene, Polyethylene , as well as Polypropylene (PP) play critical roles in TENG devices, operating as charge acquiring, trapping, and transporting materials Because of its flexibility and high surface charge retention, PDMS is widely used. TENG is commonly used to improve charge collection efficiency. Because of its relatively low surface-energy value and excellent dielectric characteristics, PTFE is also an excellent material of charge trap layers for TENG devices.

These chemically enhanced polymers have a diversified set of features and applications, resulting in them being critical materials in industries which include healthcare as well as construction through electronics and packaging. To address the changing requirements of technological advancement and sustainability, researchers continue to investigate novel changes and possible uses for these polymers.

3.2.5 Ceramic Materials

These are a different from the family of inorganic substances, non-metallic materials with a variety of qualities that make them useful for a variety of uses. Let's look at some of the most common ceramic materials:

Potassium Zirconate Titanate

PZT is a type of ferroelectric ceramic with piezoelectric characteristics. It's commonly utilized for actuators, sensors [68], as well as transducers for things like ultrasound machines, piezoelectric the engines, and inkjet printers.

Barium Titanate ($BaTiO_3$)

A ferroelectric ceramic substance with good dielectric characteristics is $BaTiO_3$. It is utilized in the manufacture of piezoelectric materials, as well as capacitors, sensors [69], and actuators.

Lithium Niobate ($LiNbO_3$)

Lithium Niobate ($LiNbO_3$) is a versatile ceramic that has excellent optical and piezo properties. It is used for electro-optical devices, telecommunications devices, and surface acoustic wave devices [70].

Aluminum Oxide (Al_2O_3)

Aluminum oxide, also known as alumina, is a high-performance ceramic widely used for its exceptional mechanical, thermal, and electrical properties [71]. It is used in cutting tools, wear-resistant components, electrical insulators, and as a substrate for electronic devices.

Silicon Carbide (SiC)

SiC is a high-temperature ceramic with excellent thermal and mechanical properties. It is used in power electronics, semiconductors [72], and abrasive applications like grinding and cutting tools.

Boron Nitride (BN):

BN is a ceramic material with exceptional thermal conductivity and high-temperature stability. It is used in applications where high thermal management is required, such as heat sinks, crucibles, and insulators in high-temperature environments. These ceramic materials offer a wide range of properties, including high hardness, electrical insulation, chemical inertness, and thermal stability [73]. Their applications span across various industries, including electronics, aerospace, automotive, medical devices, and energy production. The ongoing research and development in the field of ceramics continue to lead to new and innovative applications for these materials. Materials having high positive and negative triboelectric characteristics are those with an increased capacity to gain as well as lose electrons when coming into contact other materials listed in Figure 3.1

3.3 Triboelectric Characterization Equipment and Different Dielectric Materials

Characterization Instruments are used in the current thesis work studies to probe the structural, compositional, elemental, morphological, as well as surface work function properties of the different nanosheets and materials and Al substrate as well as other used

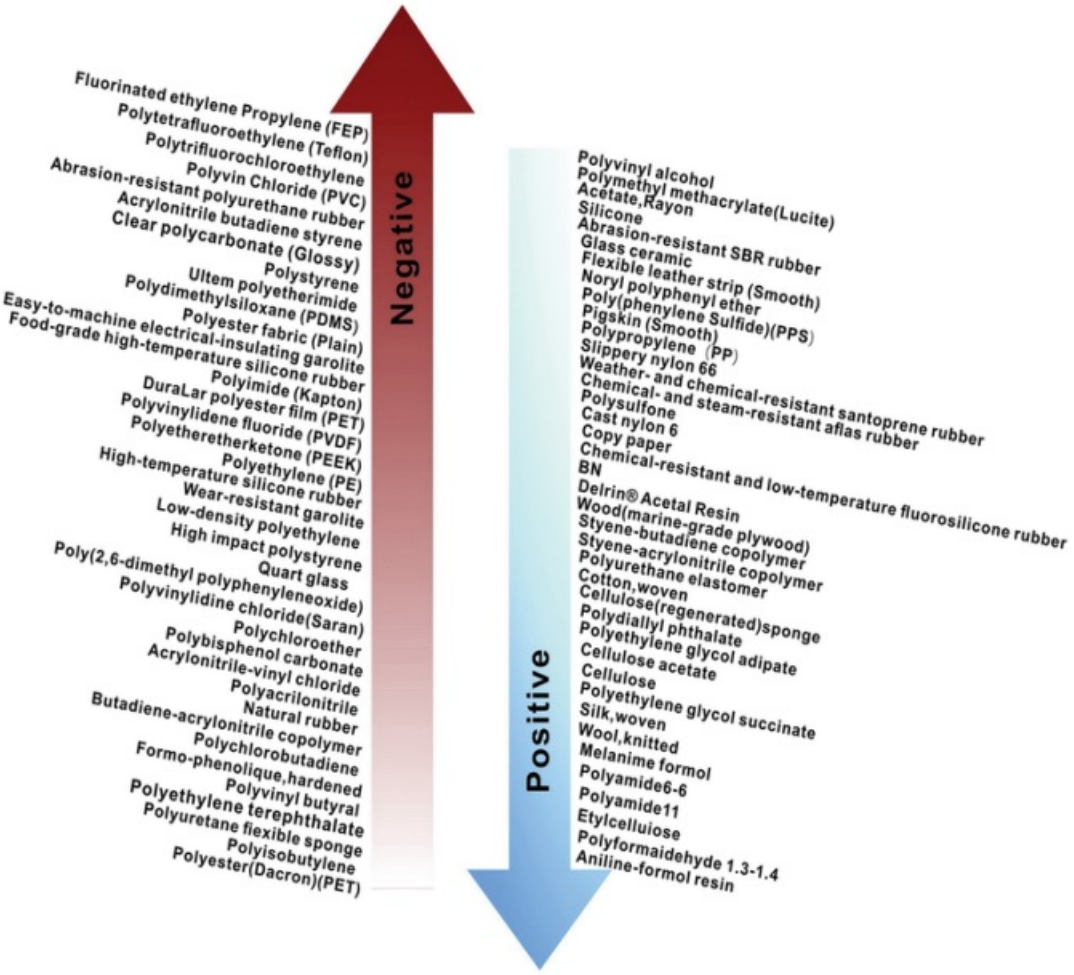

Figure 3.1: List of Triboelectric Pair.Reproduced from [8]

tribo layers. To evaluate Triboelectric Nanogenerators (TENGs), it's essential to measure their open circuit voltage (V_{OC}), short circuit current (I_{SC}), and current-voltage (I-V) characteristics. (V_{OC}) is determined by measuring voltage across the terminals with no external load. (I_{SC}) is measured by short-circuiting the terminals and recording the current. For I - V characteristics, connect the nanogenerator to varying load resistances and plot current vs. voltage. These measurements provide insights into the devices' electrical performance, aiding optimization and understanding their energy-harvesting capabilities. Multiple tests should be conducted to ensure result reliability and consistency.

3.3.1 Field-Emission Scanning Electron Microscopy

The scanning electron microscope (SEM) is a widely employed tool for high-resolution surface morphology analysis. It functions by directing an accelerated electron beam at a

sample's surface, leading to two key interactions: elastic and inelastic. Elastic interactions involve deflection of electrons by the sample's outer shell electrons, creating backscattered electrons (BSE) used for compositional and crystal structure analysis. Inelastic scattering transfers energy to the sample's atoms, exciting specimen electrons and generating secondary electrons (SE) that provide detailed surface imaging. SEM instruments consist of an electron gun, electromagnetic lenses, apertures for beam control, and specialized detectors. SEM's capacity for high-resolution imaging and compositional insight makes it indispensable in materials science, geology, biology, and other fields shown in Figure **??** The purpose of the SEM insturment is high resolution imaging, elemental analysis, and material characterisation.

The Tektronix DSO model TBS1102, a digital storage oscilloscope (DSO) developed by Tektronix, It has a 100 MHz bandwidth, a maximum real-time sampling rate of 2 GS/s (Giga-samples per second), and a record length of up to 2.5K points depict in Figure **??**.An oscilloscope's principal function is to graphically represent electrical waveforms, allowing users to monitor and analyse the amplitude, frequency, and other properties of electrical signals in real time.

The SR570 is a current preamplifier designed by Stanford Research Systems (SRS), a reputed maker of precision scientific equipment. The SR570 is especially developed for low-noise amplifiers and electrical current monitoring in a wide variety of applications Figure **??**. The SR570 current preamplifier has high sensitivity as well as performance, making it an excellent choice over research laboratories, colleges and universities, and industrial settings. It has a current gain of up to 108 V/A (volts per ampere), enabling for reliable and exact measurements of small current signals.The SR570 Current Preamplifier is intended to offer low-noise amplification of weak electrical currents, enabling precise measurement of small signals in a wide range of experimental and research applications.

An LCR meter is a precision instrument used in electronics and electrical engineering to measure the electrical parameters of passive components, namely inductance (L), capacitance (C), and resistance (R). It provides valuable information for characterizing and testing various components and circuits, helping ensure their proper functionality and performance depict in Figure **??**. Measuring the dielectric constant of aluminum (Al) foil, and parafilm is a crucial step in understanding its electrical properties.An LCR meter's

principal function is to precisely measure and characterise the electrical characteristics of passive electronic components such as inductors, capacitors, and resistors and also measuring the unkown dielectric constant of the dielectric material.

It use to measure the raw Material weight and can indirectly measure pressure when you know the force (weight) applied to a specific area. This relationship is commonly used in engineering, physics, and various practical applications where pressure and weight are interconnected. Relationship between weight and pressure, especially when dealing with objects in contact with a surface depict in Figure **??**. The relationship is described by the formula:

Pressure (P) = Force (F) / Area (A)

In this equation, pressure (P) is the force (F) exerted on a given area (A). When an object with weight (due to gravity) is placed on a surface, it exerts a force (its weight) on that surface.

3.3.2 COMSOL

To simulate TENGs output voltage, COMSOL Multiphysics software has been used. Figure 3.2 shows the electric potential distribution between two electrodes for TENG. COMSOL is a powerful Multiphysics simulation software used for modelling and analysing various physical phenomena. With COMSOL, users can create and solve mathematical models using finite element analysis (FEA), finite volume method (FVM), and other numerical techniques. The software covers a wide range of applications, including electrical, mechanical, chemical, and fluid dynamics simulations. It offers a user-friendly interface, extensive libraries of predefined models, and advanced customization options.

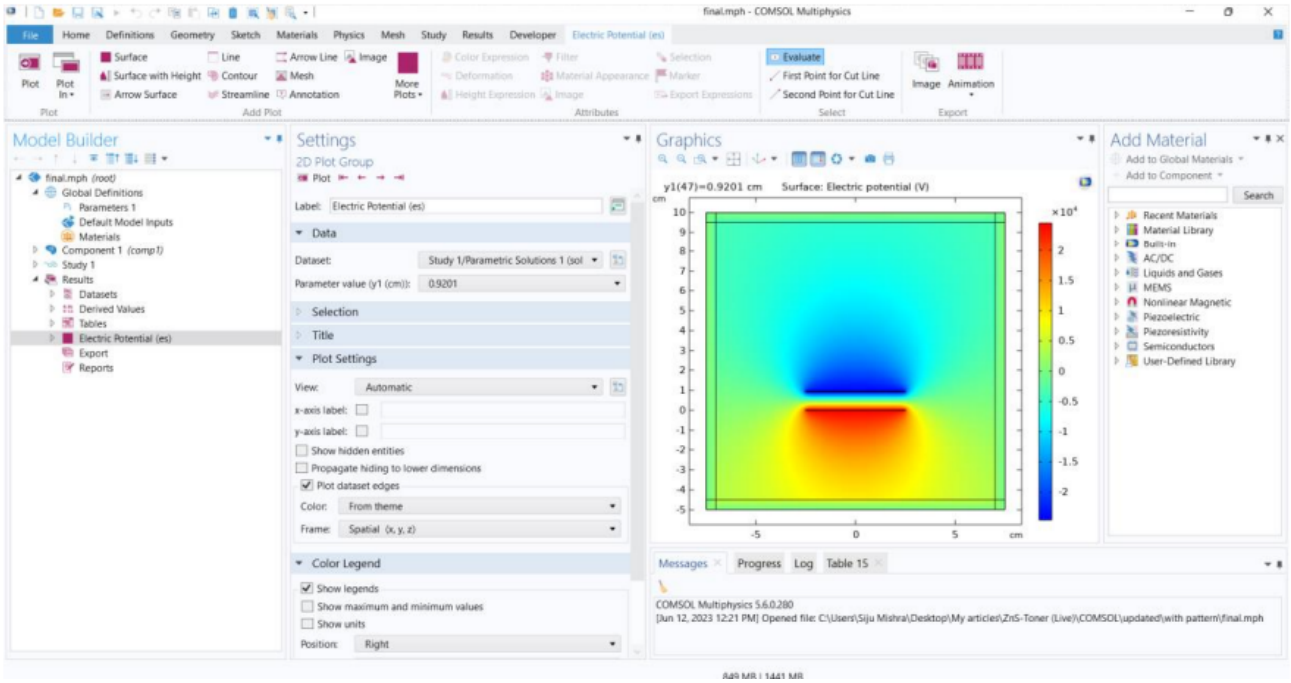

Figure 3.2: Electric Potential Distribution With COMSOL interface.

3.4 Work Function of Materials

3.5 Work Function of Materials

Work Function of two different materials is used in many different electronic applications, such as electron emission using in the field of emission devices, energy harvesting in TENG devices, and producing electricity from solar cells. To build and optimize the purpose of building and optimizing electronic devices, it is critical to comprehend the aspects affecting the work function and to use the proper measuring methodologies. Research is predicted to continue to develop materials science and nanotechnology, which will spur development across energy extraction, Electronic devices, and technologies for generating electricity from renewable sources. the workings of electrons at material surfaces. When a material comes into touch with another substance or is subjected to electromagnetic waves, the work function quantifies the energy necessary to extract one electron from its surface. The work function(Φ) is the minimum energy required to remove electrons from a material, often described as pulling them out of an "electron well" or energy barrier at the material's surfaces as well as the in order of the material Φ = Evacuation Fermi energy level (EF) Typically, the work function can be measured by electric field volts in

electron volts or joules (J).

The working function of two different materials is especially important in TENGs, as previously stated, use the triboelectric effect to transform energy from motion into electrical energy [74] . The transfer of charges occurs when two opposite substances that have distinct work functionalities come into contact and subsequently separate because of variations within their work functions Figure 3.3. This charge separation produces energy, which is able to be extracted and utilized for a variety of purposes.

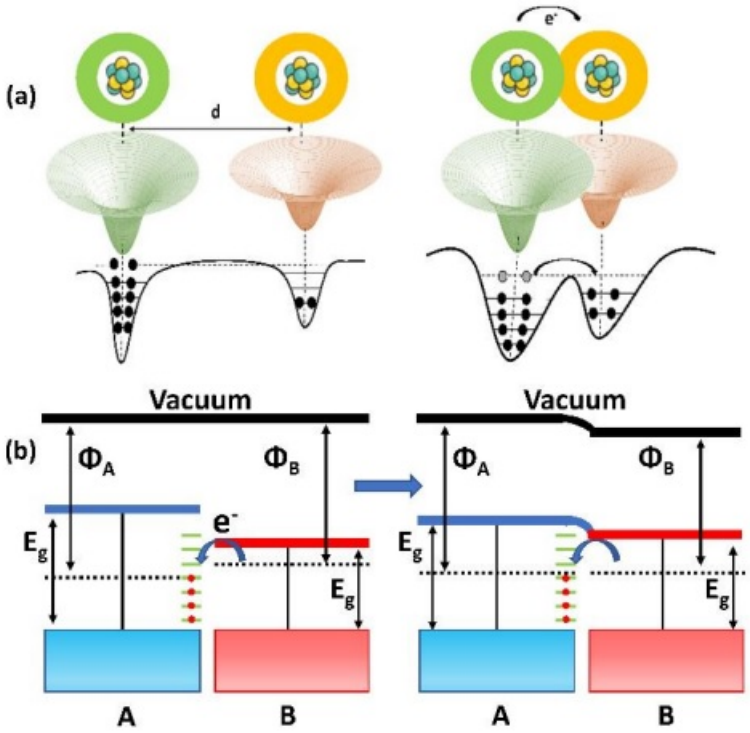

Figure 3.3: Contact Electrification based on (a) Potential Well Model, (b) Fermi Level Alignment Model.Reproduced from [2]

3.6 Elements Can Affect a Material's Work Function

Techniques for Measuring Work Function: Various experimental methods are employed to gauge the materials' work functions, such as:

a.Crystallographic Orientation: The variation in electron densities along various crystal directions, anisotropic materials' work functions can change with crystallographic orientation.

b. Surface Conditions: Surface conditions, such as adsorbents, pollutants, or surface treatments, can affect the work function by changing the surface's electrical characteristics.

c. The material's electronic structure: A material's electron distribution and energy band structure impacts how much energy is needed to extract one electron from it. Typically, materials at the Fermi level with higher electron densities and narrower band gaps have lower work functions.

d. Temperature: Thermal contraction effects and differences in electron distribution, a work associated with some materials can alter with temperature.

3.7 Methods for Measuring Work Function:

Techniques for Measuring Work Function: Various experimental methods are employed to gauge the materials' work functions, such as:

a. Ultraviolet Photoelectron Spectroscopy (UPS): UPS entails illuminating the sample with UV light and calculating the photoelectronic photons' kinetic energy. Afterward, the difference between photon energy and electron kinetic energy is used to calculate the work function.

b. Kelvin Probe: This technique measures the difference in contact potential between a materials that serves as a reference with an identified work function with the sample material, which enables the measurement of the work function of the sample.

c. Supplying an external electrical field:can change a material's work function, especially in instances with doped semiconductor products and metal-oxide surfaces.

3.8 Need for Waste Management

Resource recovery is the process of utilizing wastes as input to produce new, useful products. Reduced garbage production will lower the requirement for landfill space

and maximize the value that may be extracted from waste. The requirement to employ raw resources in the production process is postponed by resource recovery. Resources can be recovered from materials that include municipal solid trash, building, and demolition scrap, commercial garbage, and industrial waste in order to create new materials and goods. Waste materials that have value include plastic, paper, aluminum, glass, and metal. Resource recovery encompasses more than simply waste management [74] [75]. Resource recovery is a component of the circular economy, which minimizes the exploitation of natural resources and waste production and designs materials and goods more sustainably for toughness, reusability, reparability, remanufacturing, as well as recycling. It is possible to assess the potential for resource recovery of various treatment procedures using life-cycle analysis (LCA) shown in Figure 3.4.

3.9 Reusable Materials for Triboelectric Nanogenerator

Waste materials that have been investigated by researchers for use in TENGs. New waste materials could one day be discovered or used for energy harvesting because the sector is always developing. For waste material-based TENGs, waste/reused materials offer a variety of characteristics and prospective uses. The investigation of these materials for use in energy harvesting equipment is in line with sustainability and resource preservation objectives. There may yet be new wastes found and researched for TENG applications. Waste materials that have been investigated by researchers for use in TENGs. New waste materials could one day be discovered or used for energy harvesting because the sector is always developing.Various recycled/waste resources to create TENG devices. Triboelectric nanogenerators could be built from a variety of waste materials, each of which has special qualities that add to the triboelectric effect. Various waste products could be used in TENGs, including the following depict in Figure 3.5:

a. **Plastic Waste:** Because plastics have strong triboelectric characteristics, TENGs can make use of plastics like PET bottles, polyethylene, and polypropylene. There is a lot of plastic waste, which makes up a sizable fraction of the worldwide waste stream.

Figure 3.4: Waste materials used in TENG. Adapted from [43]

b. **Paper Waste:** Used paper waste, including as cardboard, newspapers, and magazines, can be used in TENGs as a triboelectric material. A paper's surface texture can increase friction and increase energy production. [46]

c. **Textile scraps:** TENGs can incorporate used or waste fabrics including cotton, polyester, or wool [76]. Fabrics frequently contain a variety of surface characteristics that enable efficient triboelectric charging.

d. **Rubber Waste:** Rubber waste, such as used tires, rubber gloves, and shoe bottoms, can be recycled into TENGs. When rubber comes into touch with different materials,

Figure 3.5: Representation from Reusable Waste to Green Energy.

there are noticeable triboelectric effects [48].

e. Electronic waste: Electronic components and Circuit boards other can be utilized in the construction of TENG. Triboelectric couples can be effectively created in e-waste by combining metal and non-metal parts [49].

f. **Organic Waste:** Biodegradable materials or organic debris, such as vegetable scraps or fruit peels, can be used in TENGs. These substances may exhibit intriguing triboelectric properties, particularly when mixed with other wastes [77].

g. **Nutshell Waste TENG:** This type of TENG is built from waste nutshells from nuts for example almonds, walnuts, or pistachios. Nutshells are environmentally benign and can have natural triboelectric capabilities [77].

h. **Metal scraps:** TENG buildings can make use of leftover metal fragments or metallic debris. Because of their high conductivity, metal materials can function as one among the triboelectric layers.

i. **Ceramic waste:** Scraps of ceramics can be used in TENGs, expanding the variety of triboelectric pairings that are conceivable.

j. **Leather waste:**Utilizing waste leather to create mechanical flexibility as well as energy

harvesting within TENG devices.

k. **Coconut Shell Waste:** Coconut Shell Waste material TENG: Utilizes waste from coconuts as a part of TENGs, which can offer sustainable and natural triboelectric qualities [78] .

l. **wasted silk:** Utilizing the special triboelectric characteristics of silk, silk waste TENGs use wasted silk materials to be dielectric layers [79].

m. **Eggshell Waste TENG:**This type of TENG is made of Egg shell waste after using the Egg [41].

n. **Feathers Waste TENG:** This type of TENG makes use of leftover feathers,

o. **Fish Gelatin Waste :** which are a byproduct from the fish processing industry, are incorporated into TENGs for environmentally friendly energy collecting [80].

Table 3.2: Table of Waste Materials and Their Triboelectric Properties

S. no	Waste material	Opposite triboelectric layer	Voltage, Current, Power Density	Applications	Stability cycles	Ref
1	Polyvinyl chloride (PVC)	Nylon	31, 3.1 μA, 11.9 mW m^{-2}	Self-powered Morse code generator	10,000	[37]
2	Waste plastic bags	Polytetrafluoroethylene (PTFE)	251, 34.1 μA, 1.74 W m^{-2}	Self-powered pencil-on-paper strain sensor	—	[38]
3	Waste tea leaves and packaging bags	Polytetrafluoroethylene (PTFE)	792, 42.8 μA, 4.88 W m^{-2}	Powering electronic office supplies	10,000	[39]
4	Aloe vera	Polydimethylsiloxane (PDMS)	32, 0.11 μA, 1.9 mW m^{-2}	Self-powered finger monitoring sensor	2,500	[40]
5	Biowaste peanut shell	Polyethylene terephthalate (PET)	910, 104.5 μA, 5.33 W m^{-2}	Self-powered devices	—	[41]

Continued on the next page

S. no	Waste material	Opposite triboelectric layer	Voltage, Current, Power Density	Applications	Stability cycles	Ref
6	Bio-waste sunflower husks	Polyethylene terephthalate (PET)	488, 28.5 μA, 0.48 W m^{-2}	Self-powered devices	—	[42]
7	Eggshell	Polytetrafluoroethylene (PTFE)	924, 1.3 μA, 0.25 W m^{-2}	Self-powered wristwatch	—	[43]
8	Bacterial cellulose	Teflon	57.6, 5.78 μA, 43 mW m^{-2}	—	1,000	[42]
9	Fish bladder film	Fluorinated ethylene propylene (FEP)	106, 7.3 μA, 200 mW m^{-2}	Smart electronic skin-based wearable electronics	850	[44]
10	Rice husks	Polytetrafluoroethylene (PTFE)	190, 1 μA, 0.12 W m^{-2}	Power source for LEDs	—	[45]
11	Rice paper	Polyvinyl chloride (PVC)	244, 6 μA, 376.4 mW m^{-2}	Power source for LEDs	10,000	[46]
12	Aluminum recyclable paper (ARP) for electrodes	Pt/PET	3.12, 82.8 nA, 3.54 mW m^{-2}	—	—	[47]
13	Waste rubber powder	Aluminum	100, 5.5 mA m^{-2}, 68 mW m^{-2}	Self-powered electronics	5,000	[48]]
14	Fluorinated wasted rubber powder (WRP)	Aluminum	265, 75 mA m^{-2}, 4.6 W m^{-2}	Self-powered electronics	—	[48]
15	Recycled plastic bags	Nylon	35.7, 1.56 μA, 152.6 mW m^{-2}	Integration with supercapacitors for powering LEDs	—	[38]
16	Plastic waste and carbon-coated paper wipes	Polytetrafluoroethylene (PTFE)	3.5 μA, 0.24 W m^{-2}	9-Segment keyboard	1,000	[49]

Continued on the next page

S. no	Waste material	Opposite triboelectric layer	Voltage, Current, Power Density	Applications	Stability cycles	Ref
17	Waste milk carton	Polyethylene (PE)	600, 40 μA, 55.9 mW m^{-2}	Power wireless sensor for environmental monitoring	65,000	[50]
18	Waste polystyrene	PTFE	250, 52 μA, 4.05 W m^{-2}	Vehicle speed monitoring sensor	20,000	[51]
19	Recycled plastic and electronic wastes	Chart paper	83.88, 101 μA, 265 mW m^{-2}	Self-powered portable electronics	5,000	[33]
20	Aseptic carton package	Oxidized low-density polyethylene	200, 400 nA, —	Power source for LEDs	97,000	[52]
21	Discarded plastic waste	PTFE	3.5 μA, 0.61 W m^{-2}	Self-powered keyboard and wearable electronics	—	[53]
22	Surgical face mask	Waste Mylar	200, 0.29 mA m^{-2}, 71.16 mW m^{-2}	Self-powered watches and calculators	10,000	[54]
23	Nylon (polyamides)	PMMA	35.7, 5.85 μA, 152.6 mW m^{-2}	Antitheft warning device	3,000	[55]
24	Household plastic waste	PU foam	44, 289 nA, —	Self-powered LED display	3,000	[35]
25	Scrap paper	PTFE	205, 18 μA, —	Human physiological monitoring	1,100	[56]
26	X-ray sheets	Silicone	201, 62.8 μA, 1.39 W m^{-2}	Self-powered devices, force sensors, LEDs, and smart buildings	10,000	[57]

3.10 A Triboelectric Nanogenerator Based on PDMS and Parafilm For Biomechanical Energy Harvesting

Technology is rapidly developing, so is the lifestyle of human society and the economy. As a result, there has been an unexceptional pick in environmental pollution like sound pollution, air & water pollution [81, 82]. Furthermore, non- renewable energy supplies such as natural gas, coal, and oil are steadily depleting. Most wearable and portable electronic devices are powered up by small replaceable chemical batteries, which also need frequent replacement. Battery replacement entails both hazards and large costs in the context of implanted medical devices. Furthermore, the chemical makeup of these batteries causes some damage to both the human body and the environment.Therefore, energy harvesting plays a significant role in reducing environmental pollution and find an alternate energy source for non- renewable energy. Various techniques such as electromagnetic induction, thermoelectric effects, piezoelectric effect, triboelectric effect, electrochemical reactions, and photoelectric effects were adapted to extract renewable energy from different sources. These techniques are helping to maintain the equilibrium between humans and nature, at the same time achieving rapid development. Mechanical energy proved itself as one of the best choices for the source from all renewable sources. The reason behind the success of mechanical energy is that it is available universally and also on a huge scale. It can be found in human body motions, vehicle motion, natural resources like air, water [83]. Among all, the triboelectric nanogenerator (TENG) technology best to harvest all types of mechanical energy. TENG is an exceptional and excellent approach that works on triboelectrification and electrostatic induction for mechanical energy harvesting [66]. Many applications were explored, such as charging energy storing devices, powering up mobile electronic devices, and self-powered sensors using TENG [84, 85, 86]. TENG is the breakthrough in the evolution of energy technology.

Commonly there are four discrete modes of operation followed and developed for energy harvesting. Triboelectric nanogenerators can operate flexibly with the help of these methods. These modes are CS, sliding, SE, and FS modes [87]. In this article, we are reporting TENG based on Polydimethylsiloxane (PDMS) and parafilm as dielectric

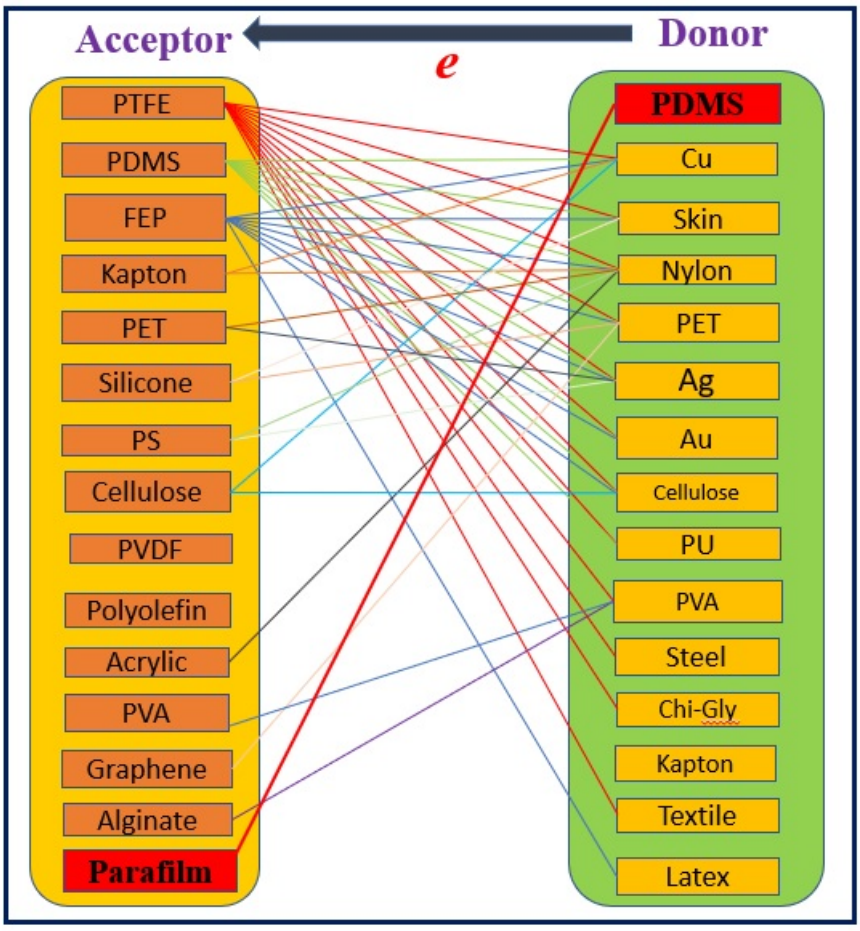

Figure 3.6: List of Triboelectric Series with Present Work.

materials for the first time. To the best of our knowledge, there are no reports on the usage of PDMS and parafilm as tribo-pair for the TENG fabrication. Previously, we have reported TENG based on aluminium foil and laboratory parafilm [88]. A large number of triboelectric pairs have been investigated for energy harvesting and proven for possible practical uses are listed in the Figure 3.6 [89, 90]. With our new design, a large improvement in the output response from ∼1 V to ∼8 V was observed for the 5 x 5 cm^2 TENG device. In this Contribution, a triboelectric nanogenerator is fabricated using parafilm, polydimethylsiloxane (PDMS) films for the first time. The fabricated TENG has been used for low- frequency mechanical energy harvesting to drive wearable and low-power electronic gadgets. The parafilm and PDMS layers act as triboelectric layers, and packaging aluminium foil acts as conducting electrodes. A flexible TENG with a dimension of 5 x 5 cm^2 generated an output voltage ∼8 V and output power of 20.25 µW at the applied load of 1 MΩ. Further, TENG was explored for switching on several LEDs. The current report presents a simple and cost-effective method for fabricating TENG and

can be used for self-powered device applications.

3.10.1 Experimental Setup

Initially, PDMS films of thickness ∼ 250 µm were prepared with the required dimension. Then, the self- standing PDMS films were prepared using elastomer and curing agent (10:1), similar to the reported literature [91]. Next, the laboratory parafilm of thickness ∼ 180 µm was taken with the required dimensions. The conducting side of the aluminium packaging films (total thickness ∼ 135 µm) were used as two conducting electrodes for TENG, as shown in Figure 3.7.

Figure 3.7: Basic Materials (a) PDMS (b) Laboratory parafilm (c) Aluminium foil.

The PDMS and parafilm were attached to the aluminium foils and further attached to acrylic sheets base supports. The sponge spacers were placed at four corners between the two acrylic base sheets to provide space for vertical movement and the separation of tribo-layers. The distance between two dielectric materials was ∼ 1.5 cm generated with spacers. (Sponge as spacer). The contact area of the TENG is 5 x 5 cm^2. Two connections from aluminium were connected to the oscilloscope to measure the output response of the TENG. The TENG response was recorded against repeated hand tapping with the help of Tekvisa software [91, 92] . The above figure 3.12 represents the basic starting materials which are used for the designing of the sensor.

Figure 3.8 represents the SEM and EDAX of aluminium foil and surface of the aluminium foil is smooth which is observed from the figure 3.13 (a) and from the EDAX we confirmed that aluminium content is present in the corresponding foil.

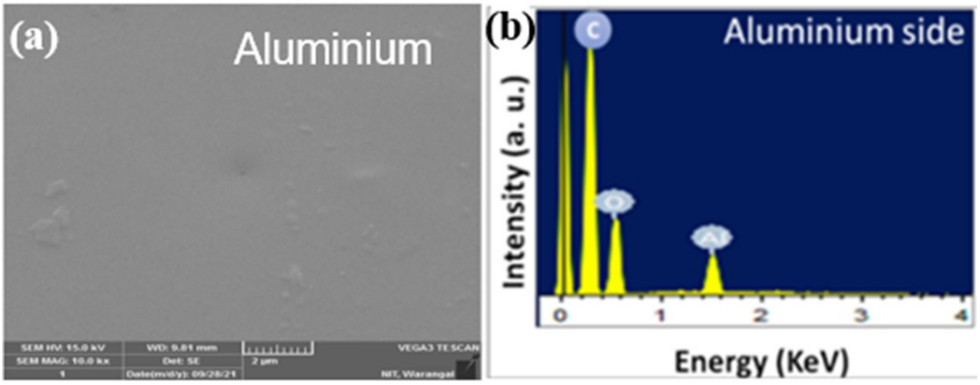

Figure 3.8: (a) SEM Image of Aluminum Foil (b) EDAX of Aluminum Foil.

3.10.2 Results and Discussion

The Figure 3.9 represents the working principle of the TENG. At the beginning as shown in figure PDMS and parafilm are separated by specified distance and there is no charge is not passed through them. In the above TENG PDMS and parafilm are acting as the dielectric materials, PDMS is the High negative triboelectric polymer and parafilm act as the medium positive tribo layer. When the two dielectric materials are completely contact to each other without no space as shown in Figure 3.9 exchange of charges will takes place. The charges from two dielectric materials will be assigned to the food packaging aluminium foils as shown in Figure 3.9. Figure 3.10 represents the fabrication steps involved for the TENG device using PDMS and parafilm. The open circuit output voltage of the TENG in response to continuous hand tapping is seen in the first half of Figure 3.16 (b). For all of the hand palming a steady output voltage of 8 V is recorded. Reversing the connections to the measuring device was also used to perform the switching polarity test.

The switching polarity test result is shown in the second half of Figure 3.16 (b). As shown in Figure 3.16 (b), the output of the TENG has shown exactly opposite responses upon reversing the connections. Thus, the switching polarity test confirms that output voltage is only from the TENG, not the instrumental noise [92, 34].The output voltage generated from the present TENG is very much higher than the previously reported TENG based on parafilm of similar dimension [86]. With the addition of PDMS to the new design, the output voltage of the current TENG device increased dramatically from 1V to 8V. In order to calculate the power density of TENG, the output voltage

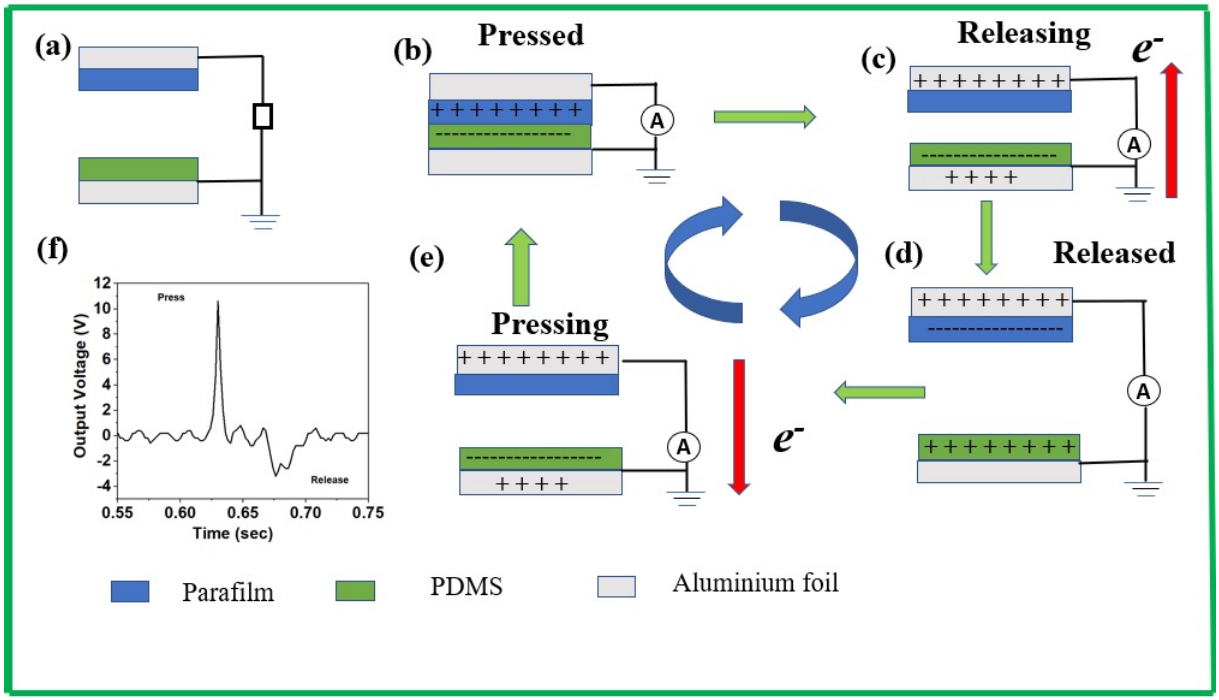

Figure 3.9: (a) – (e) Working Mechanism of TENG (f) Expanded View of One Cycle.

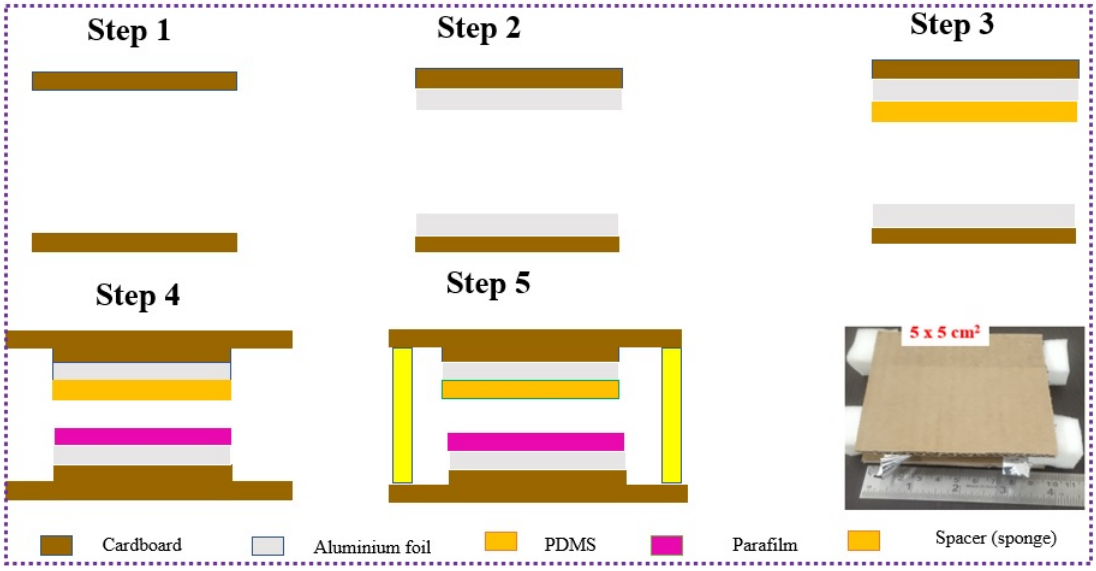

Figure 3.10: TENG Fabrication Procedures Using Parafilm and PDMS.

was measured across different load resistances in the range of 20 KΩ -100 MΩ under continuous hand palming. Figure 3.16 (c) depicts the TENG's load characteristics (c). When the load resistance was raised, the output voltage climbed and eventually settled at around 8 V. At greater resistance (100 MΩ), the output saturation voltage is roughly equivalent to the highest output voltage which is equal to forward voltage generated by the sensor [93, 94, 95]. TENG's predicted output power density as a function of varied

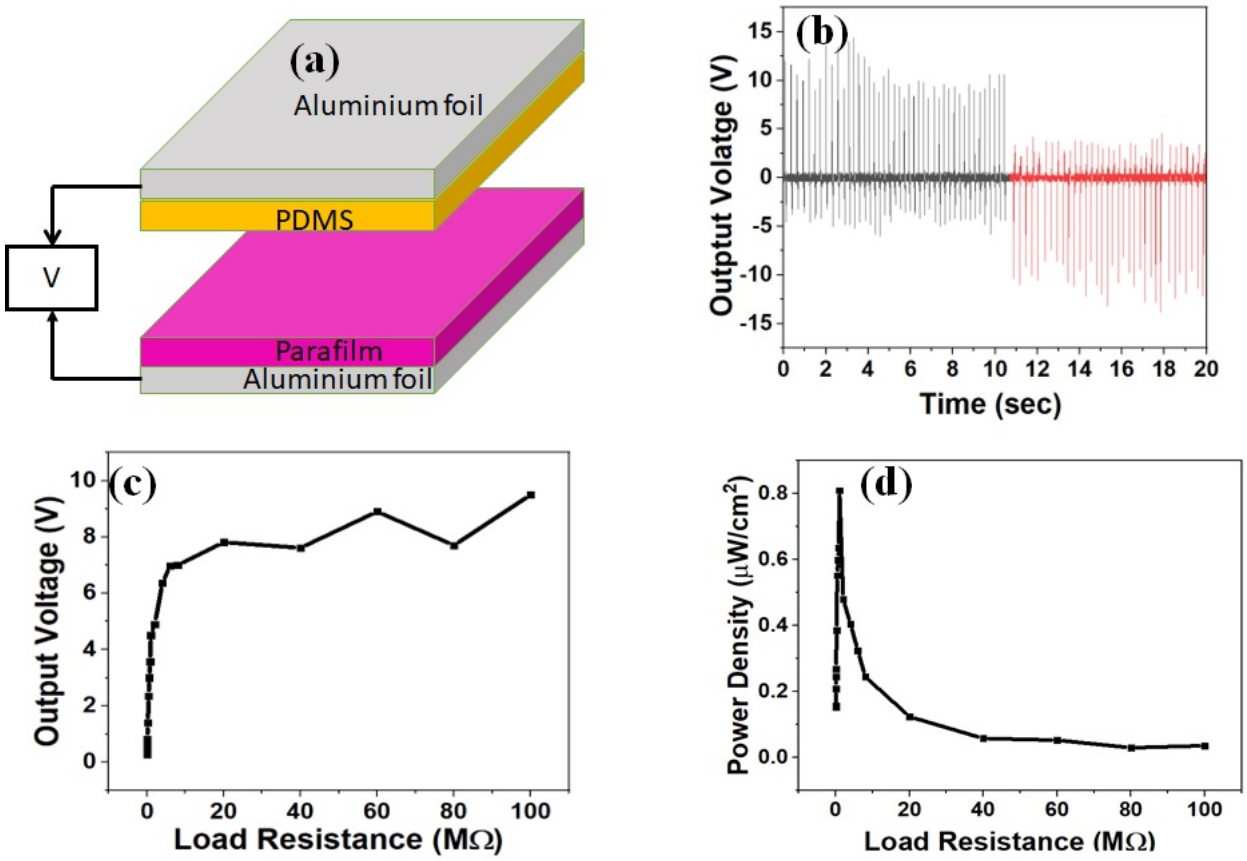

Figure 3.11: (a) Illustrative of TENG device (b) TENG output voltage in open circuit under forward and reverse connections, (c) Load Characterization of TENG, (d) Power Density of TENG.

load resistances is shown in Figure 3.16 (d). The maximum output power density of 0.81 W/cm^2, at a load resistance of 1 MΩ, was recorded. TENG output voltage needs to be

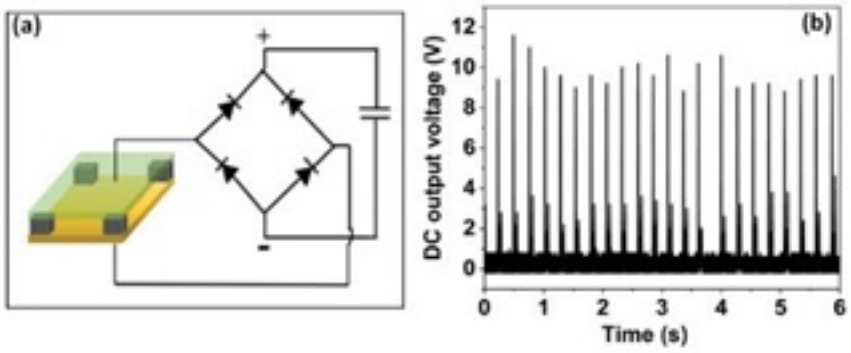

Figure 3.12: (a) Representation of DC output characteristic of the TENG with Rectifier (b) Rectified Voltage of the TENG.

rectified in order to power portable electronic devices. figure 3.17 (a) represents the block

diagram of the dc conversion process from TENG using IC bridge rectifier, and rectified output can be stored in a supercapacitor. Figure 3.17 (b) shows the TENG's rectified output voltage following the rectification procedure. Further, TENG was able to turn on the four commercial LEDs directly without using any storage element.

3.11 Triboelectric Nanogenerator Based on Different Polymers: Experimental and Simulation Study

3.11.1 Introduction

The present and future goals would be to deploy a range of sensors, including but not limited to gas, chemical, biological, motion, and navigation, to improve the functionality of electronics that are already in use. Many attempts are being undertaken to create devices that are far smaller than the size of a mobile phone many electronic gadgets that serve various human needs can be adopted including real time sensing. These small-sized electronic gadgets are in general operated on ultralow-power levels which provides us with an opportunity to power them by harvesting energy from our living environment. A sustainable power source capable of harvesting energy from the environment can be seen as one of the possible solutions to the problem mentioned. Thus, there is a need for nano energy and dependent power sources which are available, efficient, and stable [96]. Triboelectric Nanogenerator (TENG) is a new type of technology, first demonstrated in 2012 by Prof. Zhong Lin Wang's group at the Georgia Institute of Technology [13, 97]. Working in conjunction with the triboelectric effect and electrostatic induction, it is an energy harvesting device that converts tiny amounts mechanical energy into electrical energy. TENG has a wide range of applications due to its ability to produce a significant power response to drive wearable sensing devices. The literature evaluation of various Waste TENGs described based on various waste materials is shown in Table.1. Materials from bio-waste and common household trash are mixed together. Poly vinyl chloride [37] , food package covers [88] and plastic bags [60] are examples of household wastage. Biocompatible [69, 65],flexible [98] and nanoparticles [99] are also used for electrodes in the usage of electrodes.

For energy harvesting, four distinct modes of operation are often used and developed. Among those four modes contact separation (CS) mode a convenient method and less complexity in design process so, CS mode is popular in real time energy harvesting. TENG can be operated with different polymers such as PET, PTFE, PMMA, PDMS, OHP etc., In the fabrication process of TENG different types of electrodes are used such as Al, Cu, Ni, Ti etc., but for reducing cost and reusable concept food packaging Al foils are used as electrodes in this manuscript. In this paper three designs are used namely 1. AOA (Al foil OHP Al foil), 2. APA (Al foil PET Al foil) and 3. APMA (Al foil PMMA Al foil). We have previously discussed TENG, which uses PET food packaging cover surfaces, electroplated aluminium surfaces [100], and laboratory parafilm as tribo-layers [88]. Several triboelectric pairings that have been researched for energy harvesting and demonstrated for potential practical applications [89, 90]. In the present contribution food packaging Al foils (FPAF) are act as electrodes and three different polymers PET, OHP and PMMA acting as dielectrics. Our new design significantly improves the output responsiveness at 6 V, 5 V, and 25 V respectively for 5 x 5 cm^2 device (contact area). In this study, triboelectric nanogenerators are fabricated using a variety of polymers, including PET, PMMA, and OHP sheets. Packaging aluminum foil functions as conducting electrode, while the PET, OHP, and PMMA act as triboelectric layers in the design. A flexible TENG with a 5 x 5 cm^2 surface area produced an output voltage between 6 V(AOA), 5 V (APA) and 25 V (APMMA). The current work provides a simple and cost-effective method for creating TENG structure, which may be employed for applications involving self-powered devices. By using FEM analysis also for the three TENG structures obtained output response is higher for PMMA used as the dielectric in the TENG i.e. (APMMA), in the same way in practical designed TENG structures also APPMA structure is giving higher response compared to remaining to structures.Furthermore, the built APMA structured TENG was capable of turning on the 19 commercial LEDs.

3.11.2 MATERIALS AND EXPERIMENT PROCESS

Initially, the polymers OHP, PET and PMMA sheets were obtained from the local market and the sheets thickness as follows $\sim$ 49.9 µm, $\sim$ 99.8 µm and $\sim$ 345.31 µm respectively shown in Figure 3.18 (b, d, e). The conducting side of FPAF thickness ($\sim$

Table 3.3: Literature Review of Waste Materials used for TENGs Fabrication and their Electrical Characteristics

S.No.	**Waste material**	**Opposite triboelectric Layer**	**Output Voltage, current and Power Density**	**Ref.**
1	Poly vinyl chloride (PVC)	Nylon	31 V, 3.1 µA and 11.9 mW/m^2	[65]
2	Waste food packaging Al foils	Parafilm	4 V and 118 µW/m^2	[101]
3	Al Recyclable Paper	PET	3.12 V 82.8 nA and 3.54 mW/m^2	[88]
4	Recycled Plastic bags	Nylon	35.7 V 1.56 µA and 152.6 mW/m^2	[60]
5	Aloe Vera	Poly dimethylsiloxane (PDMS)	32 V and 0.11 µA and 1.9 mW/m^2	[102]
6	Bacterial cellulose	Teflon	57.6 V, 5.78 µA and 43 mW/m^2	[99]
7	Plastic waste and paper wipes	PTFE	3.5 µA and power of 0.24 W/m^2	[37]
8	Waste Rubber powder	Al	100 V, 5.5 mA/m^2 and 68 mW/m^2	[47]
9	**Waste food Packaging Al foils**	**OHP, PET, PMMA**	**6 V, 5V, 25 V and 0.12 µW/cm^2, 0.1 µW/cm^2, and 3 µW/cm^2**	**Present Work**

135 µm) acts as electrodes for the TENG. Figure 3.18 (a, c, e) represents the SEM images of the three polymers OHP, PET and PMMA respectively and the surfaces of PMMA is rough compared to that of remaining two polymers. Three polymers — OHP, PET, and PMMA — act as tribo negative layers when they are taken separately and connected to aluminium foils and then further bonded to the base supports of acrylic sheets. The schematic of the three TENG designs are seen Figure 3.14

The sponge spacers were positioned at four corners between the two acrylic base sheets to allow for vertical mobility and the separation of tribo-layers. With spacers, a

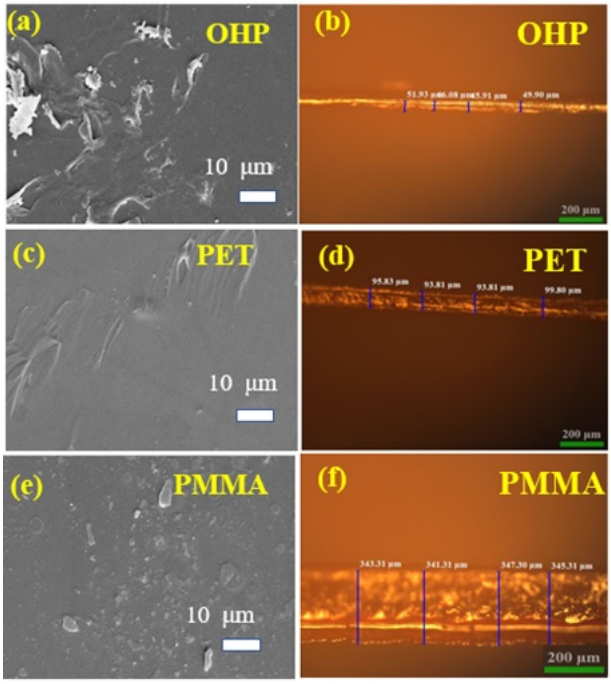

Figure 3.13: (a, c, e) SEM Images of OHP, PET and PMMA sheets, (b, d, f) Thickness Images of OHP, PET, PMMA sheets.

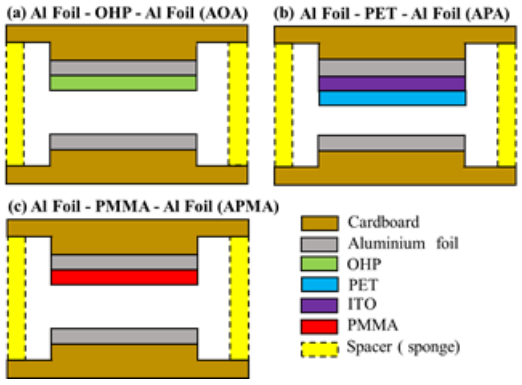

Figure 3.14: (a - c) TENG Structures (AOA, APA, APMA) using the OHP, ITO coated PET and PMMA Dielectrics.

gap of around 1.5 cm was created between dielectric material and electrode, sponge as a separator. The TENG has a 5 x 5 cm^2 contact area. In order to gauge the TENG's output responsiveness, two aluminium connectors were made and linked to an oscilloscope [91, 103]. With the use of the Tekvisa software, the TENG response to repetitive hand tapping was captured.

Parameters Selection for simulation of FEM analysis

Table 3.2 represents type of electrodes used, three different polymers (OHP, PET and

PMMA) dielectric values and thicknesses of Dielectrics and electrodes and the surface charge density given to the dielectric given to the TENG device in FEM analysis.

Steps involved in FEM Analysis to design TENG:

Step 1: select electrostatics from AC/DC module. Step 2: Design TENG model from 2D geometrics and add materials from library. Step 3: Add surface boundary conditions Step 4: Meshing Step 5: Add stationary study, Extract the results from derived values.

Table 3.4: Parameters used for FEM simulation for OHP, PET, and PMMA

Structure Component	**Parameter Utilized**	**Parameter Utilized**	**Parameter Utilized**
Electrode 1	Al	Al	Al
Electrode 2	Al	Al	Al
Charge density	8x10$^{-6}C/m^2$	8x10$^{-6}C/m^2$	8x10$^{-6}C/m^2$
Dielectric Constant	1.4 (OHP)	1.5 (PET)	4.9 (PMMA)
Length	5 cm	5 cm	5 cm
Width	5 cm	5 cm	5 cm
Thickness of electrodes	130 µm	130 µm	130 µm
Thickness of dielectrics	50 µm	100 µm	341 µm

3.11.3 Results and Discussion

Figure 3.15 shows the TENG's responses (Voc, Isc) are open circuit output voltage and short circuit current in response to repeated hand tapping. A consistent output voltage of 6 V, 5 V and 10 V is noted for every hand palming for three polymers used individually for three different designs AOA, APA and APPA respectively. The short circuit currents are of the polymers 3 A, 1.7 A and 20 A respectively. The switching polarity test was also carried out by switching the connections to the measurement apparatus. FigUre 3.20 (a, c, e) displays the results of the switching polarity test. When the connections were reversed, the output of the TENG displayed exactly opposite response, as seen in Figure 3.20 (a, c, e). The switching polarity test thereby verifies that the output voltage is only from the TENG and not from instrument noise. The obtained output power

density of TENG is shown in Figure 3.16 as a function of different load resistances. The maximum output power densities were 0.12 W /cm^2, 0.1 W/cm^2, and 3.4 W/cm^2 for load resistances of 1 MΩ, 2 MΩ, and 1 MΩ.

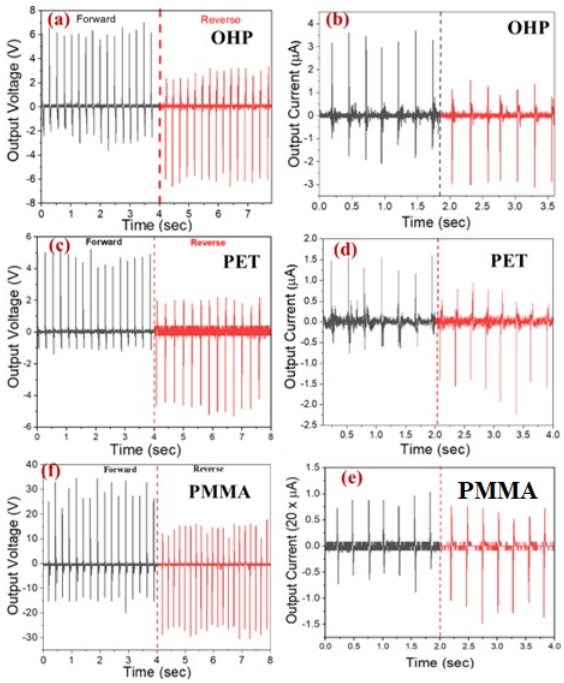

Figure 3.15: (a, c, e) - Voc and (b, d, f) – Isc of AOA, APA, APMA TENG Structures .

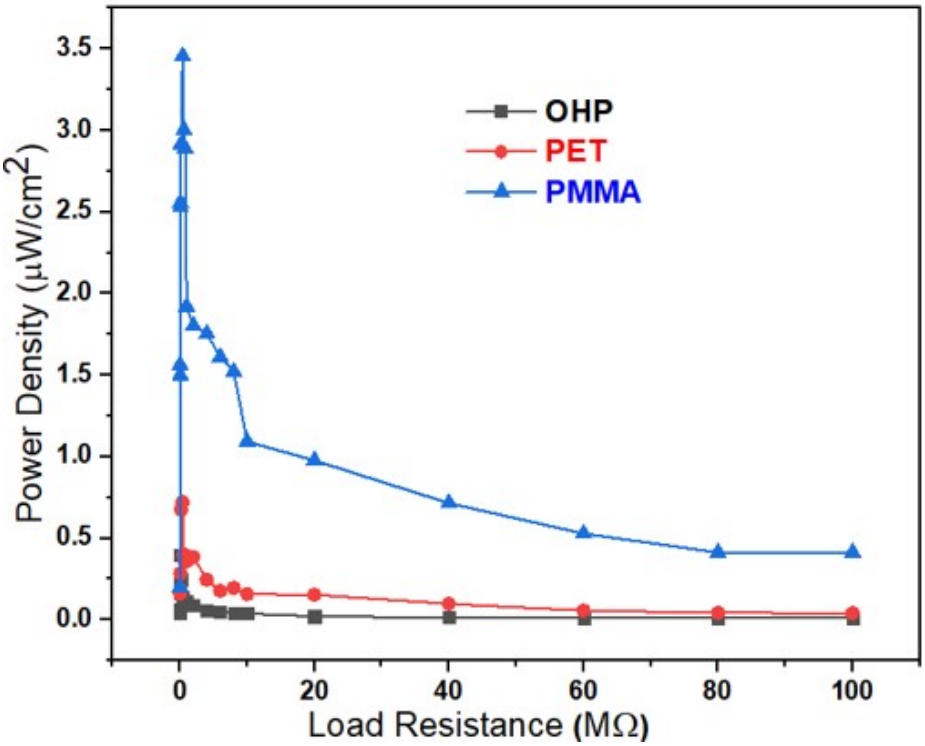

Figure 3.16: Power densities of AOA, APA, APMA TENG Structures with Load.

Powering portable devices requires rectifying the TENG output voltage. The adjusted output can be stored in a supercapacitor. Figure 3.22 depicts the block diagram of the TENG-based dc conversion procedure employing an IC bridge rectifier figure 3.22 (a). Figure 3.22 (b - d) shows the TENG's rectified output voltage following the rectification process Without a storage component.

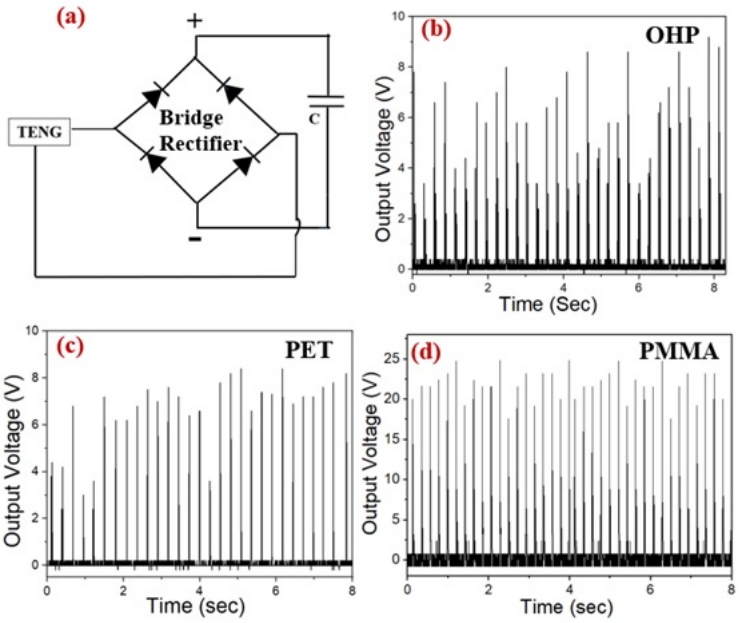

Figure 3.17: (a) Illustration of the TENG's Rectified Voltage's DC, Output Characteristics for the three polymers AOA, APA, APMA TENG structures (b – d).

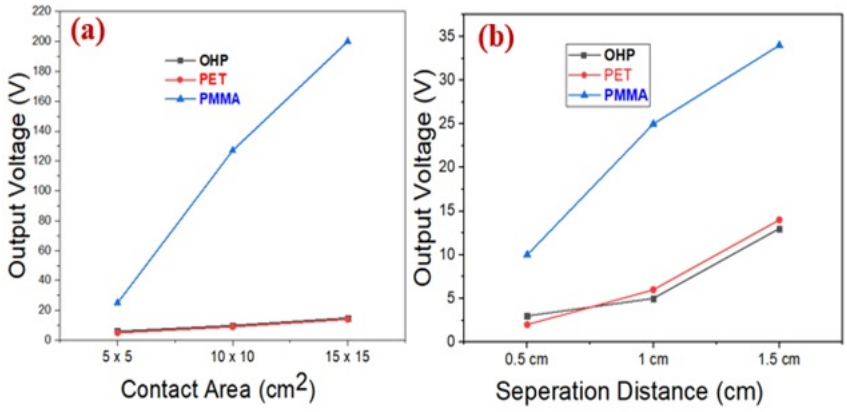

Figure 3.18: TENG devices output responses for (a) Different Area of Triboelectric Layer (b) Different Spacing between the Triboelectric Layers.

As the contact area of TENG device increases and the gap between dielectric and electrode increases corresponding output response is also increases in the both cases as

shown in Figure 3.23 (a), (b). For the three TENG devices AOA, APA, and APMMA TENG structures contact area increases from 5 x 5 cm^2 to 15 x 15 cm^2 the corresponding voltage increases 4 V to 200 V for three polymers used in the fabrication of TENG device. Similarly, the gap between the dielectric and contact electrode height increases from 0.5 cm to 1.5 cm corresponding output response increases from 2 V to 35 V for the three polymers.

Figure 3.24 represents the FEM simulations using COMSOL 6.0 Multiphysics software. In the simulation results used electrodes and dielectrics, which are practically used in the designing of the TENG devices same electrodes and polymers are used and the thickness of electrodes and polymers measured practically and the same values are used in the simulation process.The open circuit voltage is 3.28 KV, 3.27 KV and 3.29 KV AOA, APA, APMMA TENG structures respectively. Among the three polymers PMMA is having high dielectric constant and negative triboelectric charge. For that reason, APMMA structure is giving high output response compared remaining two structures. In the same way also in FEM analysis also using PMMA dielectric layer will gives more output response compared to remaining two structures. Hence, we conclude that in this report among three structures high dielectric constant and high triboelectric negative layer PMMA is giving more output response in both experimental and simulation study.

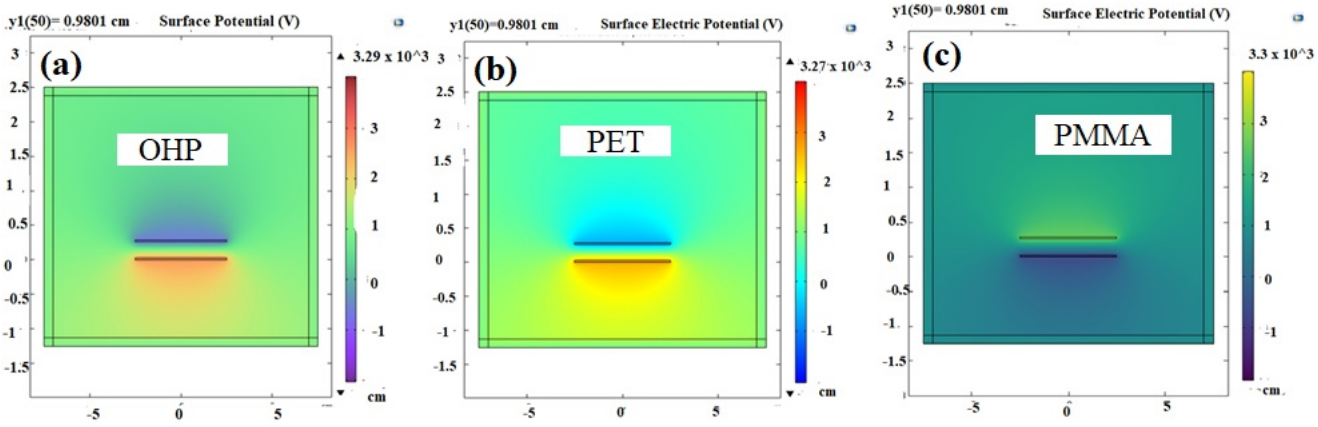

Figure 3.19: (a - c) FEM Simulations of OHP, PET and PMMA Sheets.

In the below Figure 3.25 represents the photograph of 19 LEDs are glowing continuously with hand palming of the APMA TENG device.

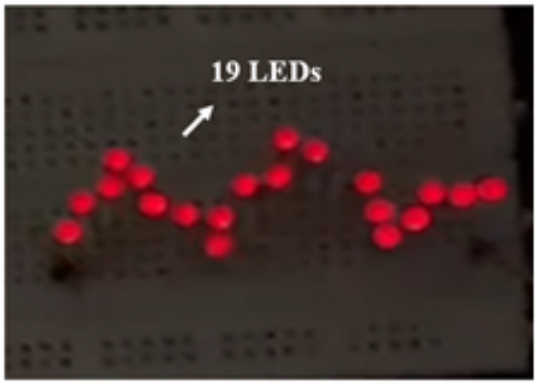

Figure 3.20: LEDs Lighting Condition Photo.

3.11.4 Conclusions

In summary, we have fabricated a material accommodated TENG is based on parafilm PDMS for the first time. The maximum output voltage of $\sim$ 8 V is produced against biomechanical energy. At the applied resistive load 1 MΩ, the maximal power density indicated is 0.81 W/cm^2. Further, fabricated TENG was able to turn on the four commercial LEDs. Further, the rectified output voltage can be stored in the capacitor and use to drive the self-powered sensors, smart wearable electronic gadgets, and implantable biomedical devices in the future.We have created a material that is TENG compatible for AOA, APA, and APMA Structures. In opposition to biomechanical energy, a maximum output voltage of 6 V, 5 V and 25 V is generated respectively. The maximum power density indicated for the applied resistive load of 0.12 W /cm^2, 0.1 W/cm^2, and 3.4 W/cm^2 for load resistances of 1 MΩ, 2 MΩ, and 1 MΩ. Furthermore, the built TENG was capable of turning on the 19 commercial LEDs. The rectified output voltage might also be utilized in the future to power implanted biomedical devices, smart wearable electronics, and self-powered sensors by storing it in a capacitor. Compared with three TENG structures APMMA produces high output voltage, it is having high dielectric constant and more negative triboelectric layer.

Finally, in this chapter, the roughness of various dielectric materials and its impact on the output response are studied, with the conclusion that higher roughness dielectric materials provide a higher output response than remaining materials with lower roughness. These results are compared in the simulation, and the same response is obtained in the case of practical data. The next chapter goes into depth about the various TENG designs that

use less expensive reusable materials and their complete nanogenerator characterizations.

Chapter 4

TENG Device Designs and Driving Hand Held Devices

This chapter deals with the different types of TENG devices with reusable waste materials and new dielectric material is also used in the making of TENG device. Further all the nanogenerator characterizations are performed for all the TENG devices and powering small gadgets like digital watch, digital calculator, digital thermometer, and series of LEDs. This chapter is divided into two parts. In the first part designing of the TENG is designed using only food packaging aluminium foils and in the second part device is fabricated with Aluminum foil acts as electrode and parafilm acts as dielectric medium.

4.1 TENG Using Food Packaging Aluminum foils

4.1.1 Introduction

The research on developing a clean and renewable energy source has given top priority due to the raising concerns about environmental pollution and limited availability of earth resources [104]. Therefore, the different energy harvesting techniques such as piezoelectric, triboelectric, thermoelectric, photovoltaic, electromagnetic were developed to harvest from the freely available renewable energy sources. Among all, triboelectric energy harvesting has attracted a lot of attention since its discovery in 2012 and named

as triboelectric nanogenerator (TENG) [13, 75]. The TENG produces an electric voltage or current in response to the mechanical stimulus through contact electrification and electrostatic induction [105, 106]. In addition, the TENG has the advantages of high energy efficiency, low cost, lightweight, and flexible. Moreover, it can harvest low, high frequency, and irregular mechanical energy from the ambient and bio-mechanical energy [107].

Researchers are exploring new triboelectric materials to reduce the cost and complexity of the TENG device and improve its efficiency significantly for energy conversion. Despite different triboelectric materials like inorganic, organic, polymer, bio-waste, and packaging materials are in existence [95, 108, 109], the energy generation process from the waste packaging materials has grabbed more attention as they help in reducing the pollution in the environment. Recently, research has been focused on developing TENG using waste materials to reduce environmental pollution. A few works that deal with some new triboelectric materials (i.e., waste materials) have been reported in energy harvesting applications. The waste materials such as the discarded milk carton [45], an eggshell membrane [110], waste tea leaves [37], orange peel [38], fish scales [88], fish bladder [23], rice husk [90] , sugar cane [111], recycled PVC cling film [112], and waste plastic bags [113]. Further, waste-based TENG's were demonstrated for different applications such as in-site real-time survey for environmental monitoring, generation of Morse code, powering commercial electronic temperature/humidity sensor, watch, calculator, intelligent wireless switch, and turn on number of LEDs ranging from 50 to 179 in number. The rapid increase of food packaging waste is a significant cause of pollution in the air, water, and land. Therefore, a triboelectric nanogenerator (TENG) is developed using only food packaging aluminium covers. The demonstrated TENG helps in reducing environmental pollution and as well as harvesting mechanical energy. In the demonstrated TENG, electroplated aluminum surface and PET surface of food packaging cover act as tribo-layers. The fabricated TENG generates voltage and instantaneous power density of $\sim$ 4 V and 40 nW/cm$_2$. The TENG stability was tested over 4000 cycles and found highly stable. The demonstrated TENG output power can be increased by using other tribo layer materials such as PDMS, PVDF, and PVC films. Therefore, it can be utilized to power up portable electronic devices in the future.

The summary of the contribution, we have used the discarded food packaging aluminium cover foils (DFACF) only for the TENG fabrication for the first time. The demonstrated TENG has several advantages, such as reducing pollution, low cost, no extra electrode deposition required, and can be scaled to large areas. The DFACF are usually thin PET foil electroplated with aluminium on one side. In this manuscript, the PET surface acts as a tribolayer and the electroplated aluminum as electrodes for the TENG. Our previous report demonstrated DFACF as electrodes for the TENG fabrication, and it has shown excellent stability [66].

In the present contribution, a novel TENG is fabricated using only food packaging aluminium cover foils for the first time and studied its detailed electrical characteristics.

4.1.2 Experimental Details

Materials used for TENG fabrication are DFACF, cardboards, and sponges. The cardboards and sponges were purchased from the local market, and DFACF were obtained from the packaged food received from a restaurant. The schematic of the fabricated TENG (10 x 10 cm^2) is shown in Figure 4.2 (a).Two electrode connections were taken from the bottom, and top aluminium surfaces, as shown in Figure 4.2 (a), to measure TENG output voltage. A digital storage oscilloscope (Tektronix-TBS1102) measured the output voltage TENG against the continuous palm tapping. Further, the effect of device size and spacing between the tribolayers were studied.

4.1.3 Results and Discussion

The surface morphology of the Aluminium and PET surface of DFACF is shown in Figures 4.1 (a) - (b). It is clear from the SEM images that, PET surface has more roughness than aluminium surface. Further, the EDX analysis was carried out on both surfaces and presented in Figure 4.1 (b) - (c). The PET side shows only C and O elements, whereas the aluminium side shows the Figure 4.2 (b) shows the open-circuit voltage of TENG (10 X 10 cm^2, spacing = 0.5 cm) against repeated palm tapping's under forward and reverse connections. The forward and reverse connection test was done by interchanging TENG connections to the oscilloscope, which is called the switching polarity test. A phase shift

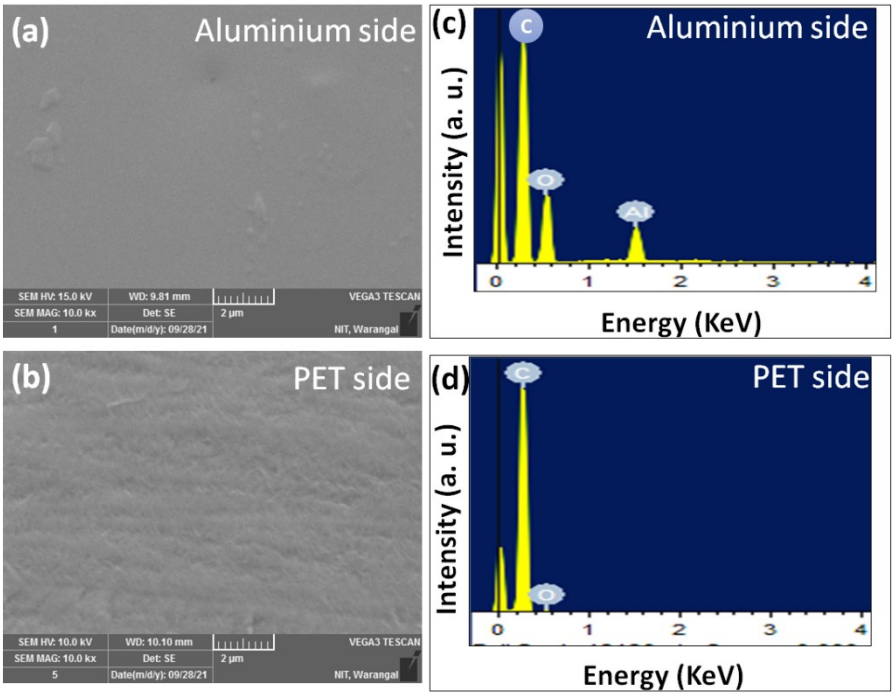

Figure 4.1: SEM Images of the (a) Aluminum Side, (b) PET Side, EDX spectrum of (c) Aluminum Side (d) PET Side.

of 180 degrees was observed in the output voltage under forward reverse connections. The switching polarity test confirmed that the generated output voltage was due to the TENG operation alone, not the instrumental noise [23]. An average output voltage of $\sim$ 4.01 V was observed for the continuous palm tapping process. The response of the TENG for one cycle of press and release is shown in figure 4.2(a).

In order to find the TENG maximum output power, the output voltage was measured under various load resistances and presented in figure 4.2(c). As the value of load resistance increases, the voltage significantly increases and reaches a saturation value of $\sim$ 3.5 V approximately. The TENG load resistance behaviour can be understood using a simple equivalent model reported in the literature [111].

The power density of TENG was calculated using the figure 4.2 (d) data and shown in figure 4.2 (e). The maximum power density is 40 nW/cm^2 was observed under the impedance matched conditions at a load resistance of 1.8 MΩ. The output voltage of TENG was further converted into direct current (DC) voltage using a bridge rectifier, as shown in figure 4.2 (f). The obtained DC voltage is helpful for practical applications such as powering portable electronic devices.

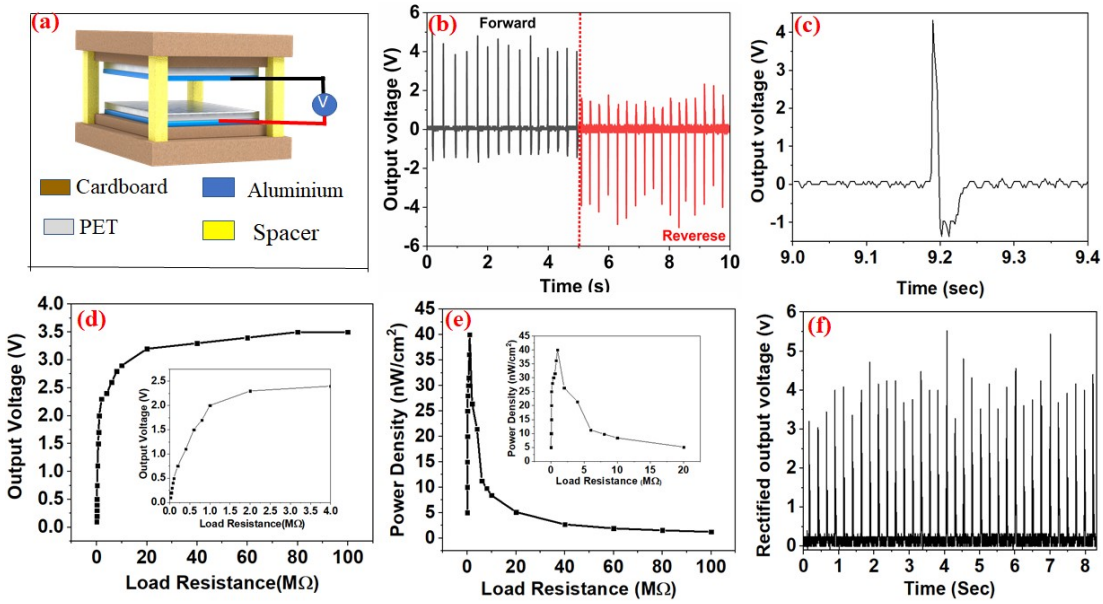

Figure 4.2: (a) Schematic of TENG structure (b) TENG response in forward and reverse connections, (c) output voltage response for one cycle, (d) TENG output voltage under different load resistance, (e) The output Power Density as a function of Load Resistance, (f) TENG output after Rectification.

At last, the effect of the triboelectric layer active area (device size) on the performance of TENG was studied under three different sizes of 5 x 5 cm^2, 7 x 7 cm^2, 10 x 10 cm^2 for separation of 1.5 cm. The approximate voltages were obtained as 0.2 V, 1 V, and 3.96 V for device dimensions of 5 x 5 cm^2, 7 x 7 cm^2, 10 x 10 cm^2 respectively. The increased output voltage is due to the increased contact area for the enhanced contact electrification. TENG performance was measured at the discrete separation between the tribo-layers of 0.5 cm, 1.5 cm, and 2.5 cm. It is observed that TENG output voltage increased initially with distance up to 1 cm and after decreased. The TENG's open-circuit output voltage (Voc) is roughly equivalent to basic expression. (i.e., Voc = $\sigma d/\epsilon$), where d, σ, and ϵ are interlayer spacing, vacuum permittivity interlayer spacing and triboelectric charge density on the surface [113]. The output voltage increased with interlayer distance up to 1 cm as per the TENG output expression. The output voltage decrease at higher spacing is due to the ineffective contact between the PET and Al . Figure 4.3(c) shows the charged voltage of different capacitors by TENG. The energy stored by each capacitor was calculated and presented in Figure 4.3 (d) and it shows the variation of maximum stored energy as a function of load capacitance (C_L) with the highest stored energy of 52.8

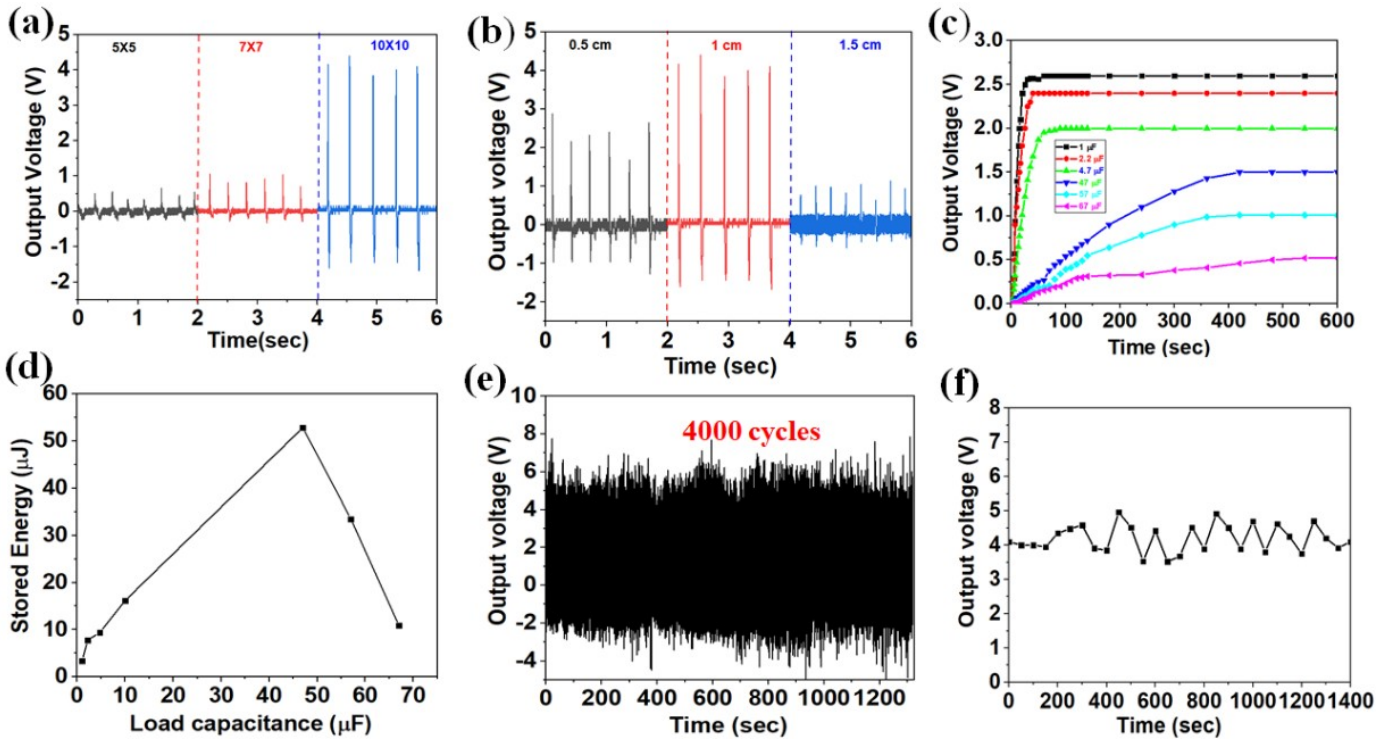

Figure 4.3: TENG output voltage as a function of (a) different active areas, (b) spacing between substrate PET and Aluminum, (c) Charging curves of different capacitors, (d) Stored energy as a function of load capacitors, (e) TENG response under 4000 cycles, (f) output voltage values for every 100 cycles.

µJ found at the optimal (C_L) of 47 µF.Further, the high stability of TENG was confirmed by testing over 4000 cycles, and the TENG response is shown in Figure 4.3 (e). Finally, the behavior of the output voltage was represented in a graphical form for every 50 th cycle (ex: 50, 100, 150), as shown in figure 4.3 (f). Here, the average value of the output voltage for TENG obtained was around $\sim 4 \pm 0.5$ V, and this deviation is because of the variation of continuous palm tapping force and frequency.

4.2 A Triboelectric Nanogenerator Based on Food Packaging Aluminium Foil and Parafilm For Self-Powered Electronics

4.2.1 Introduction

Triboelectric nanogenerators (TENG) have attracted increased attention due to their multifunctional applications in various fields such as bio-medical, healthcare, Internet of things, artificial intelligence, and self-powered electronic devices and sensors [114]. The first TENG was reported in 2012 and developed to effectively convert ambient mechanical energy, such as body motion, wind, and vibration energy into electrical energy [115]. The typical TENG consists of two different electronegativity layers. These layers generate potential difference via the coupling of the triboelectric effect and electrostatic induction during cyclic contact and separation between them [112, 20]. Subsequently, TENG has AC to DC conversion circuits, storage elements such as a battery or capacitor to power up portable electronic devices or sensors [86, 85]. Four different modes of TENG operation have been demonstrated based on electrode configuration and direction of polarization change. These four modes are vertical contact-separation, lateral-sliding, single-electrode, and free-standing triboelectric layer [116]. The contact separation mode is very well established among different modes and demonstrated for many triboelectric materials [22, 117] . In the present manuscript, also vertical contact separation mode of TENG operation is used. The main advantages of TENGs are their high energy-conversion efficiency, simple structure, cost-effectiveness, reliability, scalability, and harvesting energy from irregular, low-frequency inputs [31, 118]. A wide variety of triboelectric pairs tested for energy harvesting and demonstrated for potential practical applications are summarized in figure 1 [90, 25].

However, the search for new triboelectric materials is still considered an important area of research to reduce the TENG device's cost and complexity and improve its energy conversion efficiency. There are various triboelectric materials such as inorganic, organic, polymer, and bio-waste materials [25, 119]. The energy generation from waste attracted much attention due to the reduction of pollution in the environment. Many recent reports

are dealing with the new triboelectric materials from the waste materials for energy harvesting applications. J. Bae et al., reported the biowaste Peanut shell powder, Sunflower husks powder based TENG for biomechanical energy harvesting [120, 121] J. M. Wu et al., demonstrated high current density TENG based on rice husk [45]. Z. Zhu et al., developed TENG based on waste tea leaves and waste aluminium plastic bags [39]. Z. L. Wang et al., demonstrated a novel TENG based on the waste milk carton and used for in-situ real-time survey of environmental monitoring [122, 107], . H. Singh et al., fabricated TENG using an eggshell membrane with other triboelectric materials and demonstrated for powering the digital watch [77]. P. Zhang et al., used recycled PVC cling film as a triboelectric layer and used it for Morse code generation [37]. G. Han et al., fabricated the TENG based on waste plastic bags [123]. It is found that output voltage of waste material based TENG's in the range of 6 - 600 volts and power density in the range of 0.25 $\mu W/m^2$ - 0.84 W/m^2 . In this manuscript, waste food packing Aluminium cover (WFPAC) foil and laboratory parafilm were used as a new triboelectric pair for mechanical energy harvesting for the first time. Parafilm is a semi-transparent, flexible film composed of a proprietary blend of waxes and polyolefins. It has several advantages: flexible, moldable, self-sealing, odourless, moisture-resistant, thermoplastic, semi-transparent, and colorless. The WFPAC is a polymer (PET) film electroplated with Aluminium. The reuse of WFPAC foils for energy harvesting strongly promotes the next-generation energy technologies that will effectively avoid pollution and hazards caused by metal and hardly degradable plastic materials.

The summary of the contribution the increasing food packaging waste is a severe concern for air, water, and soil pollution. In this research work, a triboelectric nanogenerator (TENG) is fabricated using waste food packaging Aluminium cover foils and laboratory parafilm for the first time. The device novelty lies in the selection of the materials; parafilm and food packing Aluminium cover foils. The demonstrated TENG produced an output voltage and instantaneous power density of $\sim$ 4 V and 11.8 nW/cm^2, respectively, by hand excitation force. Further, TENG can easily power up 85 commercial light-emitting diodes, digital watch, thermometer, and calculator with the help of charged capacitor. The demonstrated TENG demonstrated the ease of process, simplicity, cost-effectiveness, and reduction of pollution. Further, this TENG performance can be improved with other triboelectric materials and applied in self-powered portable electronic device applications.

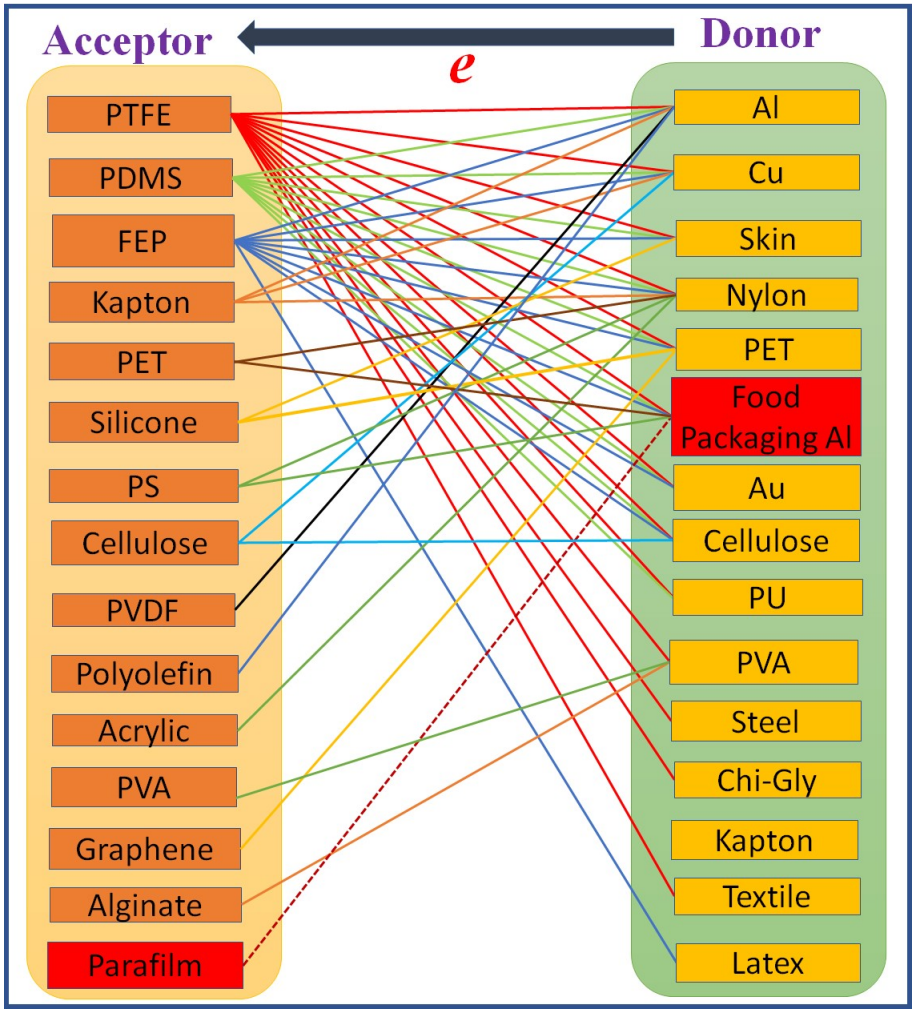

Figure 4.4: List of Triboelectric Pairs reported in the literature and our current work highlighted in dotted line

In this report, a novel TENG is fabricated based on WFPAC foil and parafilm for mechanical energy harvesting for the first time and studied its performance. Further, fabricated TENG has been demonstrated to power up portable electronic devices and a group of LEDs.

4.2.2 Materials and Methods

The materials used in this study are cardboard sheets, WFPAC foils, laboratory parafilm, and sponge. The Parafilm-M was purchased from Sigma Aldrich. The Aluminium packaging foils, cardboards, sponges were obtained from the local market . The obtained Aluminium foils were used for cooked rice packaging initially and then used for

TENG. The Parafilm and WFPAC foils are initially characterized by a scanning electron microscope (SEM). Then, TENG was fabricated using parafilm (thickness $\sim$ 180 µm) and WFPAC foil (thickness $\sim$ 35 µm), cardboard sheets, and sponge spacers. The fabrication steps of the TENG are shown in figure 4.5.

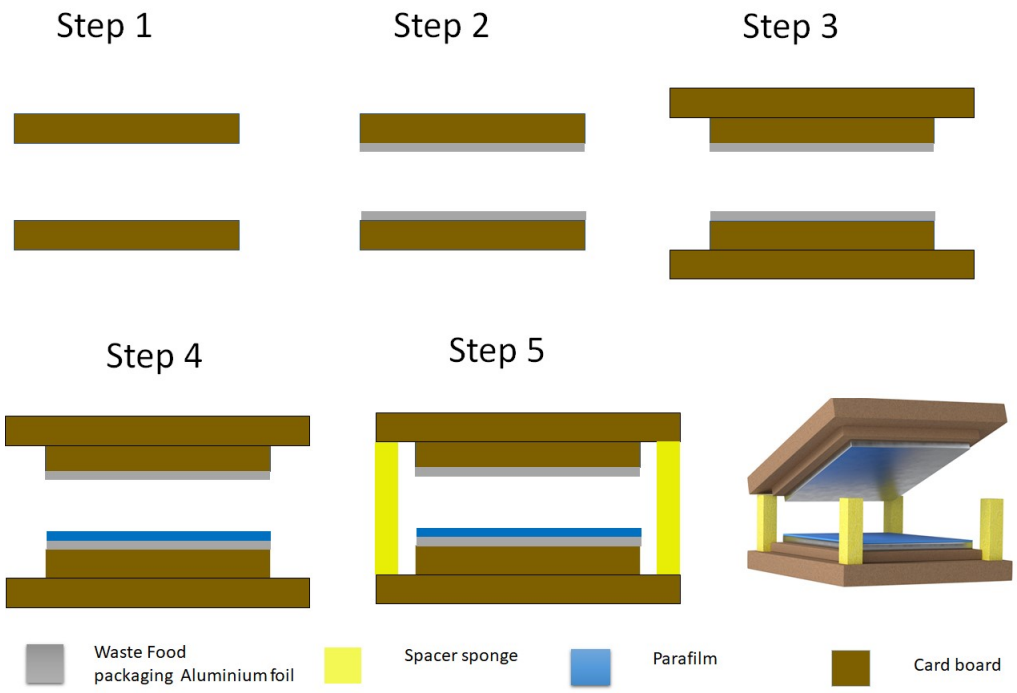

Figure 4.5: Fabrication steps of TENG based on Parafilm and Waste Food packaging Aluminium Foil.

Initially, WFPAC attached to two rigid cardboards of selected dimension firmly by scotch tape with conducting side up. Further, parafilm is firmly attached to one of the above structures on the conductive side with scotch tape. These two cardboards with electrodes and parafilm were attached to another two cardboard sheets of higher dimension than this with a spacer. Four corners of the bottom cardboard were attached with sponge spacers with the help of strong glue. Another cardboard with only WFPAC foil is placed over the spacer and attached with the help of the strong glue. A finite gap exists between the bottom parafilm and the top Aluminium electrode due to the sponge spacer. The original images of the fabricated TENG devices and fabrication steps are shown in figure 4.6.

Generally, TENG devices work in four modes: vertical contact separation, in-plane sliding, single-electrode, and free-standing triboelectric-layer [115]. In this work, TENGs

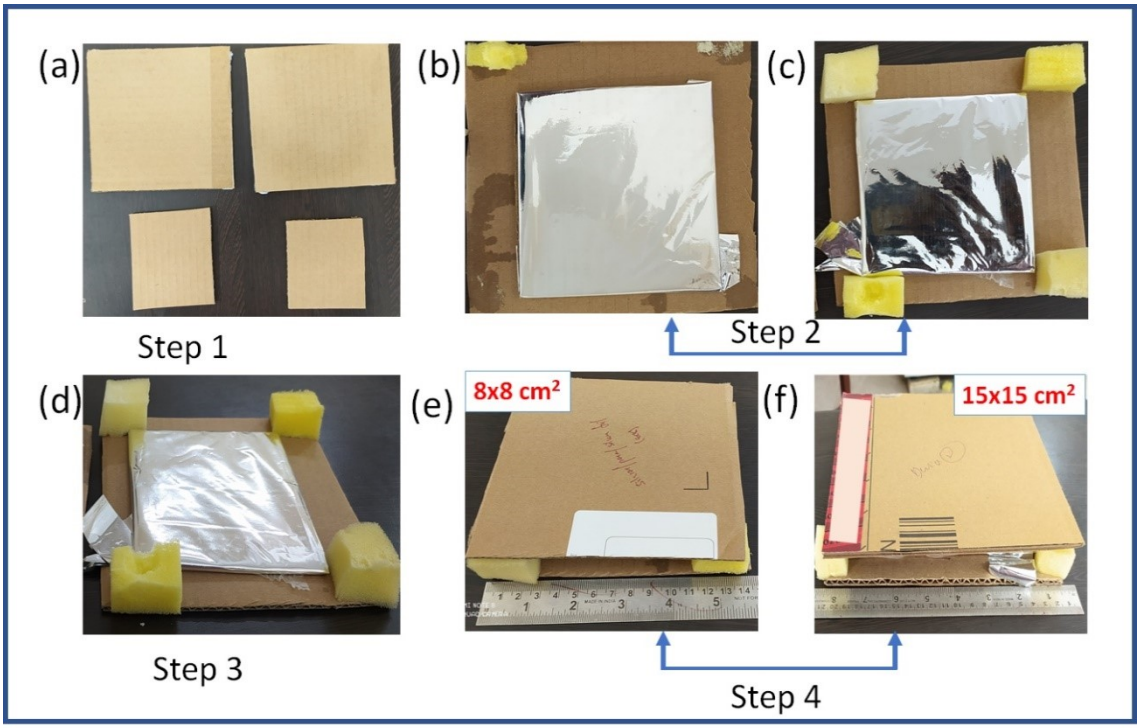

Figure 4.6: Photographs of TENG's fabrication steps based on parafilm and Waste Food packaging Aluminium foil (a) Cardboard sheets for upper (large) and inner (small) parts of the TENG, (b) - (c) Aluminium foil attached to inner cardboard sheets, (d) Parafilm attached to the Aluminium foil of figure (c), (e) - (f) packed 8x8 and 15x15 cm2 TENG device.

were designed to operate in the vertical contact mode. At open-circuit conditions, the charge generation of the TENG under cyclic force application can be understood from the coupling of the triboelectric effect and electrostatic induction [115]. Figure 4.7 schematically presents the working mechanism of the TENG with parafilm under the vertical compressive force. The mechanism is well-reported and accepted in the literature [75] .

In the initial state, before the contact of the parafilm and the top Aluminium electrode, there is no charge transfer and thus no electric potential, like shown in figure 4.7 (a). As shown in figure 4.7 (b), when parafilm and Aluminium contact each other, exchange of charges between Aluminium and parafilm due to their different abilities to gain or lose charge. The parafilm carries a negative charge while Aluminium carries the same amount of positive charge, keeping the TENG in a balanced state. When the TENG starts to separate, the balance is broken due to the electrical potential difference. The parafilm can retain charges on its surface, which remains unchanged, so a balanced state is rebuilt.

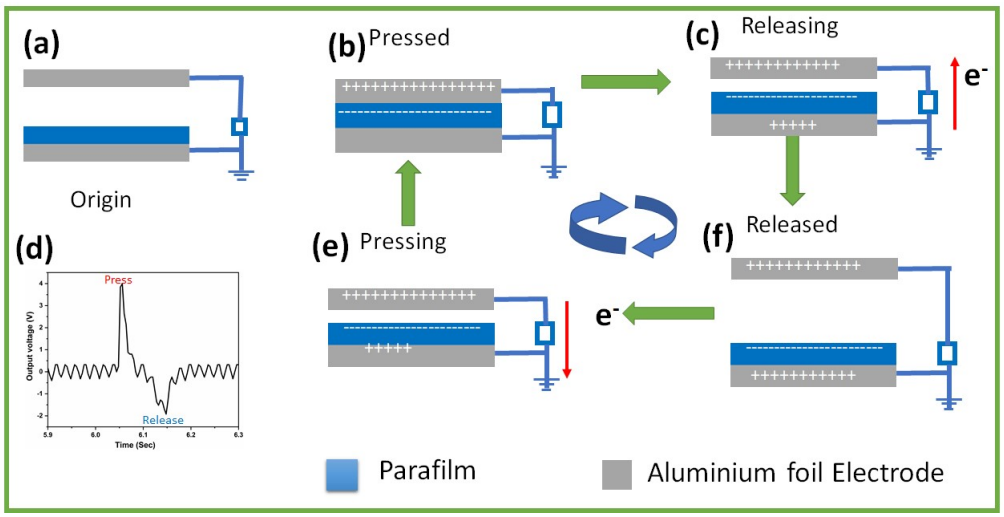

Figure 4.7: (a) - (c), e, f Working Mechanism of TENG, (d) Press and release signal output voltage pulse.

The charges on the electrode surface will transfer from the parafilm electrode to the Aluminium, as shown in figure 4.7 (c),(f). When the two surfaces are brought together again (figure 4.7 (e)), the electrical balance is broken and rebuilt again. In this state, charges transfer from Aluminium to the parafilm electrode until the balance is reached (figure 4.7 (b)). During the periodical contact-separation process, the triboelectric charges on the parafilm induce a periodical movement of the free electrons on the top and bottom Aluminium electrodes to generate electron flows in the external circuit.

The TENGs were prepared with a different active area of 5 x 5, 8 x 8, 15 x 15 cm^2 for a fixed spacing of 1.5 cm between the parafilm and WFPAC foil using the exact dimension spacer. Further, TENGs were fabricated with different spacer dimensions for a fixed active area of the device (15 x 15 cm^2) to study the spacer size. Finally, fabricated TENG output voltage against hand tapping was measured using a digital storage oscilloscope (Tektronix-TBS1102) interfaced to a computer using the software as reported in the literature [91]

4.2.3 Results and Discussion

Initially, the surface morphology of the parafilm and Aluminium foil was characterized with a scanning electron microscope. Figure 4.8 (a)-(c) and (d)-(f) shows the SEM images of parafilm and Aluminium foil surface at different magnifications. It is clear from the SEM images that, parafilm films has rougher surface compared to Aluminium foil

surface.

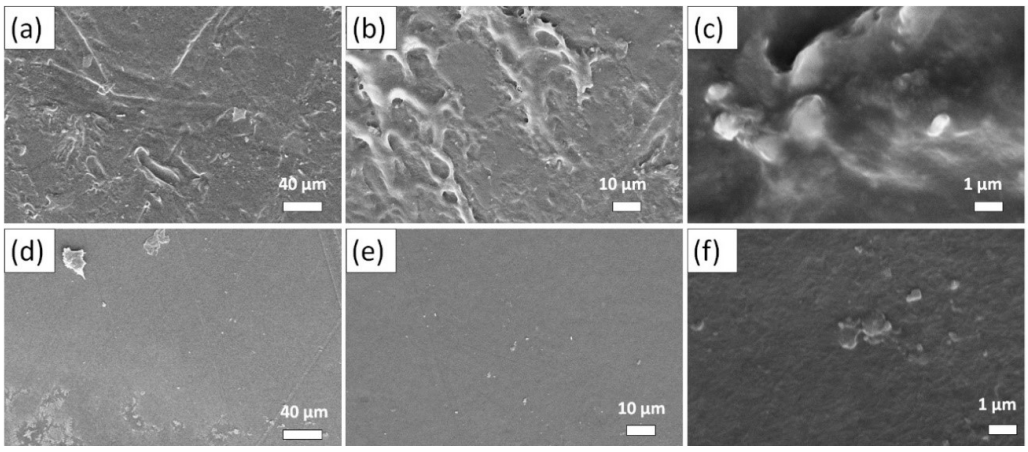

Figure 4.8: SEM Images of the (a) - (c) Parafilm, (d)- (f) Aluminium Packaging foil at Different Magnifications.

Figure 4.9 (b) shows the open-circuit voltage of the 15x15 cm^2 TENG (spacing = 1.5 cm) in response to the repeated hand tapping. An output voltage of $\sim$ 4 V was observed for repeated hand tapping. A switching polarity test was performed by reversing the TENG connections to the oscilloscope to confirm the output voltage only due to TENG operation. The TENG has shown exactly opposite electrical signal in reverse connection with respect to the forward signal, as shown in figure 4.9 (b). The switching polarity test confirms that the voltage generated is only from TENG, not from the instrument noise [34]. The enlarged view of the single cycle (press and release) output voltage signal is shown in figure 4.9 (c). We have also tested the output response of the TENG fabricated with fresh Aluminium foil - parafilm against hand tapping. It was found that no difference in their output voltage response when compared to the used Aluminium foil-based TENG. A similar output for both types of foil is due to the no abnormal changes on the surface at the microscopic level for the used foil.

Further, TENG output voltage was measured with variable load resistances ranging from 20 KΩ to 100 MΩ under uniform hand tapping to measure the optimum output power density. The variation of output voltage under different load resistances is shown in figure 4.9 (d). With an increase in load resistance, the voltage increases and saturates at a value of approximately $\sim$ 3.8 V. The saturated output voltage at higher resistance (100 MΩ) is close to the open circuit output voltage. The TENG load resistance-dependent output

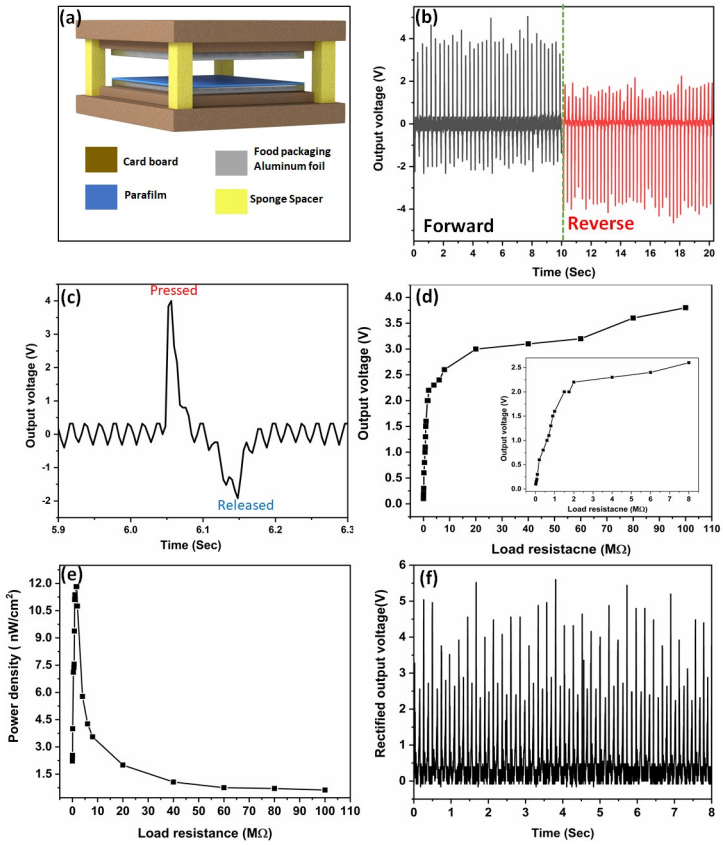

Figure 4.9: (a) Schematic of the TENG, (b) Electric output of a TENG under forward and reverse connections, (c) A zoomed-in view of output voltage generated by TENG during a single cycle of operation, (d) output voltage as a function of the load resistance, (e) output power density as a function of the load resistance, (f) Rectified Output Voltage of the TENG.

voltage shows a similar trend as reported in the literature [93, 94, 95]. The TENG load resistance can be understood with the help of a simple equivalent model demonstrated by Z L Wang and other research groups in the literature [124] The TENG is equivalent to a variable capacitor connected to a voltage source. The voltage drops across the R_L increase until the optimum R_L and saturate at the theoretically infinite load resistance similar to open-circuit voltage [24].

The output power density (Power density= $V^2/(A*R_L)$) with different load resistances was calculated and summarized in Figure 4.9 (e). Figure 6(e) shows that the maximum output power density of the TENG is 11.8 nW/cm^2, at a load resistance of 1.8 MΩ. The output power density characteristics of the TENG device can be explained with the help of the maximum power transmission theorem [125]. According to the theorem,

maximum power transmission takes place when the load resistance value equals to the source internal resistance. In the present report, the peak output power density occurred under impendence matched conditions across a load resistor value $\sim$ 1.8 MΩ. The output power density decreased with the load resistance values greater than 1.8 MΩ due to the saturated output voltage. The saturated output voltage at higher load resistance decreases the V^2/R_L ratio (power) value. The output power density of TENG with load resistance shows a similar trend as reported in the literature [126, 127]. Figure 4.9 (f) shows the rectified output voltage of the TENG after rectification via DB 107 IC bridge rectifier. The output power of the TENG can be utilized for continuously driving LEDs.

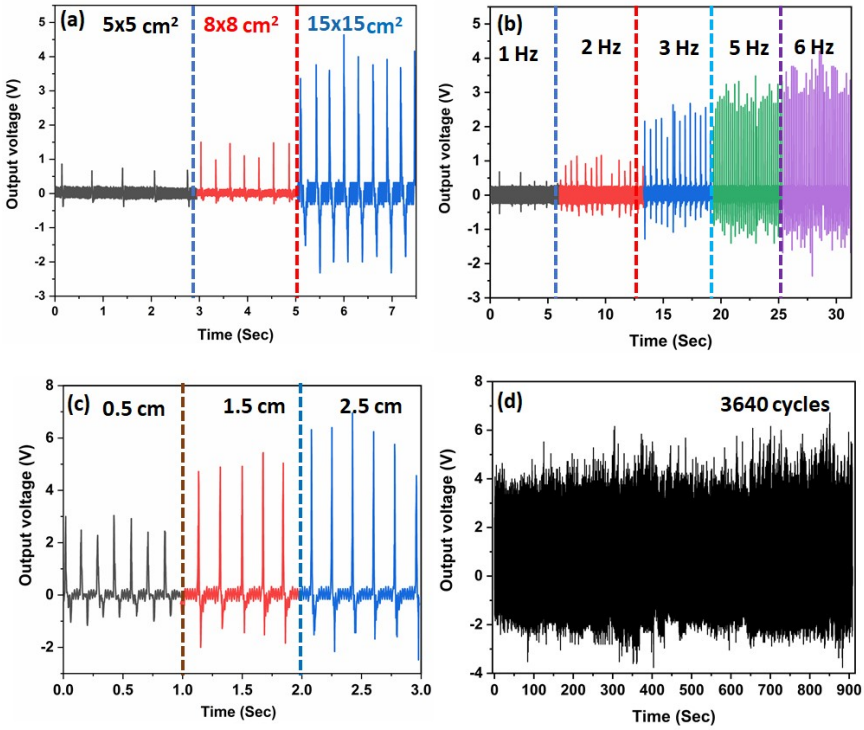

Figure 4.10: TENG output voltage as a function of (a) Different Area, (b) Different Frequency, (c) Different Spacing between Parafilm and Aluminium, (d) Output Stability of the TENG under 3640 cycles.

Further, the study was carried out to find the effect of triboelectric layer size (device size) on the TENG performance. Figure 4.10 (a) shows the TENG response against hand tapping for different device dimensions of 5 x 5, 8 x 8, 15 x 15 cm^2 for a separation distance of 1.5 cm. The averaged voltage values were obtained as 0.61 V (5 x 5 cm^2), 1.28 V (8 x 8 cm^2), and 3.96 (15 x 15 cm^2). The enhancement in the output voltage from 0.61 V to 3.96 V was observed. This enhancement is due to the increased contact

area of the triboelectric layers. Similar behaviour was reported for TENG's in earlier literature also [128] . Figure 4.10 (b) shows the TENG's output voltage characteristics under different tapping frequencies of 1, 2, 3, 5, and 6 Hz for a separation distance of 1.5 cm. It is evident from figure 4.10 (b) that the output voltage was gradually increased with an increase in tapping frequency. This enhancement in the output voltage is attributed to the imperfect neutralization of accumulated residual charges due to rapid external tapping cycles, resulting in the increasing of triboelectric potential [129, 106, 66]. At each frequency, the averaged voltage values were obtained as 0.5 V (1 Hz), 1 V (2 Hz), 2.2 V (3 Hz), 3 V (5 Hz), and 3.7 V (6 Hz).

Further, TENG performance was evaluated at the different spacing between the tribo-layers of 0.5 cm, 1.5 cm, and 2.5 cm with the help of a sponge. Figure 4.10 (c) shows the TENG's output voltage variation under the same frequency of hand tapping with different spacing. TENG output voltage was increased with an increase in spacing between the tribo-layers. The open-circuit output voltage Voc of TENG can be approximately expressed as $Voc = \sigma d/\epsilon$, where d is interlayer spacing, σ is the triboelectric charge density on the surface, and ϵ is the vacuum permittivity . According to the open-circuit output voltage expression, the output voltage will increase with increasing the interlayer distance. Similar behaviour was observed for other TENG devices in the literature [49]. The stability and durability of the TENG are essential factors to ensuring its practical applications. The output voltage was measured under external hand tapping force for 3640 cycles to examine the TENG durability for long-term operation. Figure 4.10 (d) shows that the generated voltage did not degrade after 3640 cycles, indicating the high stability of fabricated TENG. Further, TENG response was recorded at different time points, such as immediately after fabrication, one month, and three months. In all the cases, TENG exhibited a stable output response .

Figure 4.11 (a) - (b) represents the enlarged view of the stability graphs at different time points. An average voltage of $\sim$ 4 V was observed throughout all cycles. The TENG's output voltage was plotted for every 100^{th} cycle (ex: 100, 200, 300 etc.) shown in Figure 4.11 (c). The TENG's output voltage shows an average value of 4 ± 0.5 V, and this deviation is due to variation of hand tapping force and frequency.

Figure 4.12 (a) shows the charging characteristics of various rating commercial ca-

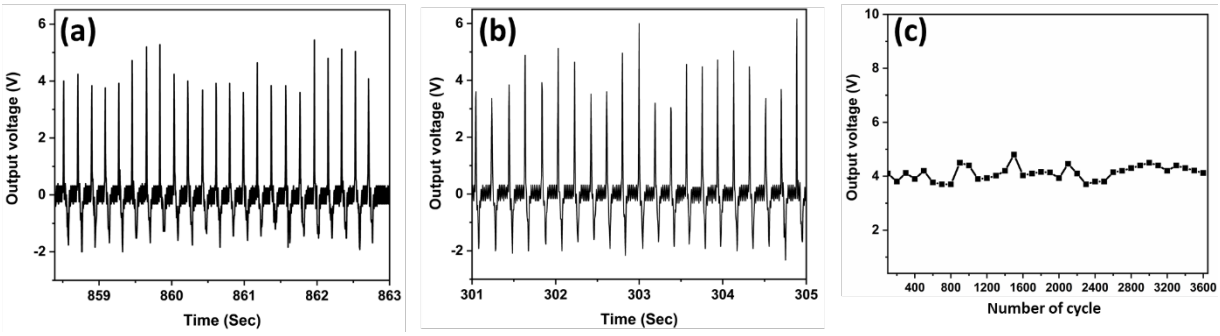

Figure 4.11: (a)-(b) Enlarged View of Few Cycles from the 3640 cycles (c) output voltage values at every 100 cycles from the stability graph.

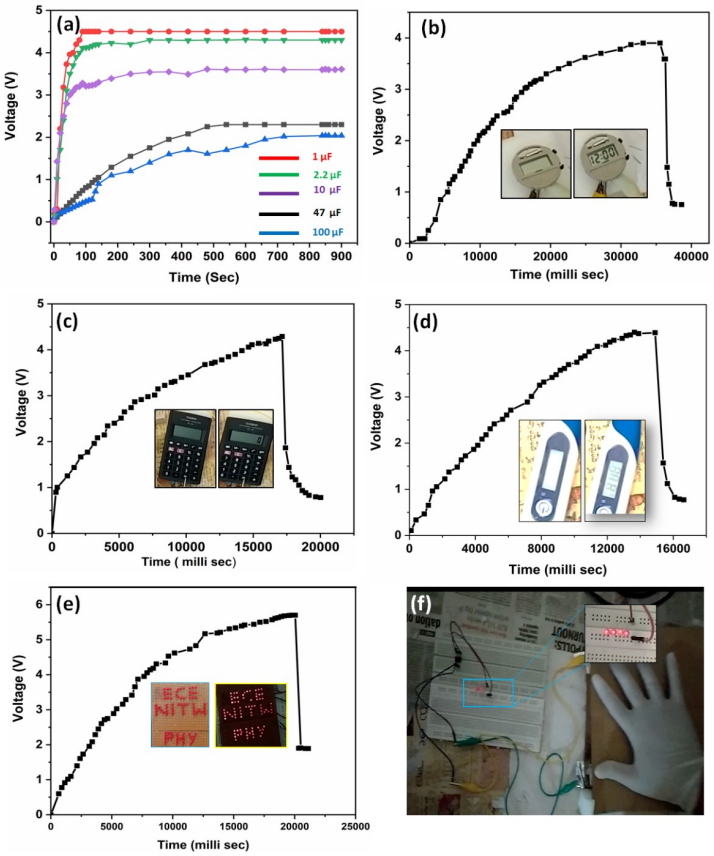

Figure 4.12: (a) Charging curves of different capacitors, charging and discharging behaviour of capacitor before and after power up the electronic devices (b) digital watch, (c) calculator, (d) thermometer and (e) 85 red LEDs, (f) Image of the Continuous Powering on 4 LEDs under Cyclic Application of Force.

pacitors such as 1 µF, 2.2 µF, 10 µF, 47 µF, and 100 µF for 900 seconds. The energy stored by the 1 µF capacitor was used to power up portable electronic devices such as a digital watch, calculator, thermometer, and 85 LEDs, as shown in Figure 4.12 (b)-(e). Further,

TENG can also power up 4 LEDs continuously with hand tapping shown in Figure 9(f) .

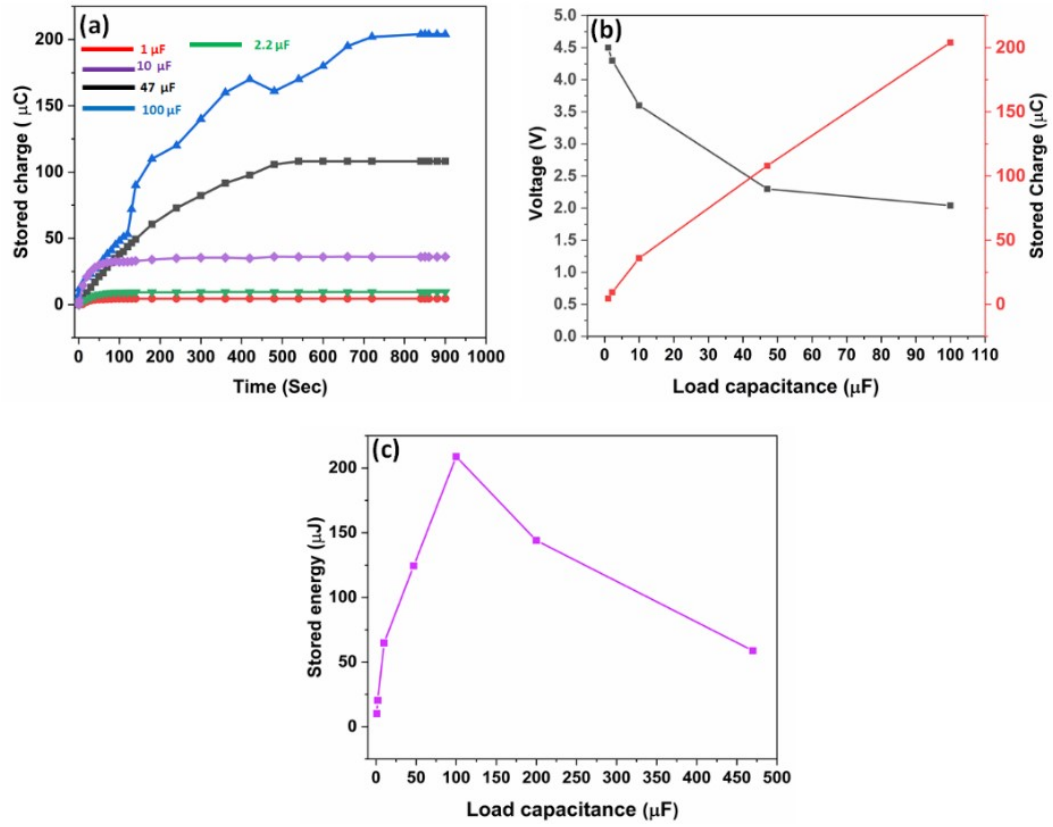

Figure 4.13: (a) Stored charge as a function of Time for Different Load Capacitors (b) The Behaviour of output voltage and stored charges as a function of Load Capacitance (C_L) (c) The Stored Energy as a function of C_L.

The stored charge on these different load capacitors was obtained using the basic equation Q = CV. Figure 4.13 (a) shows the stored charges as a function of time for various load capacitors. The capacitor with a small enough value of 1 µF store a small amount of charge and quickly reaches the saturation value. It is evident from the figure that storage capacity is increased with an increase of load capacitance value. The capacitor with a large enough value of 100 µF stored the maximum charges of 200 µC in a given time of 900 s. At a constant time duration of 600 s, 1 µF capacitor saturation voltage and maximum stored charge were 4.5 V and 4.5 µC. In the case of 100 µF capacitor, the output voltage equals 2.3 V while the stored charges reach a maximum value of 204 µC. The output voltage and stored charge characteristics were analysed as a function of different load capacitance values shown in figure 4.13 (b). There is an inversion relation

between voltage and stored charges against corresponding C_L. Figure 4.13 (c) shows the variation of maximum stored energy as a function of load capacitance. The maximum stored energy of 208.8 µJ was observed at the optimum C_L of 100 µF.

4.2.4 Conclusions

In conclusion, TENG was fabricated using only discarded food packaging aluminium foils and demonstrated to turn on 3 LEDs. The TENG's open-circuit voltage can reach up to $\sim$ 4 V and the maximum power density achieved is 40 nW/cm^2. The power density of TENG can be further improved by attaching other tribolayers to the top electrode. Thus, this study presents a novel way to utilize food packaging waste for energy harvesting applications.

In summary, a new TENG has been demonstrated based on the waste food packaging Aluminium covers foil and the parafilm to power portable electronic devices. In our design, the parafilm and conducting side of WFPAC foil serve as the triboelectric pair. TENG's open-circuit voltage can reach $\sim$ 4 V and the maximum power density 11.8 nW/cm2. The prepared TENG was demonstrated to power up portable electronic devices and LEDs. The present work opens up a new triboelectric pair for energy harvesting. This new parafilm tribo-layer can form new triboelectric pairs with other materials for enhanced mechanical energy harvesting. Furthermore, the idea of using WFPAC foil reduces environmental pollution to a certain extent.

This chapter focuses on several types of TENG devices created from reused waste materials and novel dielectric materials. We characterise these nanogenerators before demonstrating their capacity to power tiny devices including a digital watch, digital calculator, digital thermometer, and a sequence of LEDs. In the next chapter, we will validate the nanogenerator characterizations using the COMSOL platform. Only a few researchers have used this technology for such objectives so far. However, in the next chapter, we want to validate and finalise all TENG device characterizations using COMSOL. The scaling factor will be calculated as part of the validation process to ensure a significant connection between simulated and real-time data.

Chapter 5

CS TENG Simulation & Analysis

This chapter delves into the simulation of Triboelectric Nanogenerators (TENGs) using the sophisticated COMSOL framework. We continue to use the same types of electrodes and dielectric materials in the design of the TENG device as we did in Chapter 4. This consistency enables us to make a direct comparison between the simulations and earlier experimental data, assuring the dependability of our observations.

Various characterizations of the TENG device are methodically done throughout the investigation. These involve determining the contact area and surface charge density, experimenting with various electrode structures, and evaluating single and two dielectric combinations. Notably, the dielectric materials used in the simulations are pre-existing polymers from the COMSOL modelling programme. This assures that our findings remain completely associated with real applications, improving the results' relevance and applicability.

The calculation of the scaling factor for both simulation and actual instances is a significant part of the study. This aspect is meticulously evaluated to measure the relationship between simulated and real-world circumstances. Surprisingly, the results from both methodologies show an incredible level of agreement, with no noticeable variances. This amazing consistency increases the validity of our simulations and enhances reliability in the TENG device's performance prediction.

Finally, this chapter gives a thorough analysis into the TENG device utilising rigorous simulations on the COMSOL platform. We establish the accuracy of our results

by using consistent electrode and dielectric materials and completing a variety of characterizations. The extraordinary match between simulation and real outcomes verifies the TENG device's durability and efficacy, highlighting its potential as a viable and efficient energy generating technology.

Triboelectric nanogenerators have been gaining popularity in the field of renewable energy due to their ability to harness waste mechanical energy through friction. The generation of triboelectricity depends on various factors such as surface charge density, material properties, geometrical features, and operating parameters like velocity. Polymers have shown good results in the generation of triboelectricity, and nanomaterials have proven to be useful in this regard. Computational and numerical simulations have been carried out on selected pairs of triboelectric materials using software like COMSOL Multiphysics and MATLAB to evaluate the output performance in terms of Voc and Qsc, current, power, and voltage with respect to time for selected input parameters. The numerical method adopted in this study can be a useful tool for determining the output characteristics of any triboelectric pairs. The numerical performance of the device can be validated through experiments. Overall, the development of triboelectric nanogenerators holds a lot of promise in various applications ranging from powering sensors to biomedical devices.

5.1 Introduction

The topic of energy has garnered significant attention in the field of study due to the need to harvest energy from various sources. With the depletion of fossil fuels and increasing demand, there is a global interest in replacing them with renewable energy sources [130]. The projected population growth in both developed and developing nations by 2050 further emphasizes the need for renewable energy [131]. Additionally, as the world moves towards the Internet of Things (IoT) and artificial intelligence (AI), energy consumption has become a significant concern [132].

Batteries, while widely used, have limitations such as short lifespan, maintenance requirements, high cost, and the need for constant monitoring. As a sustainable alternative, a growing focus is on developing self-powered systems that can harness energy from their

own mechanisms [133]. This has led to the exploration of autonomous power sources for sensors, enabling them to operate independently [134]. Over the years, various mechanical energy harvesting techniques such as piezoelectric, triboelectric, and electromagnetic generators have been utilized to power self-sufficient devices by gathering mechanical energy from the environment [135].

Triboelectric nanogenerators (TENGs) are cost-effective and promising energy sources for low-powered systems. They overcome the limitations of other generators, like the need for heavy magnets, pre-charging, low power output, and toxicity. TENGs utilize contact electrification and generate electric charges when different materials with varying electron affinities come into contact. These material combinations, called tribo pairs, are selected based on their distinct electron affinities. TENGs operate in four modes: vertical contact, sliding, single electrode, and free-standing. The vertical contact mode is particularly important due to its consideration of mechanical wear. The shape, geometry, and material characteristics influence the effectiveness of TENGs.

Triboelectric materials are organized in a series according to their electron affinities, and polymer triboelectric materials are commonly utilized in this categorization. In the realm of TENG-based devices, researchers have primarily focused on dielectric materials such as PET, PMMA, Kapton, PDMS, FEP, and PTFE. These polymer-based dielectric materials are commonly employed in many TENG designs [136]. Experimental studies have unequivocally established that the output generation of TENGs is contingent upon numerous factors, encompassing work function, surface charge density, material properties, geometrical features, and operating parameters. Several strategies have been devised to augment the output of TENGs; however, implementing some of these strategies has proven challenging due to intricate designs and limited control over material properties. Additionally, the absence of simulation in the study of these devices is conspicuous. Simulation offers significant advantages, such as testing complex device designs and exercising precise control over material characteristics [73]. This enables a better understanding of device functionality and facilitates the identification of methods to enhance device performance.

Software tools like COMSOL Multiphysics, ANSYS, and MATLAB are commonly utilized for implementing these computational models. Among them, COMSOL Multi-

physics is frequently used for simulating basic TENG designs. However, existing studies often focus on the fundamental working principles and lack investigation into the effects of experimental parameters, such as dielectric thickness, different dielectric materials, area of the dielectric materials varying material properties (e.g., surface charge density), and diverse design geometries [137]. Experiments generally relate to the real-time measurement of materials utilising appropriate equipment, methods, and environments. In contrast, simulation uses more cost-effective software than experiments to construct a logical and numerical design model. In this work, we have simulated the TENG under different simulated experimental conditions ad presented the detailed results in support with the experimental results reported in the literature.

Many of the researchers in the TENG based devices focused on the different dielectric material based like PET, PMMA, Kapton, PDMS, FEP and PTFE. In the hardware designing part the above polymer based dielectric materials are used in designing of hardware devices only and there is a lack of scope in the simulation process and there is lack of validation is not done for above hardware devices. This COMSOL is a cross-platform finite element analysis, solver, and Multiphysics simulation software capable of combining multiple physics in any order to create physics-based models for simulations of real-world phenomena. With a consistent user interface, it provides the same experience regardless of engineering application and physics phenomena. To use generic physics models and save time is mostly preferred, but for the best access to the Multiphysics and equations regardless of the time and complexity of the model creation COMSOL is chosen as a tool for conducting electrostatic simulation analysis of various TENG models

5.2 Methodology

To simulate the electrostatic behavior of a triboelectric nanogenerator (TENG) using COMSOL, start by selecting the electrostatics AC/DC physics module and choose between a 2D or 3D study based on your requirements. Design the geometry of the TENG structure, either by creating it from scratch or importing designs from other CAD software for more complex geometries. Next, add appropriate materials to the different elements of the TENG structure, and if necessary, define new materials with specific

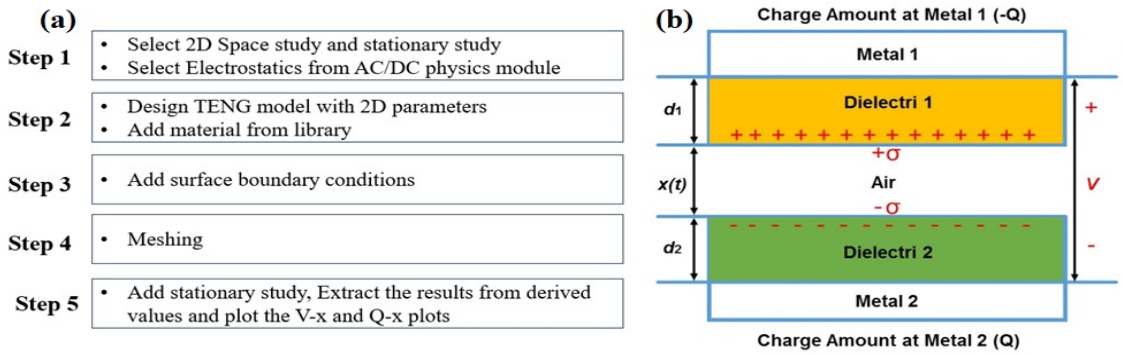

Figure 5.1: (a)The Processes of Finite Element Analysis using COMSOL Multiphysics are illustrated in a flow chart, (b) The Fundamental Structure of a Contact Separation TENG via regard to dielectric mode

Table 5.1: Symbol and its Notation

Symbol	Notation
Voc	Open Circuit Voltage
Qsc	Short Circuit Current
Q	Charge
d_1,d_2	Thicknesses of dielectrics
€r1 and €r2	Dielectric Constants
A	Contact Surface Area
$€_0$	Relative permittivity of air
x(t)	separation distance

properties. Further, For the modelling and simulation of a CS-mode TENG in this work, appropriate dielectric materials were imported from the material library of COMSOL Multiphysics. Specify boundary conditions such as initial charges, potentials, and ground references to accurately represent the TENG system. Perform meshing of the entire system to discretize the geometry for numerical calculations. Set up a stationary study to solve the electrostatic equations and analyze the outputs, including voltage (V), charge (Q), and position (x) within the TENG structure. Finally, extract the desired values and plot V-Q-x graphs using COMSOL's built-in plotting capabilities or export the data for visualization in other plotting software. The use of Gauss' electric field equations to compute the internal electric field within different portions of the TENG structure is crucial

to this approach. the computation of critical output parameters (voltage, current, and power) in a triboelectric nanogenerator (TENG) context of a triboelectric nanogenerator (TENG). The TENG structure, shown in Fig.1b, is made up of two polymer pairs with different electron affinities and linked electrodes. The methodology focuses on three dielectric zones with differing dielectric constants (€r1 and €r2), thicknesses (d1 and d2), as well as an air gap. These equations allow for the determination of electric fields, voltage (Voc), and short-circuit conditions (Qsc), establishing a solid methodological foundation for analyzing TENG performance and output.

$$E_{di-electric1} = \frac{Q}{A\epsilon_0\epsilon_{r1}} \tag{5.1}$$

$$E_{di-electric2} = \frac{Q}{A\epsilon_0\epsilon_{r2}} \tag{5.2}$$

$$E_(air - gap) = 1/e_0(Q/A - s) \tag{5.3}$$

where Q is the charge produced by the material in coulombs per metre square, A is the dielectric material's contact surface area, and ε_0 is the relative permittivity of air.

The electrical potential created across the electrode is given by Equation for a separation distance of x(t) of surface charge density.

$$V(t) = -Q/Ae_0(d_1/e_{\mathrm{r1}} + d_2/e_{\mathrm{r2}} + x(t)) + s/e_0x(t) \tag{5.4}$$

Considering open circuit (Q=0) and short circuit (V=0) conditions

$$V_{\mathrm{oc}} = (se_0)/(x(t)) \tag{5.5}$$

$$Q_{\mathrm{sc}} = (Asx(t))/((d_0 + x(t))) \tag{5.6}$$

By following these steps, one can effectively simulate and analyze the electrostatic behavior of the TENG using COMSOL

In this work, we have selected the contact-separation mode of TENG with PET and PMMA as triboelectric layers for the simulation as shown in the Figure 5.1(a) and TENG structure shown in figure 5.1(b). The table 5.2 shows the basic device parameters

used for the TENG device design in COMSOL [138]. The electrostatics submodule in COMSOL is used to analyze electrostatic force, electric field, and potential distribution. The simulations in this work take electrostatics into account. In the research part of the programme, there are choices for frequency domain, time-dependent, and stationary analysis. Because frequency change and load are not considered in this investigation, a stationary study was chosen for all simulations. Lastly, the simulation results were presented by integrating and averaging the resulting data.

The simulation process involves three major steps:

1. Geometry: In this step, the geometry of the TENG is defined and modelled using appropriate software. This includes defining the dimensions, shape, and material properties of the various components of the TENG.

2. Mesh analysis: Once the geometry has been defined, a mesh analysis is performed to create a mesh of the model. This involves dividing the geometry into small, discrete elements or cells that can be used to calculate the electrical properties of the TENG.

3. Stationary study: The final step involves performing a stationary study, which is a type of simulation that calculates the electrical properties of the TENG under steady-state conditions. This involves solving a system of equations that describe the behaviour of the TENG, taking into account the various material properties and geometrical parameters [139].

The present manuscript has studied the following
(a) In the first set of simulations, we studied the effect of surface charge density on the performance of TENG with PET-PMMA as a triboelectric pair.
(b) In the second set of simulations, we studied the effect of electrodes on the performance of TENG with PET-PMMA as a triboelectric pair.
(c) In the third set of simulations, we studied the effect of device area on the performance of TENG with PET-PMMA as a triboelectric pair.

Table 5.2: Geometries for four fundamental TENG layers with various dielectric thicknesses

Unit	Length (cm)	Width (cm)	Thickness (μm)	ε_r
Bottom electrode	5	5	130	9
Bottom dielectric (PET)	5	5	140	$\varepsilon_r = 2.3$
Top dielectric (PMMA)	5	5	125	$\varepsilon_r = 3.8, 4.2, 2, 1.8, 4$
Top electrode	5	5	130	9

5.3 Results and Discussion

Variation of surface charge density (σ) (PET, PMMA) Surface charge density plays a crucial role in the performance of a Triboelectric Nanogenerator (TENG) as it directly affects the amount of charge generated and collected during the triboelectric process. Surface charge density refers to the amount of electric charge accumulated per unit area on the surfaces of the triboelectric materials. The surface charge density directly influences the output voltage and current of the TENG. A higher surface charge density leads to a higher voltage potential difference between the electrodes, resulting in a larger open-circuit voltage (Voc). A greater surface charge density also enables a higher charge transfer, leading to increased short-circuit current (Isc) and overall power output. In this study, simulations were performed for different surface charge densities of triboelectric layers, while maintaining other parameters constant for the triboelectric pair (PMMA-PET), area of the devices, and electrodes. The detailed simulation parameters are presented in Table.5.1. The surface charge densities are varied from 8e-4 to 8e-10. Figure 5.2 (a) - (f) displays simulation images of the potential distribution during the separation of the triboelectric layers

Surface charge density was varied from 8×10^{-4} to 8×10^{-10}.

As expected with increase of surface charge density of triboelectric layers, the V_{oc} and Isc has increased as shown in Figure 5 (g). This study suggests that surface charge density enhancement by different surface modification methods helps achieve higher output powers. In the literature, few works reported on surface charge density enhancement

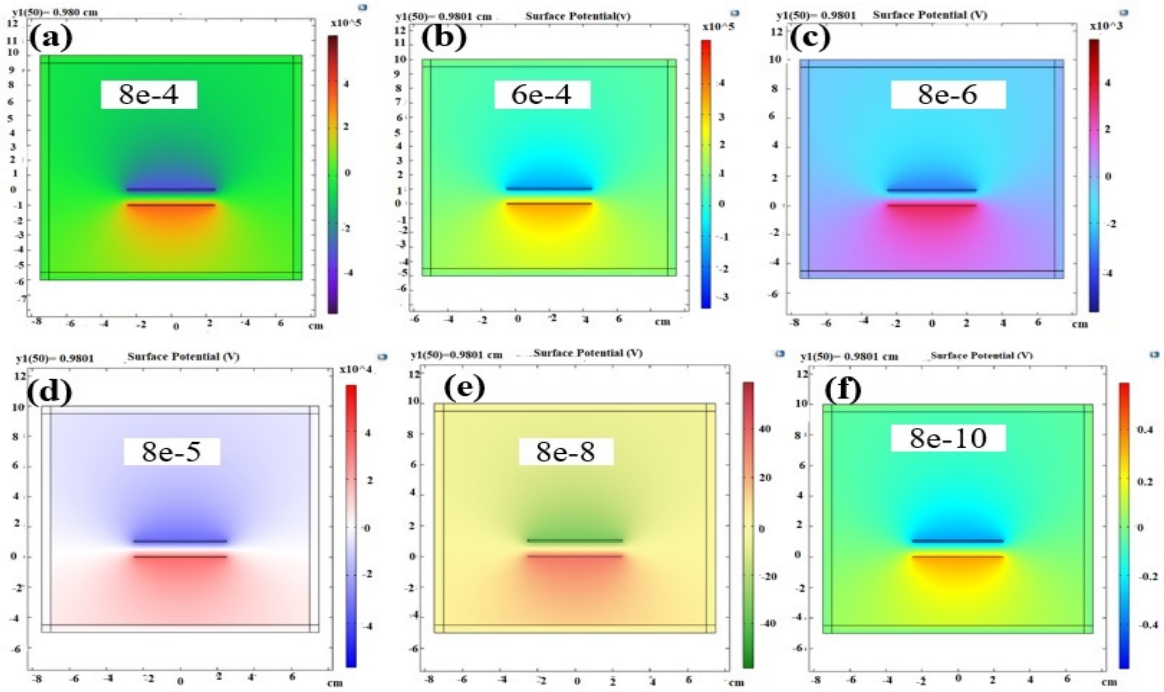

Figure 5.2: Variation of Surface Charge Densities and its corresponding open circuit voltages (a) $\sigma = 8\ e^{-4}$ (b) $\sigma = 6\ e^{-4}$ (c) $\sigma = 8\ e^{-6}$ (d) $\sigma = 8\ e^{-5}$ (e) $\sigma = 8\ e^{-8}$ (f) $\sigma = 8\ e^{-10}$

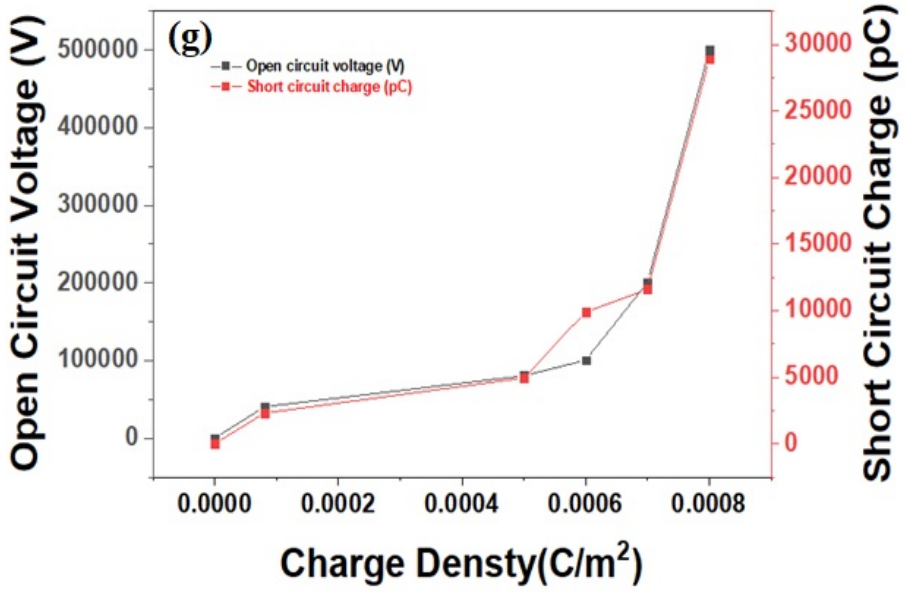

Figure 5.3: (g) Open circuit voltage and short circuit charge vs Charge density

through increasing surface roughness [140], surface treatment with plasma [141], and surface polarization with an external electric field [142].

Table 5.3: Diiferent Electrodes thicknesses used in TENG

Name of the units	Length (cm)	Width (cm)	Thickness (μm)
Aluminium	5	5	130
Bottom dielectric (PET)	5	5	140
Top dielectric (PMMA)	5	5	125
Copper	5	5	130
Gold	5	5	130
Titanium	5	5	130
Nickel	5	5	130

5.3.1 Variation of Electrode Pairs

Electrodes play a crucial role in performing a Triboelectric Nanogenerator (TENG) as they collect and transfer the generated charge. The properties and characteristics of the electrodes can significantly impact the TENG's performance. Simulations were performed using different combinations of top and bottom electrodes while maintaining constant parameters such as the triboelectric pair (PMMA-PET). The electrode combinations investigated were Al-Al, Au-Au, Cu-Cu, Ni-Ni, and Ti-Ti. The detailed simulation parameters are presented in Table.2. Figure 5.4 (a)-(e) displays simulation images of the potential distribution during the separation of the triboelectric layers. These images were captured at the same vertical distance between the layers to facilitate better comparisons. Additionally, Voc (open-circuit voltage) and Isc (short-circuit current) values were extracted from the simulations and presented in Figure 5.4 (f)-(j) and. Further, we have tested Cu-Cu, Al-Al, Au-Au,Ni-Ni,Ti-Ti- found similar results

The results indicate that the permittivity value of the electrodes has a negligible impact on the output parameters of Voc and Qsc. Consequently, any combination of metal electrodes produces nearly identical outputs for the triboelectric nanogenerator (TENG). These findings align with previous experimental research reported in the literature [143].

Figure 3(k) represents the Voc and Qsc of different electrode combinations for Al act as electrode top and bottom, PET and PMMA act as the dielectrics for the top and bottom layers, and there is no change in both the responses by changing the electrodes. In the

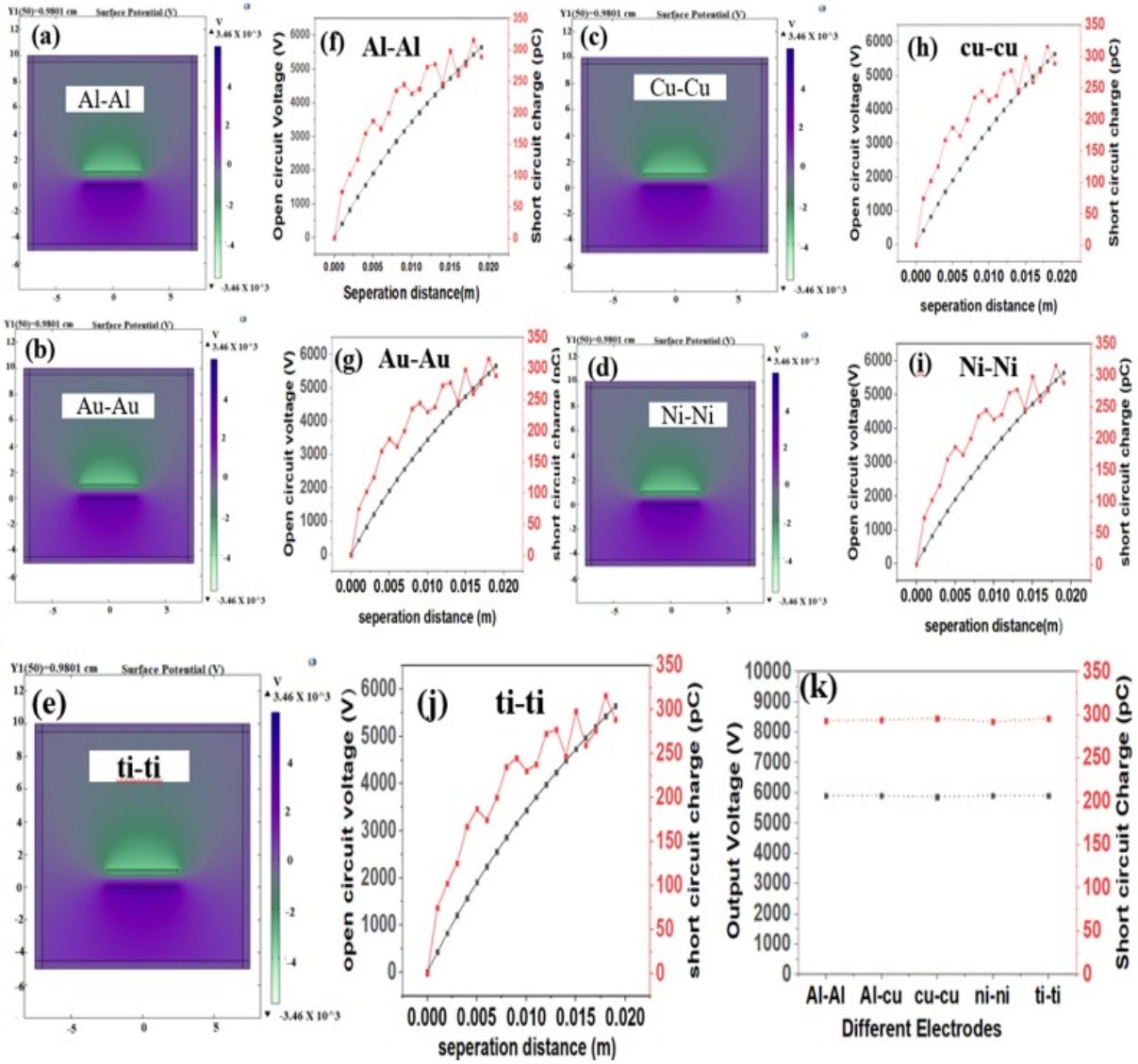

Figure 5.4: Different Electrodes Combination of TENG (a) Al-Al (b) Cu-Cu (c) Au-Au (d) Ni-Ni (e) Ti-Ti. (f – g) Voc and Qsc of different electrode combinations. (k) Open circuit voltage and short circuit charge vs electrode combinations

first set of simulations, the active contact area of the PET-PMMA triboelectric layer was varied while keeping other parameters constant, as mentioned in the Table.3. The contact area varied from 2 x 2 to 8 x 8 cm^2, and the corresponding potential distributions were illustrated in the provided Figure 4 (a-c). Additionally, the open-circuit voltage (Voc) and charge transferred (Qsc) were obtained by varying the separation distance between the triboelectric layers, as shown in the Figure 5 (a) and (b). The results clearly indicate that both Voc and Qsc increase proportionally with the device's active area enlargement. The expansion of the active area leads to an increased number of contact points between the

triboelectric layers, resulting in higher output voltage and charge generation. The impact of the device's size, represented by the area of the triboelectric layer, on the TENG output has been extensively studied by researchers worldwide, and the observed trends in both simulations and real-time experiments align with each other [144] Overall, the findings highlight the importance of the active contact area in determining the performance of the TENG, demonstrating that a larger device size leads to enhanced output characteristics. The open circuit voltage of the CS TENG device is also increases and the corresponding short circuit.

Overall, this simulation aims to provide insights into how the relative dielectric constant of the PMMA affects the performance of a CS-mode TENG, which can help in the design and optimization of TENG devices for various applications.

5.3.2 Variation of An Active Contact Area of the Device:

As shown below in the figure the contact area increases from 2 x 2 cm ^{2} to 8 x 8 cm^2 the corresponding open circuit voltage of CS TENG device is also increases and corresponding short circuit charge is also to be increased as increasing of the contact area of the device.

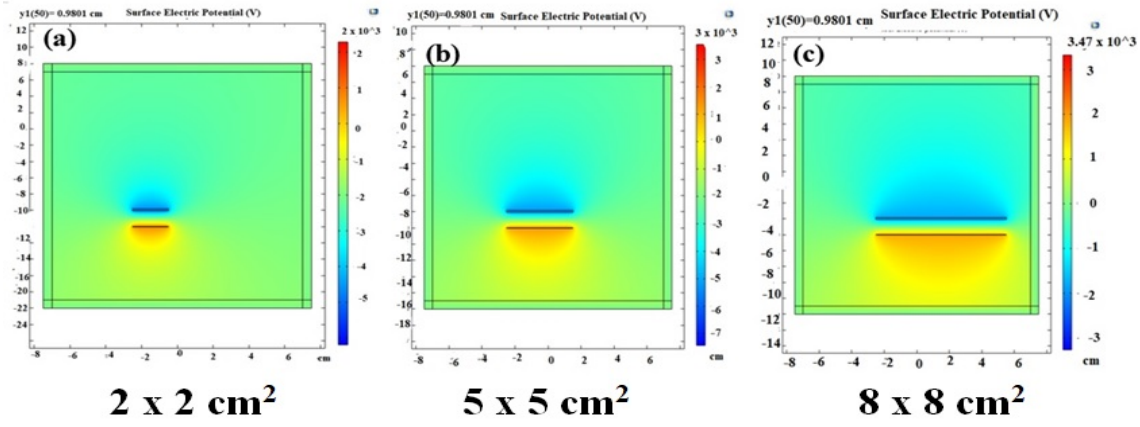

Figure 5.5: Electric Potential Distribution for CS mode TENG considering three different contact areas

In the first set of simulations, the active contact area of the PET-PMMA triboelectric layer was varied while keeping other parameters constant, as mentioned in the

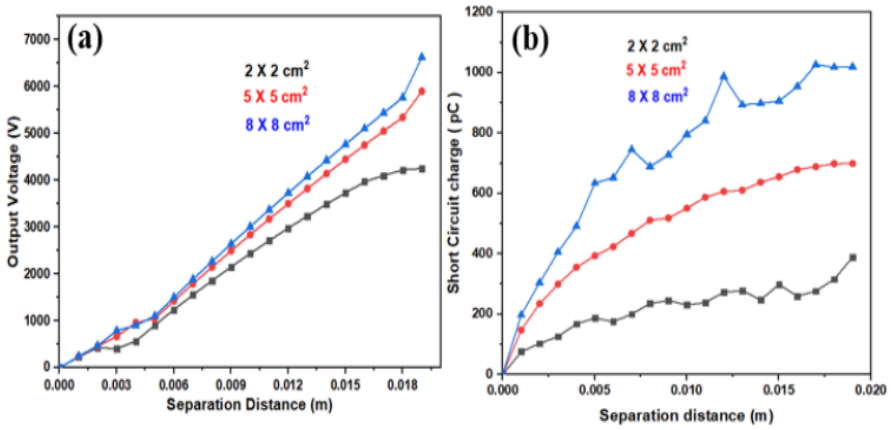

Figure 5.6: : (a) Varying Contact Area Corresponding output voltage responses (b) Short Circuit Charge

Table.3. The contact area varied from 2 x 2 to 8 x 8 cm^2, and the corresponding potential distributions were illustrated in the provided Figure 5.4 (a - c). Additionally, the open-circuit voltage (Voc) and charge transferred (Qsc) were obtained by varying the separation distance between the triboelectric layers, as shown in the Figure 5.6 (a) and (b). The results clearly indicate that both Voc and Qsc increase proportionally with the device's active area enlargement. The expansion of the active area leads to an increased number of contact points between the triboelectric layers, resulting in higher output voltage and charge generation. The impact of the device's size, represented by the area of the triboelectric layer, on the TENG output has been extensively studied by researchers worldwide, and the observed trends in both simulations and real-time experiments align with each other [17] Overall, the findings highlight the importance of the active contact area in determining the performance of the TENG, demonstrating that a larger device size leads to enhanced output characteristics. The open circuit voltage of the CS TENG device is also increases and the corresponding short circuit.

5.3.3 Scaling Factor

Scaling factor is calculated using following way

1. Measured the simulation and practical open circuit voltages for designed TENG device for different contact areas ranging from 2 x2 cm_2 to 16 x 16 cm_2.

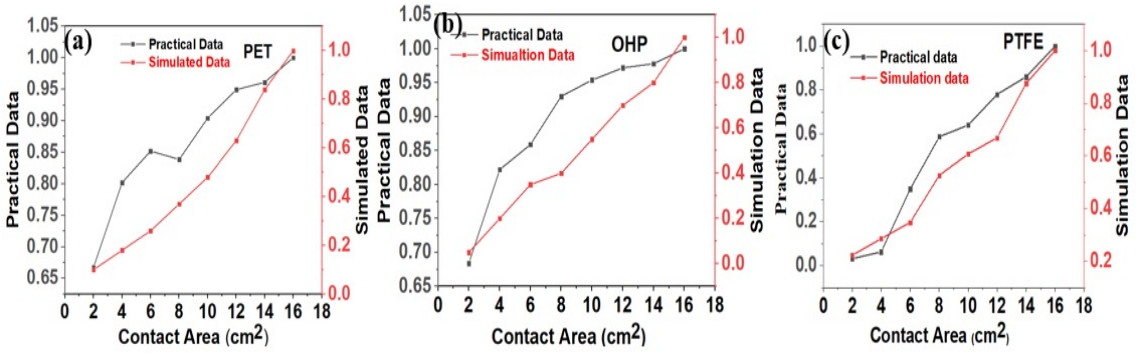

Figure 5.7: Scaling Factor for both practical and simulation data under different contact area (cm^2)

2.Calculated the scaling factor value for corresponding specific TENG area device to maximum area TENG device value.

3.Finally, measured the difference between the simulated and practical value.

Below Figure 5.7 (a - c) represents the scaling factor graph for Al/PMMA/Al, Al/PET/Al and Al/OHP/Al structures in the case of both simulation and experimental. Contact area increases from 2 x 2 cm^2 to 16 x 16 cm^2 corresponding output response is measured in both practical and simulation cases. Scaling factor is calculated for practical and simulation both the cases and conclude that the variation is nearly similar in the both the cases shown in the below Table 5.3 and maximum response is observed in simulation study.

Table 5.4: Scaling factor Comparison for Practical and Simualtion Data

Di-electric Material	**Practical Data**	**Simulation Data**
PMMA	0.8773	0.876
OHP	0.867	0.6447
PET	0.852	0.6325

5.4 Conclusion

In this work, the authors delve into the world of Triboelectric Nanogenerators (TENGs) with a particular focus on harnessing computational and numerical simulations to advance their performance in the realm of renewable energy generation. The paper extensively explores the application of software tools such as COMSOL Multiphysics and MATLAB to create simulations that provide valuable insights into the behavior of TENG systems. The methodology section guides researchers through the process of setting up and conducting these simulations, allowing for the thorough examination of TENG performance under various conditions. The study investigates three key aspects of TENG performance: the influence of surface charge density, the role of different electrode pairs, and the impact of the active contact area on TENG output. Remarkably, the results reveal that optimizing these factors can significantly enhance TENG performance, providing a promising avenue for advancing the development and utilization of TENGs in the renewable energy sector.

Summary: In this chapter, we used the COMSOL framework to simulate Triboelectric Nanogenerators (TENGs). We employed the same electrode and dielectric materials as in previous studies, allowing us to compare models to actual data. The TENG device was fully characterised in a variety of methods, including measuring contact area and surface charge density, testing alternative electrode topologies, and comparing single and two dielectric combinations. The simulations made use of pre-existing COMSOL polymers, assuring relevance to real-world applications. We carefully determined scaling factors to achieve a significant connection between simulated and actual findings, and the two techniques agreed astonishingly well. This consistency verifies our simulations and enhances confidence in the performance forecasts of the TENG device.

The previous two chapters concentrated on the device's design and simulation with the COMSOL programme. We evaluated and correlated the simulated results with our experimental data. However, in the next chapter, we will look into the feasibility of introducing AI (Artificial Intelligence) into the TENG process. This will allow us to address and investigate new TENG technology potential and uses.

Chapter 6

AI Based Power Prediction to TENG Devices

This chapter describes about the generating the own data set from designed TENG device and that dataset is divided into two parts training and testing data. Firstly, the data divided into three classifiers depending upon the output response of the voltage and each classifier also divided into training and testing divisions. Then training and testing data giving to Machine learning algorithms and finding accuracy of the model and for best model extracted the confusion matrix and from that evaluated the performance metrics.Deep learning techniques were used when the dataset had been increased to select the regression procedure with the lowest loss.

In this thesis, the entirety of machine learning (ML) and deep learning (DL) algorithms is predicated on a synthesized dataset generated from Triboelectric Nanogenerator (TENG) experiments. The dataset, accessible via the following link http://tinyurl.com/CS-TENG-DATASET, serves as the foundational source for training and evaluating the demonstrated models. By utilizing this unique dataset, derived from TENG, the research aims to enhance the robustness and applicability of the ML and DL algorithms discussed herein.

6.1 INTRODUCTION

The creation of tiny power sources has presented several difficulties to drive wearable electronic devices. The concepts of piezoelectricity [145], triboelectricity [115], pyroelectricity, elec- tromagnetism [146], and solar cells [147] have all received attention from researchers. Triboelectric nanogenerators (TENGs) are among them; they are energy harvesters that use mechanical energy to create green energy and run small electronic devices [148]. TENGs work by contact electrification and electrostatic induction principles. TENGs can operate in one of four different ways: single electrode (SE), contact separation (CS) mode, lateral sliding (LS) mode, and free standing (FS) mode in triboelectric-layer. Furthermore, machine learning (ML) approaches to prediction a data analysis are progressively gaining popularity as AI technology advances quickly. The idea behind machine learning is that a computer programme can pick up new piece of information from the operating process and adjust to it without human intervention. Artificial intelligence (AI discipline)'s of machine learning updates a computer's internal algorithms from the readout data. Artificial intelligence is the trending technology that has been used in almost every field to open new doors for the better ways to solve real world problems. Machine learning has large scope in the interdisciplinary research also, for instance in the areas of Protein structure prediction [149], drug discovery and development [150], TENG-based self-powered sensors [151], design of de novo proteins which do not exist yet , Li-plating on graphite electrode [152]. Jiao Pengcheng [153] demonstrate d that deep learning approach can take crucial role to obtain optimal design of nanogenerators and their predictive tuning in the electromechanical performance. Y. Zhou [50] demonstrate d that huge amount of data can be collected using TENG which can be further used to analyse using artificial intelligence to build deep learning models that can predict our output variable.

The CS mode is the most effective of the four operating modes in terms of power supply and wide- ranging uses in TENG. As a result, the focus of this work is on CS-mode TENGs. The study of triboelectric nanogenerators has advanced recently and been looking for answers to issues like enhancing output optimization of generator architectures, performance, and conversion efficiency. AI is able to do more in nano energy research than merely process and evaluate data. The technological restrictions of a realization for the

prediction and optimization of nano-energy are made possible by TENGs in Orientation, mechanism study, testing, prototype design, and performance estimate. This study makes use of AI techniques to gather experimental data and create databases. A training set, a validation set, and a test set were created from the data set. After the training set data was used to train an ML model that was optimized by KNN technique, the accuracy of the model was then tested using the validation set data. A wide variety of triboelectric layer pairs tested for energy harvesting and demonstrated for potential practical applications are summarized in figure 6.1. The use of Artificial Intelligence (AI) algorithms for

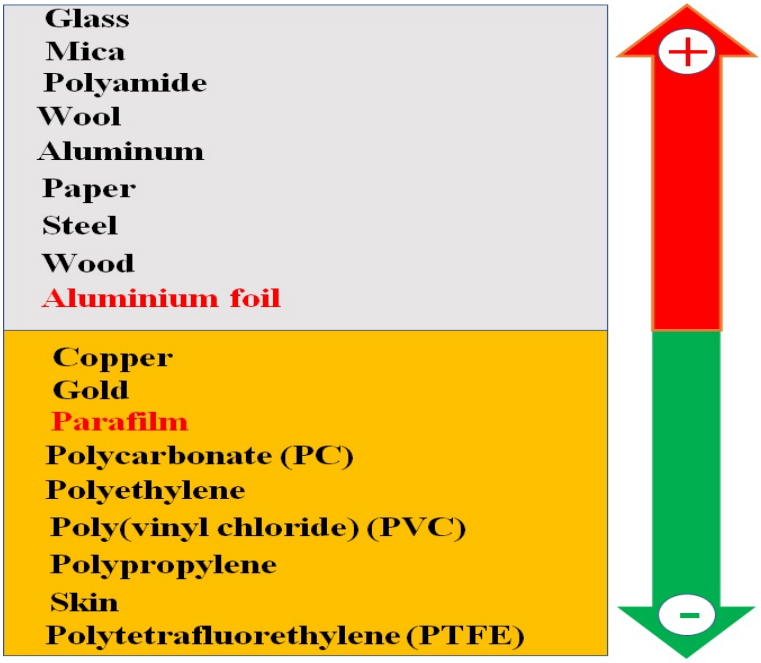

Figure 6.1: Triboelectric series including present work

analyzing practical data has increased with the advent of AI models. Combining physics and engineering has garnered a lot of interest so much, so that the triboelectric Nanogenerators (TENG) industry may also use AI technologies. In this work, the classifiers suitable for predicting the system accuracy for TENG are analyzed. The experimental data used for training and testing, and two of the Machine Learning (ML) classifiers provided promising results: K Nearest Neighbor (KNN) and Neural Network (NN). Different ML parameters are generated such as precision, recall and F1 score with the help of Confusion matrix for KNN and NN of the practical TENG energy data. Additionally, we assess the TENG's output quality in CS mode under various load factors using ML models

6.1.1 METHODOLOGY

TENG Structure and working mechanism

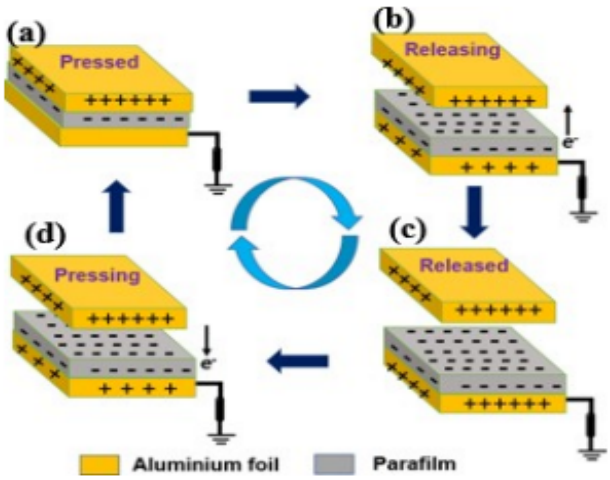

Figure 6.2: Working procedure of the TENG

The structure of TENG is electrode-dielectric (para-film) and electrode separated with spacer. In the initial state, neither a charge transfer nor an electric potential exists before the para-film makes contact with the top Aluminium electrode, as seen in Figure 6.2(a). Due to their distinct capacities for gaining or losing charge, para-film and aluminium exchange charges when they come into contact, as seen in Figure 6.2(b). The TENG is kept in a balanced condition by the parafilm's negative charge and aluminum's equal amount of positive charge. The balance is in favor of separation as the TENG begins to separate the electrical potential difference exist between the top and bottom electrodes. A balanced state is reestablished because of the parafilm's ability to hold charges on its surface while keeping it unaltered. As demonstrated in Figure 6.2(c), the parafilm transfers the charges on the electrode surface to the aluminium. The electrical balance is disrupted and then restored when the two surfaces are brought back together,and charges go from the aluminium to the parafilm electrode in this condition until equilibrium is achieved in Figure 6.2(d). Triboelectric charges on the parafilm during the process of periodic contact separation result in periodic movement of free electrons on the top and bottom of Aluminum electrodes, this process generates electron flows to drive external low power gadgets/devices and sensors.

6.1.2 Machine Learning for CTENG

Need for Machine learning

Finding the accuracy of CS TENG structure and with the help of experimental data, train and test it through ML classifiers enables accuracy of TENG.

K Nearest Neighbor (KNN)

KNN has a few benefits over other models, such as the fact that it requires no training prior to prediction and is simpler to build than other ML methods. The below Figure 6.4 represents the basic structure of KNN. The input parameters for KNN are considering for our data set is load resistance, output voltage, current and power. We divide the total number of samples into training and testing in the ratio of 80:20.KNN is having few specific features like classification learning and performance assessment with cross validation compared to other ML algorithms. KNN is effectively used for small datasets, our data set belongs to 600 samples only which is consider to small to compared to remaining datasets . Flow chart for execution of ML algorithm show in Figure 6.3:

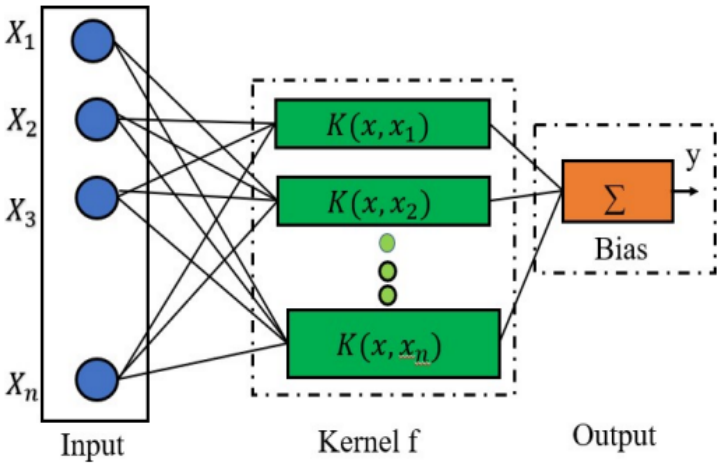

Figure 6.3: Structure of KNN

Step 1: Experimental data from the TENG can be enhanced using 3 classifiers of increasing, saturation and decreasing ranges. .

Step 2: from the experimental data classify the data as meant for training and testing purpose.

Step 3: both training and testing data will be given to ML classifiers to extract ML metrics.

Step 4: from the ML metrics obtained, admire at the best ML algorithm is suitable for TENG device.

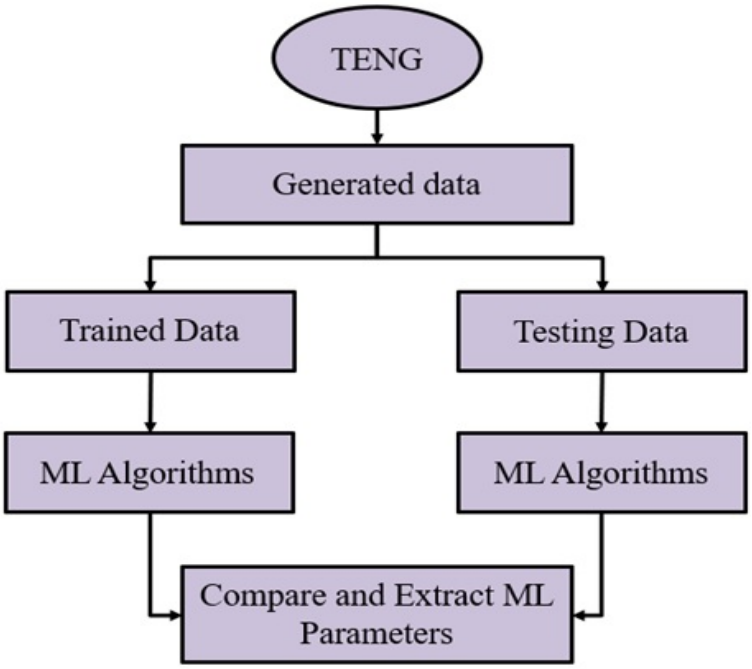

Figure 6.4: Flow chart for demonstrate d Method

6.1.3 EXPERIMENTAL RESULTS AND DISCUSSION

APA (Aluminium parafilm Aluminium) TENG The below sub section of the Figure 6.5 represents the basic structure of TENG which is operated in CS mode. In this structure, top and bottom electrodes are aluminium foils and parafilm, which act as dielectric material and their thickness is 35 µm and 180 µm respectively. According to the maximum power transmission theorem, the maximum output power density is obtained when the load resistance is equal to internal resistance. In the Figure 6.5, the maximum power is obtained at a load resistance of 1.8 MΩ because of saturated output voltage [100].Several popular machine learning models are trained and tested and promising results obtained in

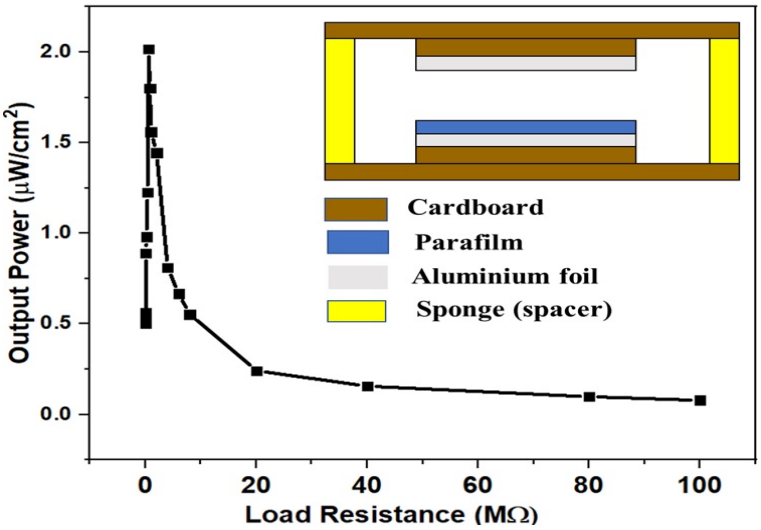

Figure 6.5: TENG Structure and Output Power Density [2]

the case of both testing and training accuracy for both KNN and neural networks (NN). In the case of MSME, the highest value is obtained for KNN in both training and testing analysis.

6.1.4 Results and Discussions

Inputs considerations for testing and training

Step 1: given data set divided into two sub sections one is used for training and second one is used for testing.

Step 2: Using MATLAB machine learning app import the training data according our classification and feed to different machine learning algorithms which are inbuilt in the software.

Step 3: After executing training data different metrics are obtained for each ML algorithm like Confusion matrix, ROC curve. From the confusion matrix calculated the Precision, recall and F1 score using the relation among them.

Step 4: Similarly step 2 is repeated for testing data also and obtained the accuracy for different ML algorithms and compare the both training and testing results.

Out of 600 samples, 480 samples assigned for training and 120 assigned for testing

including three classifiers. In the case of KNN algorithm in machine learning, the training accuracy is 97.1% and testing accuracy is 66.5%. The same classifier is used for training and testing had been done several times and there was no change in accuracy value in both training and testing case and the confusion matrix also give more promising results compared to other classifiers in ML. In the regression model also, RMSE values were effective in the case of Kernel algorithm with a training value of 0.13304 and testing value 0.66 when compared to other models in the ML. In the classifier learner module in MATLAB, excel data was provided as input and training and testing were carried out to compare the accuracy performance for all ML algorithms and it was concluded that KNN and neural networks gave most promising results in both training and testing cases. Following that, for both models, confusion matrix was generated.

The below Figures 6.6 and 6.7 represents the confusion matrix of KNN and NN for 600 samples of TENG enhanced data. Confusion matrix is classified to three classifiers labelling 1,2 and 3 as shown in Figures 6.6 and 6.7 for true and predicting classes.True positive (TP) values are represented with blue colour for both confusion matrix es for KNN and NN. With the help of confusion matrix and relation with precision, recall and F1 score calculated according to formulae as shown below equations [1-4]. Using same data Accuracy, precision, recall and F1 score represented for KNN and NN in Table 3. Table 1 describes about the different algorithms in ML is performed in case of both training and testing dataset.Figure 6.8 represents the accuracy comparison of the ML models in the case both training and testing, the difference between training testing accuracy is less for two ML methods i.e KNN and NN. So, that in the accuracy point of view in both training and testing both methods are preferable compared remaining existing methods like decision tree, KN bays and SVM. Regression method for various Machine Learning Algorithms Table 2 represents the regression process for ML algorithms and prominent results are occurred in the case KNN and NN and graphical representation of various ML algorithms are showing in figure 6.9 and in the case of training process Neural network and KNN is having less error compared to remaining ML models and in the case of testing also high values are obtaining for the both cases. So that the two models are better for our dataset and divide our data set into training and testing by using basic rule of machine learning 80:20 for the 100 samples.

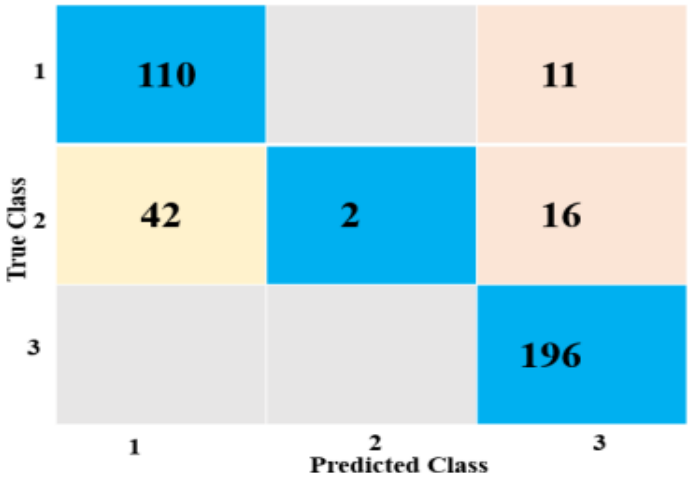

Figure 6.6: Confusion Matrix of KNN

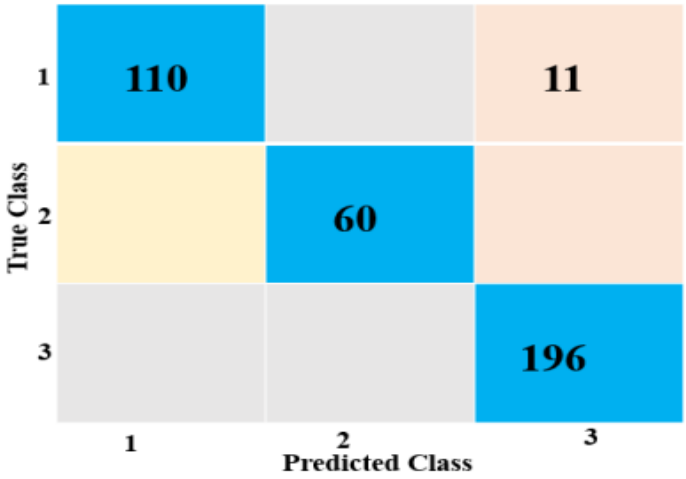

Figure 6.7: Confusion Matrix of NN

Table 6.1: Machine Learning Algorithms Comparison

Model	**Training accuracy(%)**	**Testing accuracy(%)**
Fine tree	100	78.4
Kernel Noise Bays	100	81
Linear SVM	98	60.3
Fine KNN	97.1	66.4
Coarse KNN	**81.7**	**86.2**
Neural Network	**97**	**76.7**

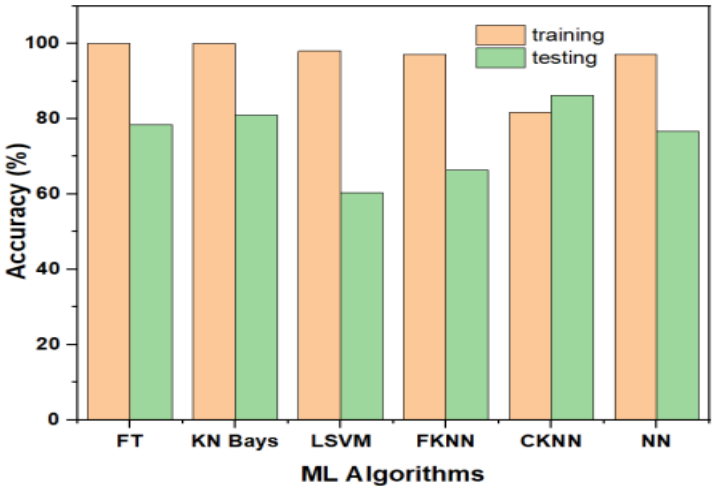

Figure 6.8: Comparative Accuracy Graph for various Machine Learning Algorithms

In the below Table 6.1 represents the ML parameters like accuracy, precision, recall and F1 are calculated with the help of confusion matrix and their related formulae for both the KNN and NN their values shown below.

$$\text{Accuracy} = \frac{TP + TN}{TP + TN + FP + FN}$$
$$\text{Specificity} = \frac{TN}{TN + FP}$$
$$\text{Precision} = \frac{TP}{TP + FP}$$
$$\text{Recall} = \frac{TP}{TP + FN}$$

Classification problems in machine learning involve pre- dicting the class labels of input data. There are several performance metrics that are commonly used to evaluate the performance of a classification model.

Accuracy: Accuracy is one of the most commonly used metrics to evaluate the performance of a classification model. It measures the proportion of correct predictions made by the model.While accuracy is a useful metric for many classifi- cation problems, it can be misleading when the classes are imbalanced, i.e., when one class has a much larger number of samples than the other. In such cases, a model that always predicts the majority class can achieve a high accuracy even though it is not a good model.

Precision: Precision measures the proportion of true positive predictions among

all positive predictions made by the model. Precision is an important metric when the cost of false positives is high, i.e., when it is important to avoid predicting a positive label when the true label is negative.

Recall: Recall measures the proportion of true positive predictions among all actual positive samples. Recall is an important metric when the cost of false negatives is high, i.e., when it is important to avoid predicting a negative label when the true label is positive.

F1 Score: The F1 score is a harmonic mean of precision and recall. It is a good metric to use when we want to balance the importance of precision and recall.

Table 6.2: Comparative Analysis for various Machine Learning Algorithms

Model Name	**Training**	**Testing**
Linear	0.16691	0.44
SVM	0.17511	0.44076
Gaussian	0.014587	0.434
NN	0.021194	0.48055
NN	0.021194	0.48055
KNN	0.13304	0.66

Table 6.3: Machine Learning performance parameters

Parameter	**KNN**	**NN**
Accuracy	97.1	97
Precision	0.9	0.93
Recall	0.82	0.90
F1	0.92	0.947

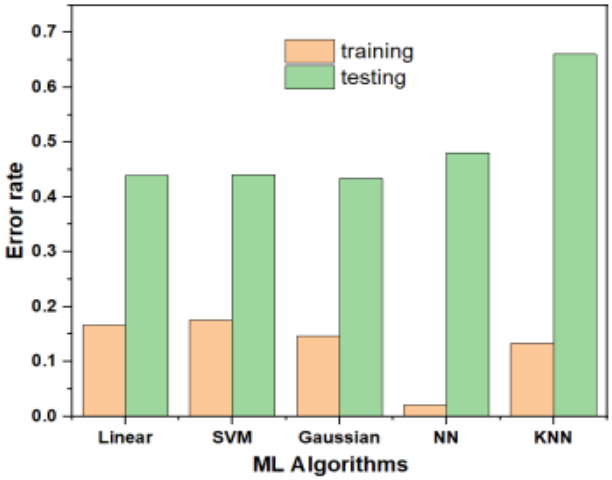

Figure 6.9: Comparison of Regression Graphs for different ML algorithms

6.1.5 CONCLUSION

In this study, a general KNN model in machine learning was suggested to predict the accuracy of the TENG. To get the output performance of TENGs, we apply the same KNN model to CS TENG structures. We create datasets from experimental data. A training set and a test set were created from the data set. Data from the test set was then used to verify the model's accuracy after the training set data was used to train KNN model.From the obtained confusion matrix of KNN and NN extracted the performance metrics of ML.KNN is giving better results in case of classification type dataset and, our enhanced data set is also classified data, for that reason KNN is having better results compared other ML models.

6.2 Accurate Output Power Prediction in TENG Devices Using Artificial Intelligence: A Comparative Analysis

6.2.1 Introduction

Numerous efforts are currently underway to develop alternative energy production technologies that can meet the increasing demand which are good for environment as well. The extraction of natural energy, such as solar energy [34], thermal energy [154], wind energy [155], and mechanical energy [156], has grown in popularity. Traditional energy harvesting systems, such as wind turbines, thermoelectric generators and solar cells, largely depend upon certain environmental parameters for reliable functioning, such as steady sunshine, wind power and temperature [157]. As a result, it is very important to create more ecological solution and energy acquisition techniques that are very optimal. Recent advancements in the technologies such as IoT, AI cloud computing have given rise to user-centric functional wearable electronics, offering new opportunities in this domain. As a result, lightweight, compact, and long-term power sources are always in demand [158, 159, 105]. These energy sources must also be adaptable, ecologically benign, lightweight, and long-lasting [160]. Mechanical energy harvesting has gained attention as a very good method in creating self-powered microsystems which are integrated and wearable. It offers a solution to the drawbacks associated with traditional energy storage systems like capacitors and batteries, including their limited capacity, short lifespan, frequent recharging, and safety concerns. By harnessing mechanical energy, these systems can overcome these limitations and provide a sustainable and reliable power source for various applications. As a result, there has been a boom in interest in micro/nanoscale energy harvesting technology. There has been so much exploration of different technologies in the mechanical energy harvesting realm, including, electromagnetic microgenerators (EMGs) and piezoelectric nanogenerators (PENGs) [161] triboelectric nanogenerators (TENGs) [162]. By using nanogenerators different applications like bio memristor [99, 65], eco-friendly green electronics [68] and security purpose also [63]. Among these, TENG has showed particular potential in turning low-frequency mechanical energy into electricity

[13]. The research in this area has been dedicated to achieving high production performance, design that is very lightweight, cost-effectiveness, appropriate selection of the material, design simplicity, and environmental sustainability [163]. The goal is to optimize TENGs for efficient energy generation by exploring different materials, designs, and manufacturing techniques, while also considering their impact on the environment.

The operation of a TENG device is mainly depends on electrostatic induction and contact electrification principles [164]. The very fundamental working principle of TENG involves the interaction between two different materials, which become electrically charged upon contact [37]. When these material surfaces come into contact, there is a transfer of charges, leading to the creation of surface charges of both positive and negative in equal amounts. Charge exchange's efficiency is determined by the materials' position that is present in the triboelectric series. This is used to classify the materials; this classification is done by the ability of the device how capable it is while gaining or losing the electrons [165]. Among all the operating modes of TENG, Vertical contact-separation mode (VCSTENG) is the most generally preferred [117]. Because of the advantages of the Vertical contact-separation mode, in [28]they used this mode in their work.

Lot of investigations have been carried out by researchers for innovative triboelectric materials for improving energy conversion efficiency while lowering the making cost and complexity of TENG devices. A growing trend is the utilization of waste materials for generating electricity, which contributes to environmental pollution reduction. Several studies have been published on the application of waste materials as novel triboelectric materials for energy harvesting. These waste materials include discarded milk cartons [166], eggshell membranes [77], tea leaves [39], orange peel [108] wastages like fish scales [109], rice husk [45], recycled PVC cling film [110], used plastic bags [37] and wastage from sugar cane [38]. By repurposing these waste materials for TENG applications, researchers aim to minimize environmental impact while achieving efficient energy harvesting.

Artificial intelligence, a popular and frequently used technology, is used in a variety of sectors to provide novel answers to real-world problems. Deep learning has large scope in the interdisciplinary research also, for instance in the areas of Protein structure prediction [167] , drug discovery and development [168, 169], solving the mechanical materials computation problems [148], TENG-based self-powered sensors [170], design of de

novo proteins which do not exist yet [171], Li-plating on graphite electrode [172]. Jiao Pengcheng [173] demonstrate d that deep learning approach can take crucial role to obtain optimal design of nanogenerators and their predictive tuning in the electromechanical performance. Y. Zhou [174] demonstrate d that huge amount of data can be collected using TENG which can be further used to analyse using artificial intelligence to build deep learning models that can predict our output variable.

The utilization of artificial intelligence (AI) algorithms in the fields of engineering and physics has experienced a substantial growth in recent years. AI technology can be helpful in analyzing experimental data, predicting outcomes, and discovering patterns in complex systems. Consequently, in the area of triboelectric nanogenerators (TENG) adopted AI technology for energy prediction, generation and usage in real-time applications. The analysis of how structural characteristics impact output performance in physical tests can present occasional challenges and limitations. TENGs' structure varies over a narrow range, which makes experiment control challenging. For anticipating the performance of triboelectric nanogenerators output on these parameters like non-identical structures and configurations. This study performs parameter evaluation of TENGs using five deep learning and five machine learning models. The results reveal that the DNN model accurately predicts the expected output power levels for TENGs with the contact separation (CS) mode structure which is very much close to the value that are obtained by doing experimentation physically. In the CS mode structure for the data of output power of TENG device which was not trained also can be predicted with the AI model. The demonstrate d model will absolutely aid researchers in their analysis of the data law over a larger range of parameter values, leading to a more accurate experimental law. The obtained error 0.0043 difference to actual value is less for the deep learning model when compared to ML model error 0.0618 based on the output power for load resistance of 0.5 MΩ.

The main contribution of this work

1. Extracted the real time data from the designed APA TENG that means by varying the output load resistance corresponding output voltage is measured and from that different dependent parameters are noted like output current, output power and its power density.

2. By using inbuilt ML and DL models from the above data we created the data set in to training and testing and that data is given to above models and predicted the output power for the Unknown resistance which is not measured practically and for the measured resistance the difference between both the values is having less error for Adam optimizer for DL and Random forest in case of ML.

6.2.2 Hardware Section

Method and Materials

We have built different ML models and DL models and trained those models with our dataset which is obtained through experimental results. Then using the test dataset each model is tested for the correctness of predictions and to check the performance of our models. And we have considered the most common performance metrics for the regression analysis like "Mean Square, Mean absolute, and Root mean square errors", "R2-score". In deep learning method we have developed Deep Neural network with different number of layers and tested with different optimizers to see which model is giving good results that predicts the output power with minimal error. The problems in TENG design such as high cost and inefficiency can be solved with this type of prediction models and provide good solution for TENG design. Triboelectric series including present work is given in Figure 6.10 (a).

6.2.3 Working of Hardware APA TENG

In summary, the initial state of the triboelectric nanogenerator (TENG) is characterized by a balanced condition with no transfer of charge or electric potential. However, when the parafilm comes into contact with the top aluminium electrode, there is a phenomenon of charge exchange. This causes a negative charge to accumulate on the parafilm and an equivalent amount of positive charge to accumulate on the aluminium electrode. So, because of this an electrical potential difference is created, leading the TENG to lose its equilibrium. Charges may be held on the surface of the parafilm, allowing charges to be moved in and out between the electrodes to restore balance. Through periodic

interaction and separation of the TENG. On the parafilm, Triboelectric charges present on it cause the passage of electrons that are free on the aluminium electrodes. Electrical output is generated in the external circuit because of electron flow. The TENG working mechanism is given in Figure 6(b).

6.2.4 Software Methodology:

Machine Learning Techniques:

In machine learning, regression analysis is a statistical method used to describe the connection between dependent and independent variables. Based on independent factors such as output current, output voltage, and load resistance, it predicts the dependent variable, in this example, output power. Regression is a type of supervised learning that builds connections between various variables. A regression line is displayed to best match the data points on a scatter plot in regression analysis, demonstrating the overall trend and the strength of the link between variables. The residual error is represented by the vertical distance between the data points and the regression line, which should be minimised. I **Linear regression:** It is a technique commonly employed for predictive

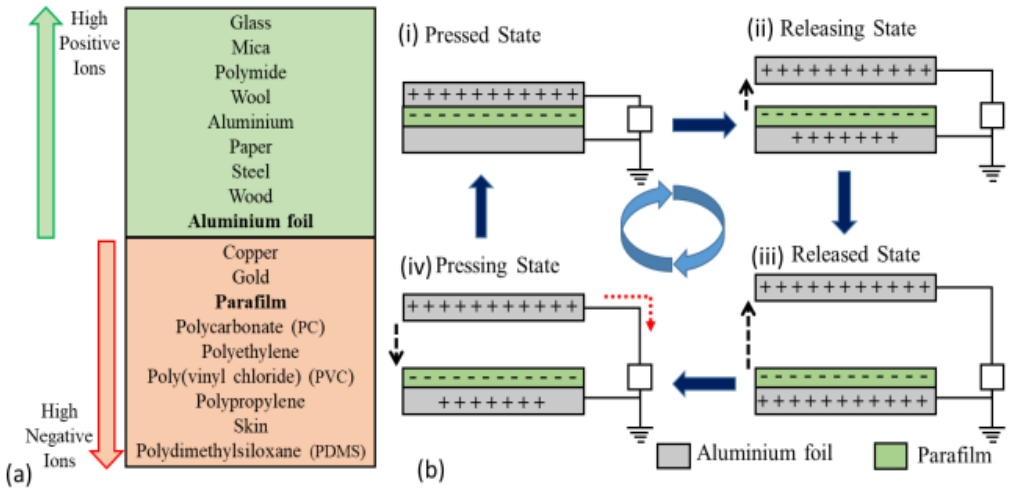

Figure 6.10: (a) Materials used in the work (b) Working mechanism of TENG

analysis. It is used to establish a relationship between continuous variables and can be applied to solve regression problems, enabling the prediction of a specific quantity. The method establishes a relationship between the independent, dependent variables. This is

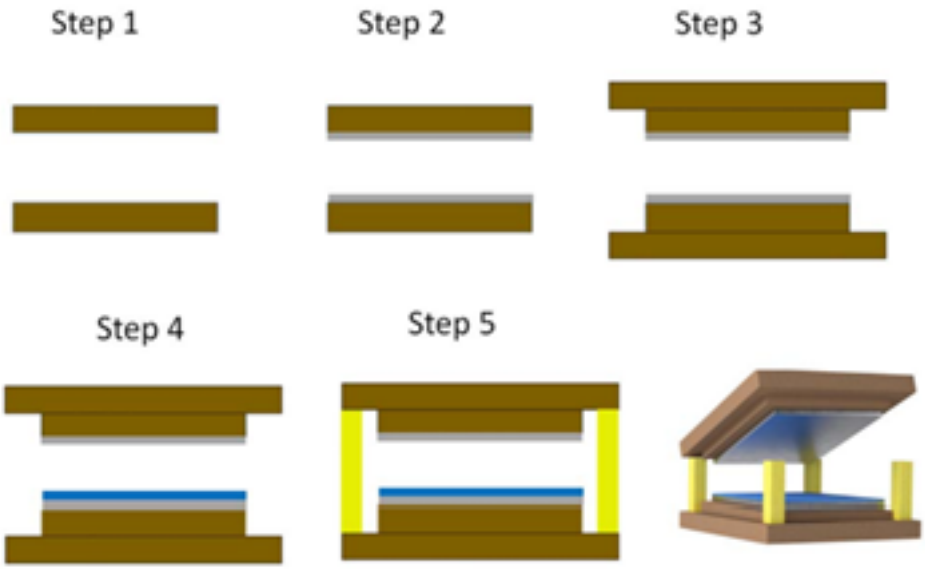

Figure 6.11: Steps for TENG Preparation.

a linear relationship between those variables. It enables us for analyzing and prediction of the target variable. In simple linear regression only one input variable is present, but in our case, there are more than one input variable which are output voltage, output current and Load resistance, so our regression problem comes under multiple linear regression which is more than one independent variable whose relationship formula becomes:

$$Y = b_0 + b_1X_1 + b_2X_2 + ... + b_nX_n$$

The coefficients are determined using the least squares approach that minimises the total of the squared deviations between the actual and expected values of the dependent variable from the regression equation.

II. **Decision Tree Regression:** It is one of the supervised learning-based algorithms. The advantage with this method is that it can be used for solving both the problems that require classification to be performed or even for regression problems as well and this is applicable to both numerical and categorical data. Since our problem is related to regression with numerical data this method can be considered to solve our regression problem. Just like the name of the regression technique it is a structure similar to a tree where each internal node indicates the decisive condition for an attribute, and each branch indicate the result of the decision, and each leaf node indicates the conclusive decision. This regression observes the important features embedded in the existing data

and utilize it for training the ML model as in a shape of a tree to predict the output values.

III. **XGB regression:** In Regression problems the output variable values are continuous values. For building supervised regression models XGBoost is a decent approach. From the XGBoost objective function and the base learners decide our method's performance. So, objective function includes a loss function and the regularization term gives the insight about the deviation of actual output power and predicted output power. XGBoost is an ensemble learning method, in ensemble learning individual models are trained and combined to obtain a single prediction.

IV. **Random Forest regression:** It is an ensemble learning technique called random forest regression which is optimal for both classification and regression tasks combines numerous decision trees and forecasts the ultimate result using the average of each tree's output. Base models are the combined decision trees. Aggregated decision trees are operated in parallel by Random Forest. So, they do not interact with one another. By generating random subsets of the dataset, Random Forest regression enables us to prevent Overfitting in the model.

V. **Support vector regression:** Support Vector Machine is a supervised learning approach that may be applied to both classification and regression issues. So, it is known as Support Vector Regression (SVR) if we use it to regression-related issues. An effective regression method for continuous data is support vector regression. The fundamental purpose of Support Vector Regression (SVR) is to include as many data points as possible within the boundary lines. The hyperplane represents the optimal fitting line, which should include a high number of data points.

6.2.5 Performance Metrics

a. Mean Square Error (MSE) The disparities between expected and the actual values are squared, summed up, and then divided by the number of data points to produce MSE. The resultant number is the average of the squared differences. Mathematically, formula

for MSE can be expressed as

$$MSE = \frac{1}{N}\sum_{j=1}^{N}(y_j - \hat{y}_j)^2 \tag{6.1}$$

MSE is a measure of a regression model's prediction accuracy. A lower MSE value indicates that the model is more accurate in predicting real values. The model seeks to provide a more exact fit to the data by minimising the squared discrepancies between anticipated values and to that of actual ones.

b. Root Mean Square Error (RMSE): It is a generally employed measure for assessing precision of a regression problem. It quantifies the disparity between the predicted values and the original values. It is given in mathematical form below,

$$RMSE = \sqrt{\frac{1}{N}\sum_{j=1}^{N}(y_j - \hat{y}_j)^2} \tag{6.2}$$

c. Mean Absolute Error (MAE): It is a statistic often used in regression analysis to calculate the average absolute difference between a dependent variable's predicted and actual values. It is computed by calculating the absolute difference between each anticipated and actual number and then averaging these differences. MAE provides a straightforward and interpretable measure of the magnitude of errors in the predictions. Mathematically, the formula for MAE is:

$$MAE = \frac{1}{N}\sum_{j=1}^{N}|y_j - \hat{y}_j| \tag{6.3}$$

d. R2-Score: R2-Score is given as R2, which reflects the amount of variation explained by the other independent factors for the dependent variable. $\mathbf{R^2}$ gives the insight about how much one variable's variance can explain about the second variable's variance. It is given in mathematical form as below,

$$R^2 = 1 - \frac{RSS}{TSS} \tag{6.4}$$

Where, Sum of squares of Residuals

$$RSS = \sum_{j=1}^{N}(y_j - \hat{y}_j)^2 \tag{6.5}$$

Total Sum of Squares

$$TSS = \sum_{j=1}^{N} (y_j - \bar{y})^2 \tag{6.6}$$

6.2.6 Deep Learning Techniques

I. **Adam:** The Adam algorithm, short for Adaptive Moment Estimation, is an optimization algorithm used in deep learning. It calculates adaptive learning rates for each parameter during each iteration. The Adam optimizer is widely used and adjusts the learning rate of each weight in the neural network based on the first and second moments of the gradients β1, β2. The algorithm computes an adaptive learning rate for each weight that takes into account the historical gradients and adjusts the learning rate for each weight accordingly. This adaptive learning rate is then utilized for updating the neural network's weights. It enables the algorithm to converge faster and more reliably than traditional stochastic gradient descent. The hyperparameters β1, β2, and ε are used to control the decay rates of the first and second moments and to prevent division by zero in the update equation, respectively. The values of these hyperparameters can affect the performance of the algorithm, and they need to be carefully tuned for each specific problem.

II. **SGD:** This is a different Gradient Descent optimizer variation that has the extra ability to operate with data and non-convex optimization problems. With such data, the cost function ends up resting at local minima, which is problematic because they are not ideal for your learning process. Instead of using batch processing, this optimizer concentrates on carrying out each update one at a time. As a result, it is typically faster, and after each repetition, the cost function decreases. It often updates with a large variance, which results in significant fluctuations in the goal function. As a result, the gradient changes to indicate a possible Global Minima. The cost function may vary about the minimum or even diverge from the global minima if we pick a learning rate that is too big. SGD can be prone to getting stuck in local minima, which can lead to suboptimal solutions. To address this, researchers have developed various techniques, such as adding momentum or adaptive learning rates, to help SGD escape local minima and converge to better solutions.

III. **Adagrad:** his is the adaptive gradient optimization approach, where the updated parameter values are heavily influenced by the learning rate. This optimizer, unlike stochastic gradient descent, employs a variable learning rate for each iteration as opposed to utilising a single learning rate to determine all the parameters. Adagrad is effective in handling sparse data and can make smaller updates for high-frequency features and greater updates for low-frequency features, leading to improved performance and accuracy.

IV. **RMSprop:** RMSprop and Adadelta are both optimization algorithms that were created to improve upon Adagrad's problem of having overly aggressive learning rates. Both of these algorithms use a similar technique to calculate the learning rate for each iteration at time t, which involves an exponential weighted average. RMSprop, which was developed by Geoffrey Hinton, is an adaptive learning rate approach that takes an exponentially weighted average of the squared gradients. The learning rate is then divided by this weighted average, which allows for more stable and consistent updates to the model's parameters. This is because the squared gradients can act as a proxy for the curvature of the loss function and help prevent the model from making large updates in the wrong direction. In practice, a value of gamma around 0.95 is often recommended for RMSprop. This value has been found to work well across a range of different datasets and models. However, the optimal value of gamma can depend on the specific problem being addressed, and it may need to be tuned accordingly.

V. **Adamax:** The AdaMax algorithm builds on this idea by considering the alleged infinite norm of the previous gradients in the place of the scaled L2 norm. Infinite norm is a way to measure the magnitude of a vector by taking the maximum absolute value of its elements. By considering the infinite norm of the previous gradients, the AdaMax algorithm can make some optimizations more successful. This is because the infinite norm provides a more robust measure of the magnitude of the gradients and can prevent the algorithm from getting stuck in local minima. Overall, the AdaMax algorithm is a powerful extension of the Adam optimization technique which improve the deep learning model' performance by providing more robust measure of the magnitude of the gradients.

VI. **Adadelta:** This modified version of the adaptive gradient optimizer addresses the issue of aggressive reduction of the learning rate in the original algorithm. Instead

of using the sum of previous squared gradients, this modification calculates a weighted average of all prior squared gradients. This helps prevent the learning rate from becoming excessively small.

Model: "sequential" **DNN with 7 layers:**

Layer (type)	Output Shape	Param #
dense (Dense)	(None, 128)	512
dense_1 (Dense)	(None, 64)	8256
dense_2 (Dense)	(None, 32)	2080
dense_3 (Dense)	(None, 16)	528
dense_4 (Dense)	(None, 8)	136
dense_5 (Dense)	(None, 4)	36
dense_6 (Dense)	(None, 1)	5

Total params: 11,553
Trainable params: 11,553
Non-trainable params: 0

Model: "sequential" **DNN with 5 layers:**

Total params: 833
Trainable params: 833
Non-trainable params: 0

Model: "sequential" **DNN with 9 layers:**

Total params: 178,337
Trainable params: 178,337
Non-trainable params: 0

Model: "sequential" **DNN with 11 layers:**

Total params: 966,817
Trainable params: 966,817
Non-trainable params: 0

Figure 6.12: Number of layers used and its parameters

The main problem with simple linear regression is that it can only learn the linear relationship between the features and target variable and when there is complex non-linear relationship then the simple linear regression cannot learn. So, to overcome this problem we need a different technique where neural networks come into picture. Artificial neural network is the approach comes under deep learning which has the ability to learn the complex relationship by making use of activation function in each layer of our neural network.

Our DNN model summary with the layers used is shown in Fig 4. Overall, increasing the layers can provide certain benefits. This can improve the model accuracy, and can lead to challenges in training time, vanishing or exploding gradients, overfitting, and the need for more data and computational resources. The below are few consequences.

1. Increased Training Time: As we are increasing the number of layers, model computational complexity also increases, leading to longer training times.

2. Vanishing or Exploding Gradients: With very deep networks, the gradients (which are used to update the model's parameters during training) may become very small (vanishing gradients) or very large (exploding gradients), making it difficult to train the model effectively.

3. Require More Data: If the number of layers are increased then the neural network may require more training data to prevent overfitting and effectively learn the underlying patterns in the data.

4. Require More Computational Resources: Deeper models require more computational resources, including memory and processing power, making them more expensive.

Deep neural networks are one of the deep learning algorithms that mimics the behaviour of neurons in the human brain. Recurrent Neural Networks (RNN), Convolutional Neural Networks (CNN) have the ability to process the unstructured data which are part of ANNs. Before fitting the dataset to the training set, Data is transformed into array representations. In the DNN model, the input for forecasting the power at the output consists of the grating width and sliding velocity. With the help of ReLU function hidden layer is activated as shown in the above Figure 6.17, and the loss function is adjusted with clarified variance ratio of every element. Developed model provides the output forecasts for previously unseen data in the CS mode.

There are three layers in artificial neural networks: input, hidden, and output. There may be more than one hidden layer. A layer has n number of neurons in it. Each layer's neurons will each have an associated activation function. The function that introduces non-linearity into the relationship is the activation function. In our situation, a linear activation function is required in the output layer. Regularizers may be connected to each layer. The role of regularizers is to prevent overfitting.

6.2.7 Optimizers in Deep Learning models

When our DNN models are trained, we must adjust the weights at each epoch and strive to decrease the loss function as much as feasible. We must employ an optimizer for this task, which is an algorithm that modifies our neural network's weights and its learning

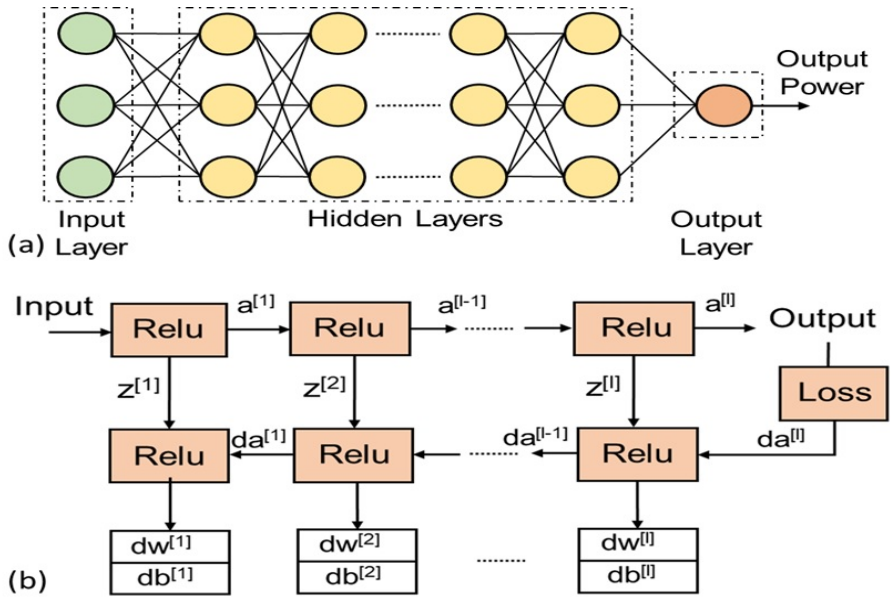

Figure 6.13: (a) Layer Construction (b)Workflow of modelling process

rate. So, an optimizer is essential for increasing our model's accuracy and decreasing loss. But picking the right weights for the model is a difficult undertaking. We can use utilize different optimizers to tune the weights and learning rate. We have to choose the optimizer that best suites our application. We have tested different optimizers with our DNN model and observed the performance metrics of all optimizers in predicting the output power.

6.2.8 Proposed Methodology:

Data Pre-Processing

In order to build a reliable neural network model, it is important to have a sizable amount of experimental data that is extracted from reliable references or sources [88, 100]. So, a good amount of data needs to be collected through experimental results. In Fig.6.11 which illustrates the experimental setup of the system is developed to give an idea on the flow of work, which represents the dataset, DNN model with hidden and responses correspond to validation and prediction. In our dataset, we have removed the power density and classifier features as they are not contributing much in predicting the output power. After this our dataset is split into 2 parts for making it useful for testing as well so 30 percent of data is reserved for training and 30 percent for testing The training data

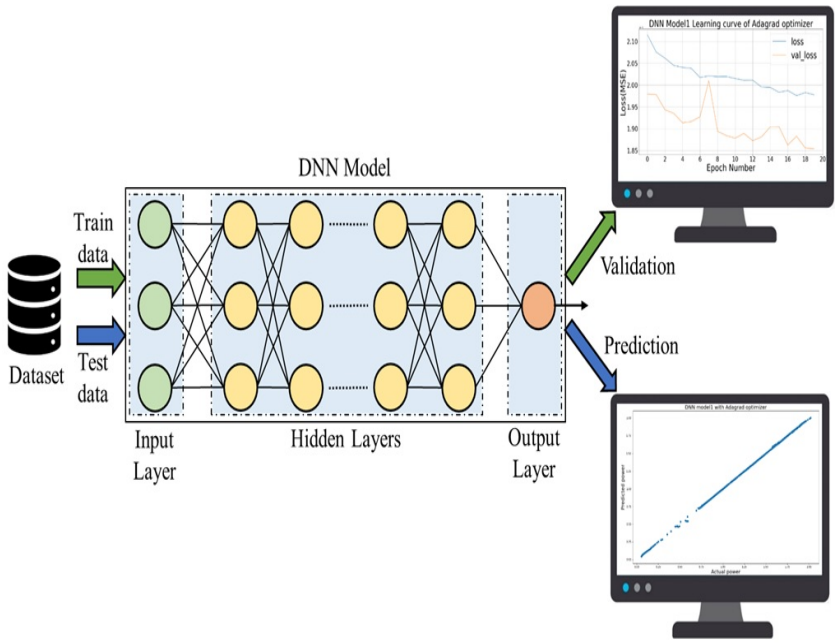

Figure 6.14: Experimental Setup

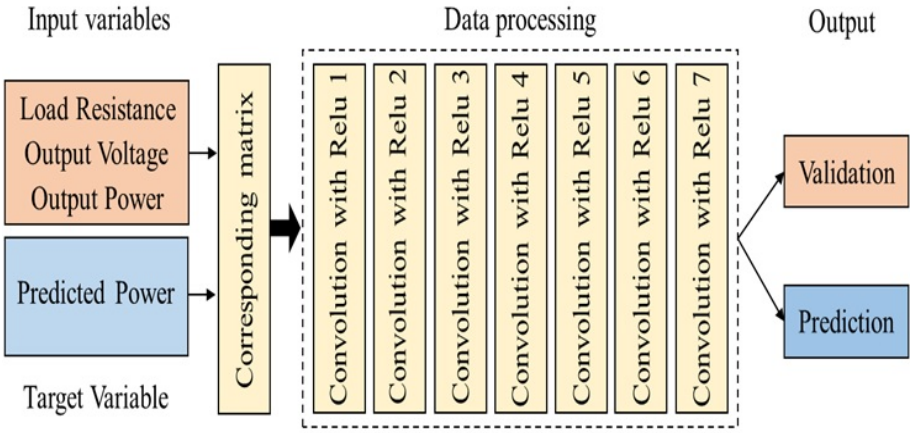

Figure 6.15: Layered structure flow chart for prediction of the output power

which is 70 percent of original data is made use for training our model and test data is the untrained data which our developed model doesn't come across used to test how our model is performing the output power prediction. The layered structure flowchart is shown in above Fig. 6.12.

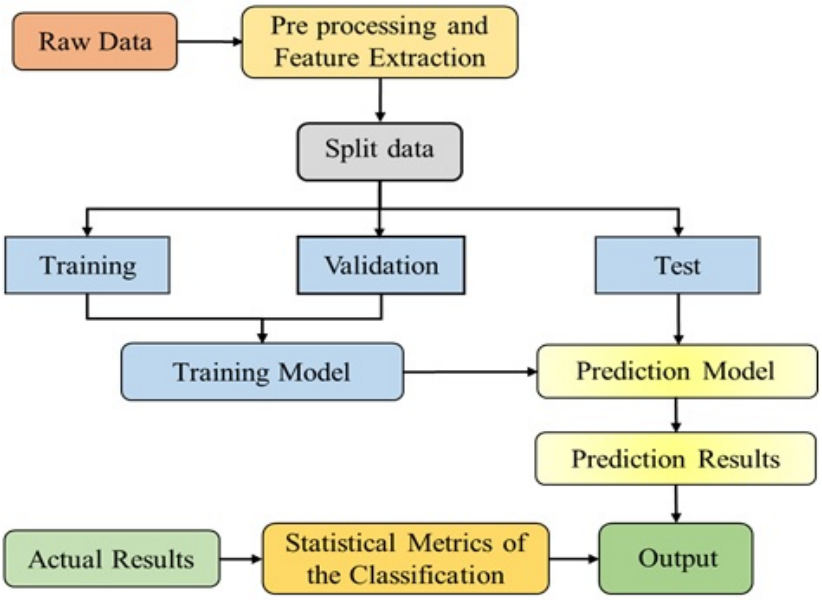

Figure 6.16: Overall model flow chart from experimental data

Construction of Proposed model and optimization

By making use of our dataset prepared from experimental results, we can predict the output power by using regression analysis. We have 2 options to solve this regression problem which are ML and DL methods. In our work we analysed both the techniques. in Fig. 6.13 the flowchart of overall model is given.

We have demonstrate d a deep neural network architecture. Our demonstrate d model contains one input layer that takes input features data, some hidden layers and one output layer to predict the output variable in our case it is output power. Our model makes use of several weight coefficient vectors wi where, i = 1, 2, 3, ... N. We need to make use of 'b' and 'x' to perform the sequence of linear operations, where 'b' is bias vector and 'x' is an input vector, which is given by

$$y[l] = w[l] \cdot x[l] + b[l]. \tag{6.7}$$

We have used one of the most widely used activation function which is ReLU. The working of ReLU activation function is mathematically given as g(x) = max (0, x) data from the input layer passes through the hidden layers gives the result at the end of output layer, it is given as x[l] = g[l](y[l]). The loss function L(ϑ) after completing the forward propagation can be obtained as,

$$L(j) = 1/N_(j = 1)^N (y_j - y_j)^2. \tag{6.8}$$

The model propagation starts at this point through the input of dx[l]. We get the output as dx[l-1], dw[l], db[l]. Our model parameters get updated in the following fashion,

$$dx[l-1] = w[l]Tdy[l] \tag{6.9a}$$

$$dw[l] = dy[l]x[l-1] \tag{6.9b}$$

$$db[l] = dy[l] \tag{6.9c}$$

$$dy[l] = w[l+1]T.dy[l+1]g[l](y[l]) \tag{6.9d}$$

6.2.9 Results and Discussion

Experimental data formed as a dataset is utilized to train the models and is divided them into a training and testing. For training our neural network 70 percent of data used for training and the test dataset with is 30 percent of our total dataset size is used to test the performance our model. Below figures show the experimental output power and the prediction of Random Forest regressor which is performing best among other tested machine learning techniques and the same comparison of our DNN models with different optimizers. We observed that our Deep neural network model performs very well in predicting the output power and the Adadelta optimizer is performing better in terms of all the performance metrics compared to other optimizers. The reasons are,

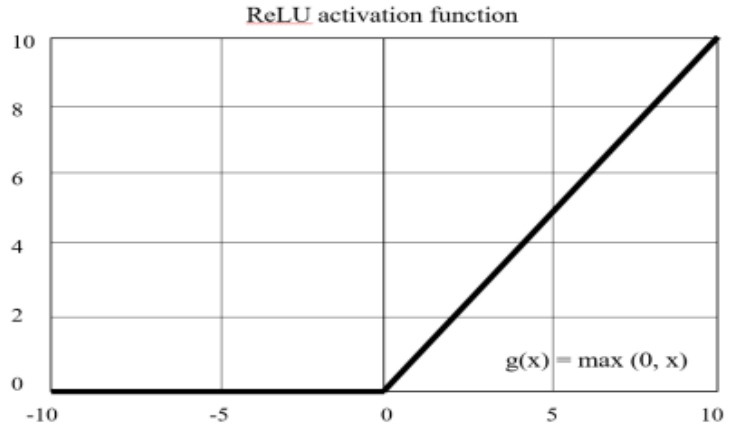

Figure 6.17: ReLU function

1.Adaptive Learning Rate: The Adadelta optimizer is an adaptive learning rate opti-

mizer, which means that it can adjust model's learning rate with respect to the gradient updates in each iteration. This ensures that the model converges quickly to the optimal solution without overshooting or oscillating.

2.Robustness to Noisy Data: Adadelta is a robust optimizer that can handle noisy data and small gradients. This is because it uses a moving average of the past gradients to update the learning rate, which reduces the impact of individual noisy gradients.

3.No Learning Rate Decay: Unlike other optimizers, such as Adam and RMSprop, Adadelta does not require a learning rate decay schedule. This reduces the need for hyperparameter tuning and makes the optimization process simpler.

4.Faster Convergence: Adadelta optimizer can converge faster than other optimizers, especially in the case of deep neural networks. This is because it uses an efficient gradient update method that requires fewer iterations to reach convergence.

In machine learning techniques Random Forest regression performs better than other regression techniques because of following reasons.

1.Overfitting Reduction: Random Forest Regressor generates many decision trees for prediction decision then integrates all results to get the last prediction, which helps to decrease model overfitting since the average of multiple trees is more stable and accurate than a single tree.

2.Non-Linear Relationships: Random Forest Regressor can gather non-linear relationships between the features and the target variable, which is not always possible in linear regression models.

3.Robustness to Outliers: Random Forest Regressor is robust to outliers as it uses a combination of decision trees to make predictions. A single decision tree can be biased by outliers, but combining multiple trees reduces the effect of any single outlier.

4.Feature Importance: Random Forest Regressor provides an estimate of feature importance, which helps to identify the most significant features that affect the target variable. This can be useful for feature selection and dimensionality reduction.

5.Easy to Use: Random Forest Regressor is relatively easy to use and requires less parameter tuning compared to other complex models like XGB Regressor.

6.2.10 Prediction Using Machine Learning Technique

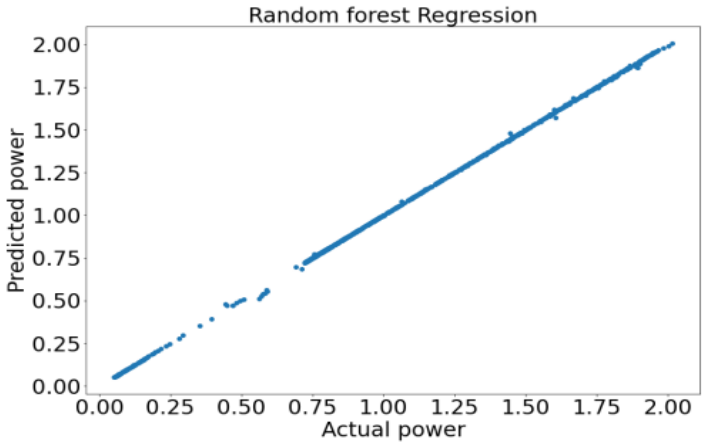

Figure 6.18: Graph between prediction vs actual power

The output power is predicted for the corresponding Load resistance, Output voltage and Output current using the Random Forest regression technique. For the Load resistance of 3MΩ the predicted power is obtained as 1.013555125µW which is very much close to the actual power of 1.013867295µW with a very minimal deviation value of 0.00031217µW. The variation of the predicted power to the actual output power is shown graphically in the above Figure 6.17 and the deviation error is tabulated below.

Table 6.4: Machine learning data between actual and predicted under specified load

Load resistance M ohm	**Actual power(µW)**	**Predicted power(µW)**	**Difference(µW)**
3	1.01386	1.01355	0.00031217
1.3	1.777230	1.77643	0.000798
0.35	1.255875	1.255664	0.0002115
4.65	0.747844	0.74784116	3.00085E-06
0.75	1.6113	1.6145	-0.003108
1.1	1.8877	1.887-0.000207	
3.2	0.97020	0.97006	0.000136
0.5	1.7309	1.7296	0.00126
2.9	1.0482269	1.048244	-1.79866E-05
2.25	1.2985673	1.2984243	0.000142958

The output power is predicted for the corresponding Load resistance, Output voltage and Output current using the Deep Neural Network with Adadelta optimizer technique. With the Adadelta optimizer, For the Load resistance of 3MΩ the predicted power is obtained as 1.014077187µW which is very much close to the actual power of 1.013867295µW with a very minimal deviation value of -0.000209892µW. The variation of the predicted power to the actual output power is shown graphically in the above Figure 6.18 and the deviation error is tabulated below. Loss fitting curves with different optimizers in DNN model are shown in above figures Figure 6.19 (a), (b), (c), (d) (e). After applying the Adadelta technique to the contact separation, the model achieved after 20 epochs, a final loss value of 0.0000182317 which very small when compared to other optimizers which are as follows. For Adam optimizer, the loss (MSE) is 0.000582385. For SGD optimizer, the loss (MSE) is 0.0000207074. For Adagrad optimizer, the loss (MSE) is 0.0000185393. For RMSprop optimizer, the loss (MSE) is 0.000450456. For Adamax optimizer, the loss (MSE) is 0.0000210353.

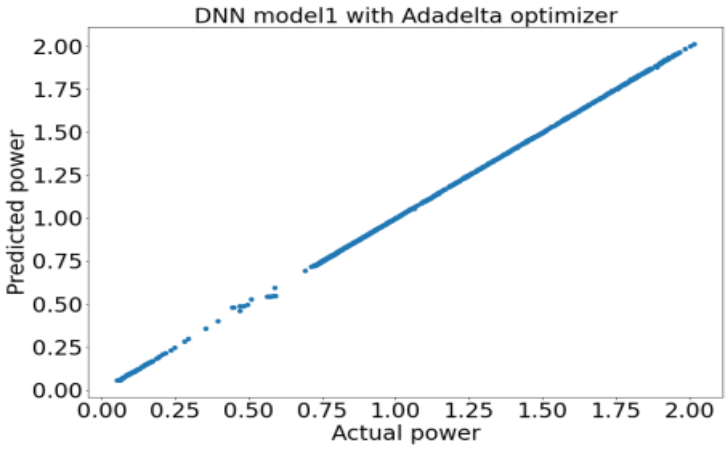

Figure 6.19: DL curve between Actual power and predicted power

Table 6.5: comparison of DL data for actual and predicted power under specified load

Load resistance M	**Actual power(µW)**	**Predicted power(µW)**	**Difference(µW)**
3	1.01386729	1.014077187	-0.0002098
1.3	1.777230	1.776497	0.000733167
0.35	1.255875661	1.2584078	-0.00253217
4.65	0.747844	0.746639729	0.001204433
0.75	1.611398438	1.615246773	-0.003848335
1.1	1.887768759	1.889030457	-0.00126169
3.2	0.97020	0.970205903	-4.65305E-06
0.5	1.730939	1.7317159	-.000776524
2.9	1.048226938	1.047286034	0.000940904
2.25	1.298567321	1.298773289	-0.000205968

Performance Metrics

Performance metrics for the regression analysis such as MSE, MAE, RMSE, R2-Score are obtained for the ML methods and Deep learning techniques with different optimizers. As per the above graph in Figure 6.20 (a) of R2-Score, Linear Regression and SVM Regression are not good compared to other techniques. Among all Adadelta optimizer is

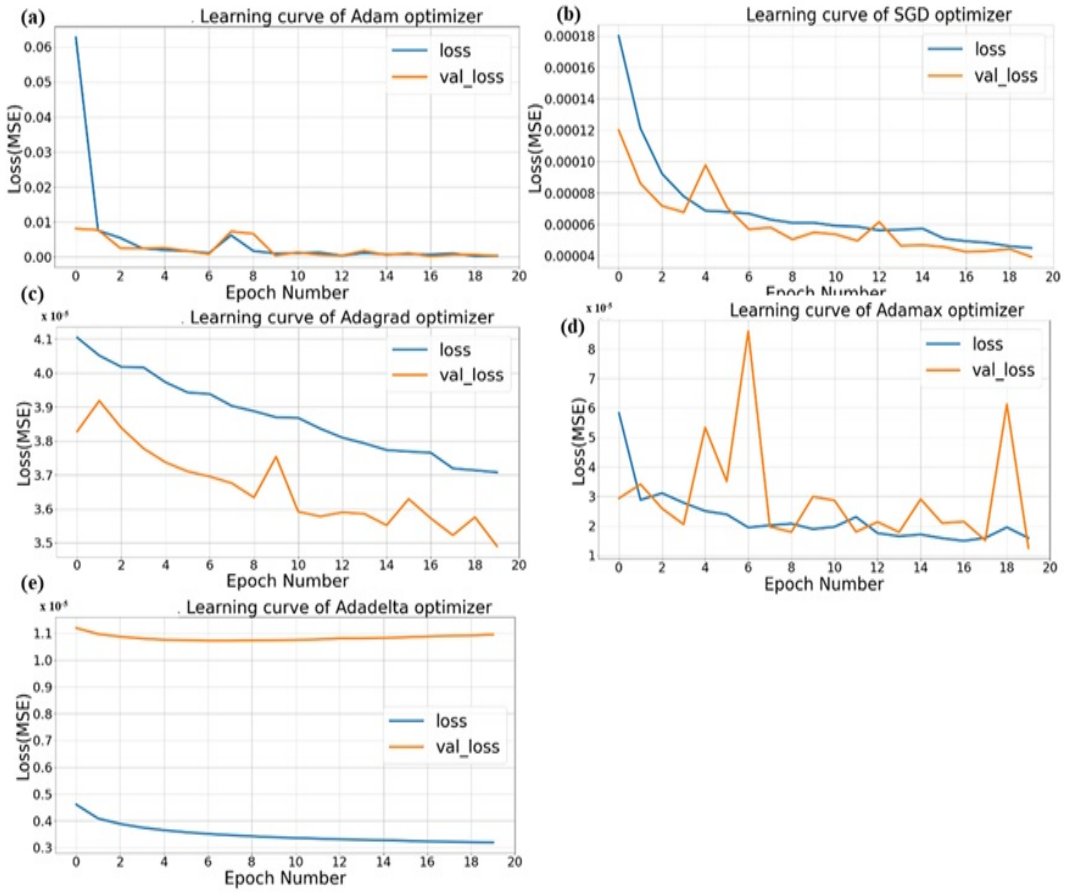

Figure 6.20: (a). Adam optimizer's Loss fitting curve, (b). SGD optimizer's Loss fitting curve, (c). Adagrad optimizer's Loss fitting curve, (d). Adamax optimizer's Loss fitting curve, (e). Adadelta optimizer's Loss fitting curve

giving better R2-Score value. From the above graph in Figure 6.20 (b) which represents the Mean Absolute Error (MAE) of all the techniques used, it is clear that among all the ML techniques Random Forest Regression technique achieves the least MAE value of 0.00139354. And among all the deep learning techniques with different optimizers, Adadelta optimizer obtains a much lower MAE value of 0.001267. As per the above graph in Figure 6.20 (c) of MSE metric comparison among the ML and Deep Learning techniques, Linear Regression and SVM Regression are having high MSE values compared to other techniques. Among all Adagrad and Adadelta optimizers are giving very low MSE. From the Fig. 6.20 (d) which represents the metric RMSE value comparison among all the techniques which is similar to MSE, because RMSE is nothing but square root of MSE, so similar to MSE among all techniques Adadelta optimizer gives very low RMSE value of 0.00426986.

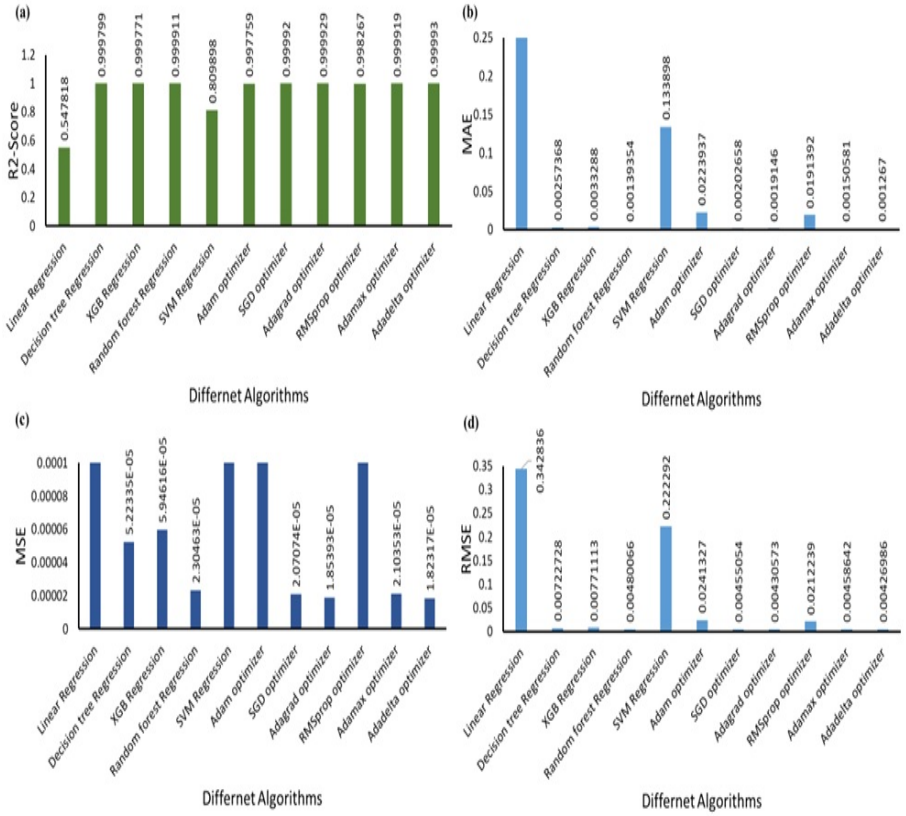

Figure 6.21: (a). R2 score for ML and DL Regression models, (b). MSE for ML and DL Regression models, (c). RMSE for ML and DL Regression models, and (d). MAE for ML and DL Regression models.

Table 6.6: Comparison of different performance metrics for ML and DL regression models

Model	**R2_Score**	**MAE**	**MSE**	**RMSE**
Linear Regression	0.547818	0.251831	0.117537	0.342836
Decision tree Regression	0.999799	0.00257368	5.22E-05	0.00722728
XGB Regression	0.999771	0.0033288	5.95E-05	0.00771113
Random forest Regression	0.999911	0.00139354	2.30E-05	0.00480066
SVM Regression	0.809898	0.133898	0.0494138	0.222292
DNN model with Adam	0.997759	0.0223937	0.000582385	0.0241327
DNN model with SGD	0.99992	0.00202658	2.07E-05	0.00455054
DNN model with Adagrad	0.99929	0.0019146	1.85E-05	0.00430573
DNN model with RMSprop	0.998267	0.0191392	0.000450456	0.0212239
DNN model with Adamax	0.999919	0.00150581	2.10E-05	0.00458642
DNN model with Adadelta	0.99993	0.001267	1.82E-05	0.00426986

The below Tables 3 4 illustrates about the related information about ML and DL regression models with their performance metrics. Among the all-regression models in machine learning Random Forest regression giving better results compared to remaining regression techniques present. Table represents the actual and predicted power for a given load resistance, the comparison of powers that are actually getting and our predicted ones in case of both ML regression methods and DL regression methods and in the both cases for ML less error is getting in the case of random forest regression and DL less error is getting in the case of Adadelta.

The TENG Device construction of real images is shown in fig. 6.21 (i) and its operating principle and isometric view is represented in the Fig 6.21(ii). Fig. 6.21 rep-

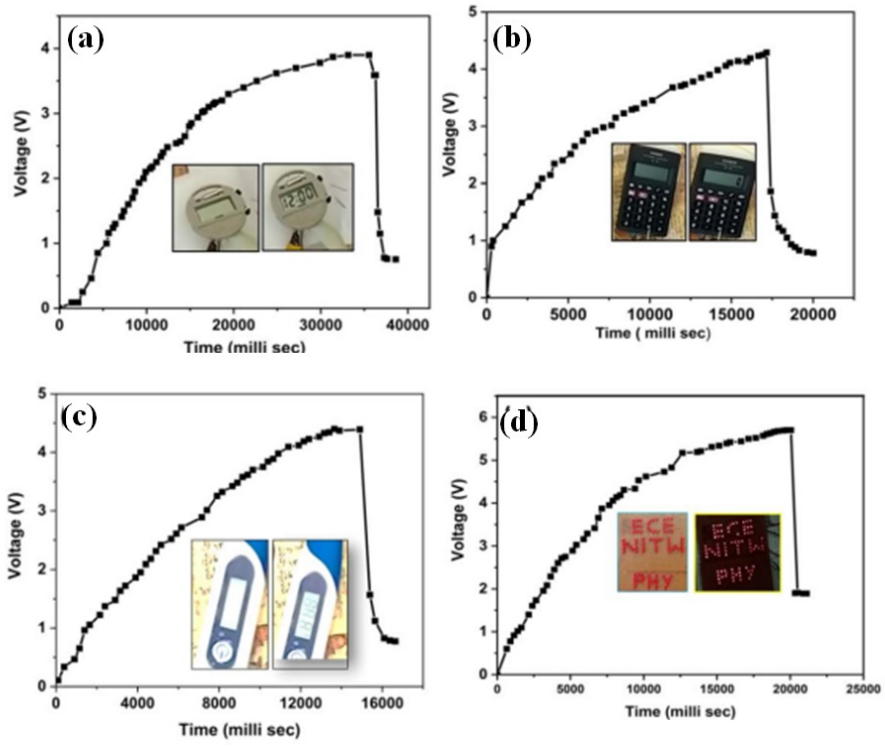

Figure 6.22: Applications of TENGs (a) glowing of watch (b) calculator (c) Thermometer (d) 85 LEDs Reproduced from [100]

resents the different electronic applications are demonstrated by using designed sensor APA (Aluminium foil parafilm Aluminium foil) TENG which are earlier published in the article [100].

6.2.11 Conclusion

In this work we have tested both machine learning as well as deep learning methods for predicting power at the output based on the load resistance and other parameters. In machine learning we observed that Random Forest regressor gives good predictions compared to other models. In Deep learning techniques, Adadelta optimizer performs better than other optimizers. With the help of this deep learning approach compared to conventional experimentation method for finding the output power, we can predict the output power even without doing the experimentation for getting that result with the help of training the model. This saves lot of cost incurred for experimentation and minimizes the errors. From the results obtained for 1.3M Ω load resistance, the actual output power is 1.7772 µW and the prediction from Random Forest regressor is 1.7764 µW and the predicted output power by our deep neural network with Adagrad optimizer is 1.7774 µW. So, in the deep learning technique the error is very small compared to machine learning technique.

Summary: In this chapter, we built our own dataset using a TENG (Triboelectric Nanogenerator). The dataset was divided into two sections: training data and testing data. Based on the output voltage response, we separated the data into three groups, and each group was further divided into training and testing sets. The data was then trained and tested using machine learning methods, and the accuracy of each model was assessed. Extraction of the confusion matrix and evaluation of performance measures yielded the best-performing model. Then, we expanded the dataset and used deep learning techniques to assess multiple regression algorithms and select the one with the lowest loss.

Chapter 7

Conclusions and Future Scope

This chapter concludes the thesis by underlying the main contributions. The chapter also discusses the possible scope for future research.

7.1 Conclusions

In this thesis, we have presented five types TENG devices to increase the output response. For the demonstrated hardware designed TENG devices evaluated the results with simulation platform COMSOL and compare both the results and calculated the scaling factor and concluding that both the results are giving same results without any deviation.We created our own experimental dataset, using machine learning and deep learning techniques to forecast output power under unknown load conditions. The variation between showed and actual results illustrates a little loss.

The introductory part of the thesis has been presented in the opening chapter 1. It comprises of the overview of the thesis, an introduction to TENG, resources used and organization of the thesis. Chapter 2 is composed of an extensive overview of the different types of nanogenerators, types of modes present in TENG and their merits and demerits are also discussed. Our contribution begins with chapter 3 and are concluded as follows:

In chapter 3, mainly focused on the material selection in that also mainly focused on the reusable waste materials like waste food packaging aluminum foil as an electrode and design the TENG device with help of different dielectric materials which are easily

available in the local market with less cost like OHP, PET and PMMA. Here we given the conclusion i.e with higher roughness of the dielectric is giving prominent output response compared to that of remaining dielectrics and their comparison with different nano generation characterizations. Finally, how each characterization of TENG device explains briefly.

In chapter 4, divided into two contributions. In the first contribution waste food packaging aluminum foil back-to-back assembled and designed the TENG device with out using any other new separate dielectric material. For the above TENG device all the nanogenerator characterizations are studied. In the second contribution APA TENG new dielectric material is used i.e. Laboratory film (Parafilm) for the first time and for the designed TENG device all the characterizations are performed. From the above two contributions following are salient features.

1. Reuse of waste food packaging Aluminium covers reduce air, water and soil pollution
2. demonstrated a new triboelectric pair for mechanical energy harvesting
3. demonstrated Triboelectric nanogenerator (TENG) with waste food packaging covers only and parafilm as new dielectric material used first time.
4. demonstrated APA (Aluminium foil Parafilm Aluminium foil) TENG is able to power up 85 LEDs
5. demonstrated APA TENG produced an VOC up to 4 V and power density 40 nW/cm2
6. demonstrated TENG exhibits stable output response more than 4000 cycles.

In chapter 5, analysis of the TENG device by using COMSOL platform. In that the design parameters are taken which are already used in the design of Hardware TENG like contact area, type of materials used and gap existing between the material. The output which is obtained in the simulation giving prominent results same as that of practical data and finally calculated the scaling factor and concluding that there is no deviation the response in simulation hardware.

In chapter 6, created the own data set from designed TENG device, in the first contribution data set divided into three classifiers and divided into training and testing. Corresponding data given to ML classifiers and find out the best algorithm for that all the performance metrics are extracted. In the second contribution increased the data set by augmentation process and applying the regression method for both Machine learning and deep learning concepts, finds the less loss for both ML and DL compared to different algorithms.

1. Various dielectric studies were conducted, and their findings were compared with simulation results, determined the scaling factor for each Triboelectric Nanogenerator (TENG) device. It was observed that both the experimental and simulation results yielded consistent outcomes, with no significant deviation. Consequently, it can be concluded that the experimental and simulated values align closely, demonstrating the reliability of the scaling factor for each TENG device.

2. An experimental study was conducted utilizing various Machine Learning (ML) and Deep Learning (DL) algorithms. The aim was to evaluate their performance in analyzing the data. The results revealed that the Random Forest regression algorithm exhibited a lower error rate in the ML model, indicating its superior predictive accuracy. Additionally, in the DL model, the Adamdelta regression algorithm demonstrated a lower error rate compared to other algorithms. These findings highlight the efficacy of Random Forest regression in the context of ML and Adamdelta regression in the realm of DL, underscoring their potential for accurate data analysis and prediction.

7.2 Limitations and Future Scope

In this section, limitations and the potential research direction for future research is presented. Finding the materials is the challenging task for generating more output response. Increasing the current from the designed TENG device is also challenging task because if we generate the power in milli amperes to drive the small electronic devices up to one minute. During the thesis work, some issues were identified. These issues form the basis for future scope.

1. To enhance the output voltage of a device, researchers often focus on improving the dielectric constant (also known as relative permittivity) of the material.

2. Enhancing the current density is vital for applications that require high-power output or faster operation.

3. Development of specialized dielectric materials for biomedical sensors holds in advancing healthcare technologies.

4. Powering smart cities, streetlights, and infrastructure monitoring.

Publications

List of International Journals:

1. **Sankar PR, Prakash K,** et al., "A triboelectric nanogenerator based on food packaging Aluminium foil and parafilm for self-powered electronics", *Physica Scripta*, Sep 6;96(12):125005 (2021): **(SCI-Indexed) Impact Factor: 2.9**

2. **Sankar PR, Prakash K,** et al., "A novel triboelectric nanogenerator based on only food packaging aluminium foils", *Materials Letters*, Mar 1;310:131474 (2021). **(SCI-Indexed) Impact Factor: 3**

3. **Sankar PR, Prakash K, et al.,** "Accurate output power prediction in TENG devices using Artificial Intelligence: A Comparative Analysis", *The International Arab Journal of Information Technology* , (2023). **(SCI-Indexed)** (Submitted & Under Review) **Impact Factor: 1.75**

4. **Sankar PR, Prakash K,** et al., "Finite element analysis of Triboelectric Nanogenerator Performance: Insights for Renewable Energy Optimization ", *Engineering Research Express*, (2023). **(SCI-Indexed)** (Submitted & Under Review) **Impact Factor: 1.7**

List of Co-Author International Journals:

1. Supraja P, Kumar RR, Mishra S, Haranath D, **Sankar PR, Prakash K**, Jayarambabu N, Rao TV, Kumar KU, "A simple and low-cost triboelectric nanogenerator based on two-dimensional ZnO nanosheets and its application in portable electronics", *Sensors and Actuators A:Physical*, Sep Jan 7:113368 (2022):**(SCI-Indexed) Impact Factor :4.6**

2. Mishra, Siju, Supraja Potu, **Ravi Sankar** Puppala, Rakesh Kumar Rajaboina, **Prakash Kodali**, and Haranath Divi "A novel ZnS nanosheets-based triboelectric nanogenerator

and its applications in sensing, self-powered electronics, and digital systems", *" Materials Today Communications*, 103292. (2022). **(SCI-Indexed) Impact Factor :4.6**

3. Supraja P,**Sankar PR**, Kumar RR, **Prakash K**, Jayarambabu N, Rao TV, ". Characteristics of 2D ZnO-based piezoelectric nanogenerator and its application in non-destructive material discrimination", *Advances in Natural Sciences: Nanoscience and Nanotechnology*, (2021) Jun 14;12(2):025011. **(SCI-Indexed) Impact Factor :2.3**

4. Supraja, P., Rakesh Kumar, Siju Mishra, D. Haranath, **P. Ravi Sankar**, and **K. Prakash**, "A simple and low-cost approach for the synthesis and fabrication of ZnO nanosheet-based nanogenerator for energy harvesting and sensing", *: Engineering Research Express*, (2023). **(SCI-Indexed)** (Under Review) **Impact Factor :1.8**

5. Supraja P, **Sankar PR**, Kumar RR, **Prakash K**, Jayarambabu N, Rao TV, ". Characteristics of 2D ZnO-based piezoelectric nanogenerator and its application in non-destructive material discrimination", *Advances in Natural Sciences: Nanoscience and Nanotechnology*, (2021) Jun 14;12(2):025011. **(SCI-Indexed) Impact Factor :6.8**

6. Mishra, Siju, P. Supraja, **P. Ravi Sankar**, R. Rakesh Kumar, **K. Prakash**, and D. Haranath., "Controlled synthesis of luminescent ZnS nanosheets with high piezoelectric performance for designing mechanical energy harvesting device", *: Materials Chemistry and Physics*, (2023). **(SCI-Indexed)** 277 (2022): 125264 **Impact Factor :3.8**

7. Mishra, Siju, P. Supraja, Vishnu V. Jaiswal, **P. Ravi Sankar**, R. Rakesh Kumar, **K. Prakash**, K. Uday Kumar, and D. Haranath, "Enhanced output of ZnO nanosheet-based piezoelectric nanogenerator with a novel device structure", *: Engineering Research Express*, (2023). **(SCI-Indexed)** 4 (2021): 045022 **Impact Factor :1.7**

List of International Conferences:

---

1. **Sankar PR, Prakash K**, et.al, "A Triboelectric Nanogenerator Based on PDMS and Parafilm For Biomechanical Energy Harvesting", in . *In2022 2nd International Conference on Power Electronics IoT Applications in Renewable Energy and its Control (PARC) 2022 Jan 21 (pp. 1-3). IEEE. (IEEE Xplore) (Published)*

2. **Sankar PR, Prakash K**, et.al, "Performance Prediction of Contact Separation Mode Triboelectric nanogenerators using Machine Learning Models" in *2023 2nd International Conference on Paradigm Shifts in Communications Embedded Systems, Machine Learning and Signal Processing (PCEMS) (IEEE Xplore) (Published)* .

3. **Sankar PR, Prakash K**, et.al, "Triboelectric Nanogenerator Based on Different Polymers: Experimental and Simulation Study" in *Submitted to INDICON Conference* ***(Presented)*** .

Book Chapter:

---

1. **Sankar PR, Prakash K**, et.al, "Triboelectric Nanogenerators Competency to Wireless Device Applications,", in **. Submitted to Springer Nature (Accepted)**

Bibliography

[1] Z. L. Wang, "On the first principle theory of nanogenerators from maxwell's equations," *Nano Energy*, vol. 68, p. 104272, 2020.

[2] A. Yu, P. Jiang, and Z. Lin Wang, "Nanogenerator as self-powered vibration sensor," *Nano Energy*, vol. 1, no. 3, pp. 418–423, May 2012. [Online]. Available: https://linkinghub.elsevier.com/retrieve/pii/S2211285511000437

[3] C. Bao Han, C. Zhang, X. H. Li, L. Zhang, T. Zhou, W. Hu, and Z. Lin Wang, "Self-powered velocity and trajectory tracking sensor array made of planar triboelectric nanogenerator pixels," *Nano Energy*, vol. 9, pp. 325–333, Oct. 2014. [Online]. Available: https://linkinghub.elsevier.com/retrieve/pii/S2211285514001748

[4] A. K. Kasi, J. K. Kasi, M. Uddin, M. Bokhari *et al.*, "Triboelectric nanogenerator as self-powered impact force sensor for falling object," *Current Applied Physics*, vol. 20, no. 1, pp. 137–144, 2020.

[5] M.-F. Lin, J. Xiong, J. Wang, K. Parida, and P. S. Lee, "Core-shell nanofiber mats for tactile pressure sensor and nanogenerator applications," *Nano Energy*, vol. 44, pp. 248–255, 2018.

[6] X. Zhao, G. Wei, X. Li, Y. Qin, D. Xu, W. Tang, H. Yin, X. Wei, and L. Jia, "Self-powered triboelectric nano vibration accelerometer based wireless sensor system for railway state health monitoring," *Nano Energy*, vol. 34, pp. 549–555, Apr. 2017. [Online]. Available: https://linkinghub.elsevier.com/retrieve/pii/S2211285517301143

[7] L. Zheng, Z.-H. Lin, G. Cheng, W. Wu, X. Wen, S. Lee, and Z. L. Wang, "Silicon-

based hybrid cell for harvesting solar energy and raindrop electrostatic energy," *Nano Energy*, vol. 9, pp. 291–300, 2014.

[8] X. Cheng, B. Meng, X. Chen, M. Han, H. Chen, Z. Su, M. Shi, and H. Zhang, "Single-step fluorocarbon plasma treatment-induced wrinkle structure for high-performance triboelectric nanogenerator," *Small*, vol. 12, no. 2, pp. 229–236, 2016.

[9] L. Jin, B. Zhang, L. Zhang, and W. Yang, "Nanogenerator as new energy technology for self-powered intelligent transportation system," *Nano Energy*, vol. 66, p. 104086, Dec. 2019. [Online]. Available: https://linkinghub.elsevier.com/retrieve/pii/S2211285519307931

[10] Y. Yang and Z. L. Wang, "Hybrid energy cells for simultaneously harvesting multi-types of energies," *Nano Energy*, vol. 14, pp. 245–256, May 2015. [Online]. Available: https://linkinghub.elsevier.com/retrieve/pii/S2211285514002651

[11] I. Aazem, D. T. Mathew, S. Radhakrishnan, K. V. Vijoy, H. John, D. M. Mulvihill, and S. C. Pillai, "Electrode materials for stretchable triboelectric nanogenerator in wearable electronics," *RSC Advances*, vol. 12, no. 17, pp. 10 545–10 572, 2022. [Online]. Available: http://xlink.rsc.org/?DOI=D2RA01088G

[12] S. Wang, L. Lin, and Z. L. Wang, "Nanoscale triboelectric-effect-enabled energy conversion for sustainably powering portable electronics," *Nano letters*, vol. 12, no. 12, pp. 6339–6346, 2012.

[13] F.-R. Fan, Z.-Q. Tian, and Z. Lin Wang, "Flexible triboelectric generator," *Nano Energy*, vol. 1, no. 2, pp. 328–334, Mar. 2012. [Online]. Available: https://linkinghub.elsevier.com/retrieve/pii/S2211285512000481

[14] Y. Yang, H. Zhang, G. Zhu, S. Lee, Z.-H. Lin, and Z. L. Wang, "Flexible Hybrid Energy Cell for Simultaneously Harvesting Thermal, Mechanical, and Solar Energies," *ACS Nano*, vol. 7, no. 1, pp. 785–790, Jan. 2013. [Online]. Available: https://pubs.acs.org/doi/10.1021/nn305247x

[15] C. Zhang and Z. L. Wang, "Tribotronics—A new field by coupling triboelectricity and semiconductor," *Nano Today*, vol. 11, no. 4, pp. 521–536, Aug. 2016. [Online]. Available: https://linkinghub.elsevier.com/retrieve/pii/S1748013216301372

[16] A. Kumar, K. Kumar, N. Kaushik, S. Sharma, and S. Mishra, "Renewable energy in India: Current status and future potentials," *Renewable and Sustainable Energy Reviews*, vol. 14, no. 8, pp. 2434–2442, Oct. 2010. [Online]. Available: https://linkinghub.elsevier.com/retrieve/pii/S1364032110001140

[17] C. Yu, M. Moslehpour, T. K. Tran, L. M. Trung, J. P. Ou, and N. H. Tien, "Impact of non-renewable energy and natural resources on economic recovery: Empirical evidence from selected developing economies," *Resources Policy*, vol. 80, p. 103221, Jan. 2023. [Online]. Available: https://linkinghub.elsevier.com/retrieve/pii/S030142072200664X

[18] Y. Zi and Z. L. Wang, "Nanogenerators: An emerging technology towards nanoenergy," *APL Materials*, vol. 5, no. 7, p. 074103, Jul. 2017. [Online]. Available: https://pubs.aip.org/apm/article/5/7/074103/1023864/Nanogenerators-An-emerging-technology-towards

[19] R. D. I. G. Dharmasena, K. D. G. I. Jayawardena, C. A. Mills, J. H. B. Deane, J. V. Anguita, R. A. Dorey, and S. R. P. Silva, "Triboelectric nanogenerators: providing a fundamental framework," *Energy & Environmental Science*, vol. 10, no. 8, pp. 1801–1811, 2017. [Online]. Available: http://xlink.rsc.org/?DOI=C7EE01139C

[20] S. Niu, S. Wang, L. Lin, Y. Liu, Y. S. Zhou, Y. Hu, and Z. L. Wang, "Theoretical study of contact-mode triboelectric nanogenerators as an effective power source," *Energy & Environmental Science*, vol. 6, no. 12, p. 3576, 2013. [Online]. Available: http://xlink.rsc.org/?DOI=c3ee42571a

[21] Y. Chu, R. Han, F. Meng, Z. Cao, S. Wang, K. Dong, S. Yang, H. Liu, X. Ye, and F. Tang, "Theoretical study on the output of contact-separation triboelectric nanogenerators with arbitrary charging and grounding conditions," *Nano Energy*, vol. 89, p. 106383, Nov. 2021. [Online]. Available: https://linkinghub.elsevier.com/retrieve/pii/S2211285521006388

[22] B. Yang, W. Zeng, Z. Peng, S. Liu, K. Chen, and X. Tao, "A Fully Verified Theoretical Analysis of Contact-Mode Triboelectric Nanogenerators as a Wearable Power Source," *Advanced Energy Materials*, vol. 6, no. 16, p. 1600505, Aug. 2016. [Online]. Available: https://onlinelibrary.wiley.com/doi/10.1002/aenm.201600505

[23] S. Ankanahalli Shankaregowda, R. F. Sagade Muktar Ahmed, Y. Liu, C. Bananakere Nanjegowda, X. Cheng, S. Shivanna, S. Ramakrishna, Z. Yu, X. Zhang, and K. Sannathammegowda, "Dry-Coated Graphite onto Sandpaper for Triboelectric Nanogenerator as an Active Power Source for Portable Electronics," *Nanomaterials*, vol. 9, no. 11, p. 1585, Nov. 2019. [Online]. Available: https://www.mdpi.com/2079-4991/9/11/1585

[24] S. Niu, Y. S. Zhou, S. Wang, Y. Liu, L. Lin, Y. Bando, and Z. L. Wang, "Simulation method for optimizing the performance of an integrated triboelectric nanogenerator energy harvesting system," *Nano Energy*, vol. 8, pp. 150–156, Sep. 2014. [Online]. Available: https://linkinghub.elsevier.com/retrieve/pii/S2211285514001025

[25] R. Zhang and H. Olin, "Material choices for triboelectric nanogenerators: A critical review," *EcoMat*, vol. 2, no. 4, p. e12062, Dec. 2020. [Online]. Available: https://onlinelibrary.wiley.com/doi/10.1002/eom2.12062

[26] X. Pu, M. Liu, L. Li, C. Zhang, Y. Pang, C. Jiang, L. Shao, W. Hu, and Z. L. Wang, "Efficient Charging of Li-Ion Batteries with Pulsed Output Current of Triboelectric Nanogenerators," *Advanced Science*, vol. 3, no. 1, p. 1500255, Jan. 2016. [Online]. Available: https://onlinelibrary.wiley.com/doi/10.1002/advs.201500255

[27] X. He, H. Zhang, J. Jiang, and X. Liu, "Output characteristics of series-parallel triboelectric nanogenerators," *Nanotechnology*, vol. 34, no. 15, p. 155403, Apr. 2023. [Online]. Available: https://iopscience.iop.org/article/10.1088/1361-6528/aca599

[28] S. Mishra, P. Supraja, D. Haranath, R. R. Kumar, and S. Pola, "Effect of surface and contact points modification on the output performance of triboelectric nanogenerator," *Nano Energy*, vol. 104, p. 107964, Dec. 2022. [Online]. Available: https://linkinghub.elsevier.com/retrieve/pii/S2211285522010424

[29] C. Jiang, K. Dai, F. Yi, Y. Han, X. Wang, and Z. You, "Optimization of triboelectric nanogenerator load characteristics considering the air breakdown effect," *Nano Energy*, vol. 53, pp. 706–715, Nov. 2018. [Online]. Available: https://linkinghub.elsevier.com/retrieve/pii/S2211285518306803

[30] Z. L. Wang, "On Maxwell's displacement current for energy and sensors: the origin of nanogenerators," *Materials Today*, vol. 20, no. 2, pp. 74–82, Mar. 2017. [Online]. Available: https://linkinghub.elsevier.com/retrieve/pii/S1369702116303406

[31] H. Zhao, M. Xu, M. Shu, J. An, W. Ding, X. Liu, S. Wang, C. Zhao, H. Yu, H. Wang, C. Wang, X. Fu, X. Pan, G. Xie, and Z. L. Wang, "Underwater wireless communication via TENG-generated Maxwell's displacement current," *Nature Communications*, vol. 13, no. 1, p. 3325, Jun. 2022. [Online]. Available: https://www.nature.com/articles/s41467-022-31042-8

[32] J. Chen, H. Guo, X. He, G. Liu, Y. Xi, H. Shi, and C. Hu, "Enhancing Performance of Triboelectric Nanogenerator by Filling High Dielectric Nanoparticles into Sponge PDMS Film," *ACS Applied Materials & Interfaces*, vol. 8, no. 1, pp. 736–744, Jan. 2016. [Online]. Available: https://pubs.acs.org/doi/10.1021/acsami.5b09907

[33] S. Xu, L. Zhang, W. Ding, H. Guo, X. Wang, and Z. L. Wang, "Self-doubled-rectification of triboelectric nanogenerator," *Nano Energy*, vol. 66, p. 104165, Dec. 2019. [Online]. Available: https://linkinghub.elsevier.com/retrieve/pii/S2211285519308729

[34] X. Wang, Y. He, X. Liu, L. Shi, and J. Zhu, "Investigation of photothermal heating enabled by plasmonic nanofluids for direct solar steam generation," *Solar Energy*, vol. 157, pp. 35–46, Nov. 2017. [Online]. Available: https://linkinghub.elsevier.com/retrieve/pii/S0038092X17306849

[35] G. Khandelwal, A. Chandrasekhar, N. R. Alluri, V. Vivekananthan, N. P. Maria Joseph Raj, and S.-J. Kim, "Trash to energy: A facile, robust and cheap approach for mitigating environment pollutant using household triboelectric nanogenerator," *Applied Energy*, vol. 219, pp. 338–349, Jun. 2018. [Online]. Available: https://linkinghub.elsevier.com/retrieve/pii/S0306261918303611

[36] V. Nguyen and R. Yang, "Effect of humidity and pressure on the triboelectric nanogenerator," *Nano Energy*, vol. 2, no. 5, pp. 604–608, Sep. 2013. [Online]. Available: https://linkinghub.elsevier.com/retrieve/pii/S2211285513001389

[37] Q.-y. Zhang, J.-l. Mu, J.-b. Mu, X.-y. Yang, S.-n. Zhang, X.-t. Han, Y.-f. Zhao, Y.-j. You, J.-b. Yu, and X.-j. Chou, "A Design of Flexible Triboelectric Generator Integrated with High-Efficiency Energy Storage Unit," *Energy Technology*, vol. 9, no. 2, p. 2000962, Feb. 2021. [Online]. Available: https://onlinelibrary.wiley.com/doi/10.1002/ente.202000962

[38] X. Feng, Q. Li, and K. Wang, "Waste plastic triboelectric nanogenerators using recycled plastic bags for power generation," *ACS Applied Materials & Interfaces*, vol. 13, no. 1, pp. 400–410, 2020.

[39] K. Xia, Z. Zhu, J. Fu, Y. Li, Y. Chi, H. Zhang, C. Du, and Z. Xu, "A triboelectric nanogenerator based on waste tea leaves and packaging bags for powering electronic office supplies and behavior monitoring," *Nano Energy*, vol. 60, pp. 61–71, Jun. 2019. [Online]. Available: https://linkinghub.elsevier.com/retrieve/pii/S2211285519302447

[40] N. R. Alluri, N. P. Maria Joseph Raj, G. Khandelwal, V. Vivekananthan, and S.-J. Kim, "Aloe vera: A tropical desert plant to harness the mechanical energy by triboelectric and piezoelectric approaches," *Nano Energy*, vol. 73, p. 104767, Jul. 2020. [Online]. Available: https://linkinghub.elsevier.com/retrieve/pii/S2211285520303244

[41] Q. M. Saqib, R. A. Shaukat, M. U. Khan, M. Chougale, and J. Bae, "Biowaste Peanut Shell Powder-Based Triboelectric Nanogenerator for Biomechanical Energy Scavenging and Sustainably Powering Electronic Supplies," *ACS Applied Electronic Materials*, vol. 2, no. 12, pp. 3953–3963, Dec. 2020. [Online]. Available: https://pubs.acs.org/doi/10.1021/acsaelm.0c00791

[42] S. Jakmuangpak, T. Prada, W. Mongkolthanaruk, V. Harnchana, and S. Pinitsoontorn, "Engineering Bacterial Cellulose Films by Nanocomposite Approach and Surface Modification for Biocompatible Triboelectric Nanogenerator," *ACS Applied Electronic Materials*, vol. 2, no. 8, pp. 2498–2506, Aug. 2020. [Online]. Available: https://pubs.acs.org/doi/10.1021/acsaelm.0c00421

[43] J. Kaur, R. S. Sawhney, H. Singh, and M. Singh, "Electricity nanogenerator from

egg shell membrane: a natural waste bioproduct," *International Journal of Green Energy*, vol. 17, no. 5, pp. 309–318, 2020.

[44] J. Ma, J. Zhu, P. Ma, Y. Jie, Z. L. Wang, and X. Cao, "Fish Bladder Film-Based Triboelectric Nanogenerator for Noncontact Position Monitoring," *ACS Energy Letters*, vol. 5, no. 9, pp. 3005–3011, Sep. 2020. [Online]. Available: https://pubs.acs.org/doi/10.1021/acsenergylett.0c01062

[45] J. M. Wu, C. K. Chang, and Y. T. Chang, "High-output current density of the triboelectric nanogenerator made from recycling rice husks," *Nano Energy*, vol. 19, pp. 39–47, Jan. 2016. [Online]. Available: https://linkinghub.elsevier.com/retrieve/pii/S2211285515004322

[46] Y. Chi, K. Xia, Z. Zhu, J. Fu, H. Zhang, C. Du, and Z. Xu, "Rice paper-based biodegradable triboelectric nanogenerator," *Microelectronic Engineering*, vol. 216, p. 111059, Aug. 2019. [Online]. Available: https://linkinghub.elsevier.com/retrieve/pii/S0167931719302163

[47] Y. Yetri, A. T. Hoang, Mursida, D. Dahlan, Muldarisnur, E. Taer, and M. Q. Chau, "Synthesis of activated carbon monolith derived from cocoa pods for supercapacitor electrodes application," *Energy Sources, Part A: Recovery, Utilization, and Environmental Effects*, pp. 1–15, Aug. 2020. [Online]. Available: https://www.tandfonline.com/doi/full/10.1080/15567036.2020.1811433

[48] X. Ren, H. Fan, J. Ma, C. Wang, Y. Zhao, and S. Lei, "Triboelectric Nanogenerators Based on Fluorinated Wasted Rubber Powder for Self-Powering Application," *ACS Sustainable Chemistry & Engineering*, vol. 5, no. 2, pp. 1957–1964, Feb. 2017. [Online]. Available: https://pubs.acs.org/doi/10.1021/acssuschemeng.6b02756

[49] B. Dudem, R. D. I. G. Dharmasena, R. Riaz, V. Vivekananthan, K. G. U. Wijayantha, P. Lugli, L. Petti, and S. R. P. Silva, "Wearable Triboelectric Nanogenerator from Waste Materials for Autonomous Information Transmission *via* Morse Code," *ACS Applied Materials & Interfaces*, vol. 14, no. 4, pp. 5328–5337, Feb. 2022. [Online]. Available: https://pubs.acs.org/doi/10.1021/acsami.1c20984

[50] L. Zhou, D. Liu, J. Wang, and Z. L. Wang, "Triboelectric nanogenerators: Fundamental physics and potential applications," *Friction*, vol. 8, no. 3, pp. 481–506, Jun. 2020. [Online]. Available: https://link.springer.com/10.1007/s40544-020-0390-3

[51] S. M. Nawaz, M. Saha, N. Sepay, and A. Mallik, "Energy-from-waste: A triboelectric nanogenerator fabricated from waste polystyrene for energy harvesting and self-powered sensor," *Nano Energy*, vol. 104, p. 107902, Dec. 2022. [Online]. Available: https://linkinghub.elsevier.com/retrieve/pii/S2211285522009806

[52] K. S. Moreira, Y. A. Santos Da Campo, E. Lorenzett, and T. A. Burgo, "Low-cost triboelectric nanogenerator based on aseptic carton package," *Results in Engineering*, vol. 17, p. 100965, Mar. 2023. [Online]. Available: https://linkinghub.elsevier.com/retrieve/pii/S2590123023000920

[53] A. B. Makar, K. E. McMartin, M. Palese, and T. R. Tephly, "Formate assay in body fluids: application in methanol poisoning," *Biochemical Medicine*, vol. 13, no. 2, pp. 117–126, Jun. 1975.

[54] Aminullah, A. K. Kasi, J. K. Kasi, M. Uddin, and M. Bokhari, "Triboelectric nanogenerator as self-powered impact force sensor for falling object," *Current Applied Physics*, vol. 20, no. 1, pp. 137–144, Jan. 2020. [Online]. Available: https://linkinghub.elsevier.com/retrieve/pii/S1567173919302767

[55] S. Sripadmanabhan Indira, C. Aravind Vaithilingam, K. S. P. Oruganti, F. Mohd, and S. Rahman, "Nanogenerators as a Sustainable Power Source: State of Art, Applications, and Challenges," *Nanomaterials*, vol. 9, no. 5, p. 773, May 2019. [Online]. Available: https://www.mdpi.com/2079-4991/9/5/773

[56] T. Wang, S. Li, X. Tao, Q. Yan, X. Wang, Y. Chen, F. Huang, H. Li, X. Chen, and Z. Bian, "Fully biodegradable water-soluble triboelectric nanogenerator for human physiological monitoring," *Nano Energy*, vol. 93, p. 106787, Mar. 2022. [Online]. Available: https://linkinghub.elsevier.com/retrieve/pii/S2211285521010363

[57] M. Navaneeth, S. Potu, A. Babu, R. K. Rajaboina, U. K. K, H. Divi, P. Kodali, and B. K., "A medical waste X-ray film based triboelectric nanogenerator

for self-powered devices, sensors, and smart buildings," *Environmental Science: Advances*, vol. 2, no. 6, pp. 848–860, 2023. [Online]. Available: http://xlink.rsc.org/?DOI=D3VA00018D

[58] S. Rathore, S. Sharma, B. P. Swain, and R. K. Ghadai, "A Critical Review on Triboelectric Nanogenerator," *IOP Conference Series: Materials Science and Engineering*, vol. 377, p. 012186, Jun. 2018. [Online]. Available: https://iopscience.iop.org/article/10.1088/1757-899X/377/1/012186

[59] V. Slabov, S. Kopyl, M. P. Soares Dos Santos, and A. L. Kholkin, "Natural and Eco-Friendly Materials for Triboelectric Energy Harvesting," *Nano-Micro Letters*, vol. 12, no. 1, p. 42, Dec. 2020. [Online]. Available: http://link.springer.com/10.1007/s40820-020-0373-y

[60] X. Feng, Q. Li, and K. Wang, "Waste Plastic Triboelectric Nanogenerators Using Recycled Plastic Bags for Power Generation," *ACS Applied Materials & Interfaces*, vol. 13, no. 1, pp. 400–410, Jan. 2021. [Online]. Available: https://pubs.acs.org/doi/10.1021/acsami.0c16489

[61] E. Kersten, "6th International Symposium on Maritime Medicine 1974," *Bulletin of the Institute of Maritime and Tropical Medicine in Gdynia*, vol. 26, no. 2, pp. 131–132, 1975.

[62] K. K. Carroll and G. J. Hopkins, "Dietary polyunsaturated fat versus saturated fat in relation to mammary carcinogenesis," *Lipids*, vol. 14, no. 2, pp. 155–158, Feb. 1979.

[63] B. Yalagala, S. Khandelwal, D. J, and S. Badhulika, "Wirelessly destructible MgO-PVP-Graphene composite based flexible transient memristor for security applications," *Materials Science in Semiconductor Processing*, vol. 104, p. 104673, Dec. 2019. [Online]. Available: https://linkinghub.elsevier.com/retrieve/pii/S1369800119312594

[64] A. Chen, C. Zhang, G. Zhu, and Z. L. Wang, "Polymer Materials for High-Performance Triboelectric Nanogenerators," *Advanced Science*, vol. 7, no. 14,

p. 2000186, Jul. 2020. [Online]. Available: https://onlinelibrary.wiley.com/doi/10.1002/advs.202000186

[65] B. P. Yalagala, S. A. Sankaranarayanan, A. K. Rengan, and S. R. K. Vanjari, "Biocompatible, Flexible, and High-Performance Nanowelded Silver Nanowires on Silk Fibroin for Transparent Conducting Electrodes toward Biomemristor Application," *ACS Sustainable Chemistry & Engineering*, vol. 10, no. 14, pp. 4473–4485, Apr. 2022. [Online]. Available: https://pubs.acs.org/doi/10.1021/acssuschemeng.1c08227

[66] T.-C. Hou, Y. Yang, H. Zhang, J. Chen, L.-J. Chen, and Z. Lin Wang, "Triboelectric nanogenerator built inside shoe insole for harvesting walking energy," *Nano Energy*, vol. 2, no. 5, pp. 856–862, Sep. 2013. [Online]. Available: https://linkinghub.elsevier.com/retrieve/pii/S2211285513000360

[67] F.-R. Fan, Z.-Q. Tian, and Z. Lin Wang, "Flexible triboelectric generator," *Nano Energy*, vol. 1, no. 2, pp. 328–334, Mar. 2012. [Online]. Available: https://linkinghub.elsevier.com/retrieve/pii/S2211285512000481

[68] B. P. Yalagala, A. S. Dahiya, R. Dahiya, and Bendable Electronics and Sensing Technologies (BEST) Group, University of Glasgow, Glasgow G12 8QQ, U.K, "ZnO nanowires based degradable high-performance photodetectors for eco-friendly green electronics," *Opto-Electronic Advances*, vol. 6, no. 2, pp. 220 020–220 020, 2023. [Online]. Available: http://www.oejournal.org//article/doi/10.29026/oea.2023.220020

[69] B. P. Yalagala, S. Deswal, S. R. K. Vanjari, and R. Dahiya, "Flexible and ultra-fast bioresorbable nanofibers of silk fibroin-PVA composite," in *2021 IEEE International Conference on Flexible and Printable Sensors and Systems (FLEPS)*. Manchester, United Kingdom: IEEE, Jun. 2021, pp. 1–4. [Online]. Available: https://ieeexplore.ieee.org/document/9469701/

[70] X. Chen, D. Taguchi, T. Manaka, and M. Iwamoto, "Organic double layer element driven by triboelectric nanogenerator: Study of carrier behavior by non-contact optical method," *Chemical Physics Letters*, vol. 646, pp. 64–68, Feb. 2016. [Online]. Available: https://linkinghub.elsevier.com/retrieve/pii/S0009261416000117

[71] N. Akamatsu, H. Nakajima, M. Ono, and Y. Miura, "Increase in acetyl CoA synthetase activity after phenobarbital treatment," *Biochemical Pharmacology*, vol. 24, no. 18, pp. 1725–1727, Sep. 1975.

[72] Y. Yang, H. Zhang, J. Chen, Q. Jing, Y. S. Zhou, X. Wen, and Z. L. Wang, "Single-Electrode-Based Sliding Triboelectric Nanogenerator for Self-Powered Displacement Vector Sensor System," *ACS Nano*, vol. 7, no. 8, pp. 7342–7351, Aug. 2013. [Online]. Available: https://pubs.acs.org/doi/10.1021/nn403021m

[73] S. P. Borderud, Y. Li, J. E. Burkhalter, C. E. Sheffer, and J. S. Ostroff, "Electronic cigarette use among patients with cancer: characteristics of electronic cigarette users and their smoking cessation outcomes," *Cancer*, vol. 120, no. 22, pp. 3527–3535, 2014.

[74] H. Zou, L. Guo, H. Xue, Y. Zhang, X. Shen, X. Liu, P. Wang, X. He, G. Dai, P. Jiang, H. Zheng, B. Zhang, C. Xu, and Z. L. Wang, "Quantifying and understanding the triboelectric series of inorganic non-metallic materials," *Nature Communications*, vol. 11, no. 1, p. 2093, Apr. 2020. [Online]. Available: https://www.nature.com/articles/s41467-020-15926-1

[75] X. Wang, S. Niu, Y. Yin, F. Yi, Z. You, and Z. L. Wang, "Triboelectric Nanogenerator Based on Fully Enclosed Rolling Spherical Structure for Harvesting Low-Frequency Water Wave Energy," *Advanced Energy Materials*, vol. 5, no. 24, p. 1501467, Dec. 2015. [Online]. Available: https://onlinelibrary.wiley.com/doi/10.1002/aenm.201501467

[76] M. M. Rastegardoost, O. A. Tafreshi, Z. Saadatnia, S. Ghaffari-Mosanenzadeh, C. B. Park, and H. E. Naguib, "Recent advances on porous materials and structures for high-performance triboelectric nanogenerators," *Nano Energy*, vol. 111, p. 108365, Jun. 2023. [Online]. Available: https://linkinghub.elsevier.com/retrieve/pii/S2211285523002021

[77] J. Kaur, R. S. Sawhney, H. Singh, and M. Singh, "Electricity nanogenerator from egg shell membrane: A natural waste bioproduct," *International Journal of Green Energy*, vol. 17, no. 5, pp. 309–318, Apr. 2020. [Online]. Available: https://www.tandfonline.com/doi/full/10.1080/15435075.2020.1727482

[78] P. S. Bhandari and P. R. Gogate, "Kinetic and thermodynamic study of adsorptive removal of sodium dodecyl benzene sulfonate using adsorbent based on thermo-chemical activation of coconut shell," *Journal of Molecular Liquids*, vol. 252, pp. 495–505, 2018.

[79] D.-L. Wen, X. Liu, H.-T. Deng, D.-H. Sun, H.-Y. Qian, J. Brugger, and X.-S. Zhang, "Printed silk-fibroin-based triboelectric nanogenerators for multi-functional wearable sensing," *Nano Energy*, vol. 66, p. 104123, 2019.

[80] Q. Sun, L. Wang, X. Yue, L. Zhang, G. Ren, D. Li, H. Wang, Y. Han, L. Xiao, G. Lu *et al.*, "Fully sustainable and high-performance fish gelatin-based triboelectric nanogenerator for wearable movement sensing and human-machine interaction," *Nano Energy*, vol. 89, p. 106329, 2021.

[81] P. Bai, G. Zhu, Z.-H. Lin, Q. Jing, J. Chen, G. Zhang, J. Ma, and Z. L. Wang, "Integrated Multilayered Triboelectric Nanogenerator for Harvesting Biomechanical Energy from Human Motions," *ACS Nano*, vol. 7, no. 4, pp. 3713–3719, Apr. 2013. [Online]. Available: https://pubs.acs.org/doi/10.1021/nn4007708

[82] Z. L. Wang, "Triboelectric Nanogenerators as New Energy Technology for Self-Powered Systems and as Active Mechanical and Chemical Sensors," *ACS Nano*, vol. 7, no. 11, pp. 9533–9557, Nov. 2013. [Online]. Available: https://pubs.acs.org/doi/10.1021/nn404614z

[83] J. Han, N. Xu, Y. Liang, M. Ding, J. Zhai, Q. Sun, and Z. L. Wang, "Paper-based triboelectric nanogenerators and their applications: a review," *Beilstein Journal of Nanotechnology*, vol. 12, pp. 151–171, Feb. 2021. [Online]. Available: https://www.beilstein-journals.org/bjnano/articles/12/12

[84] X. He, Y. Zi, H. Guo, H. Zheng, Y. Xi, C. Wu, J. Wang, W. Zhang, C. Lu, and Z. L. Wang, "A Highly Stretchable Fiber-Based Triboelectric Nanogenerator for Self-Powered Wearable Electronics," *Advanced Functional Materials*, vol. 27, no. 4, p. 1604378, Jan. 2017. [Online]. Available: https://onlinelibrary.wiley.com/doi/10.1002/adfm.201604378

[85] S. S. K. Mallineni, H. Behlow, Y. Dong, S. Bhattacharya, A. M. Rao, and R. Podila, "Facile and robust triboelectric nanogenerators assembled using off-the-shelf materials," *Nano Energy*, vol. 35, pp. 263–270, May 2017. [Online]. Available: https://linkinghub.elsevier.com/retrieve/pii/S2211285517301829

[86] T. Huang, M. Lu, H. Yu, Q. Zhang, H. Wang, and M. Zhu, "Enhanced Power Output of a Triboelectric Nanogenerator Composed of Electrospun Nanofiber Mats Doped with Graphene Oxide," *Scientific Reports*, vol. 5, no. 1, p. 13942, Sep. 2015. [Online]. Available: https://www.nature.com/articles/srep13942

[87] M. Xuan, J. Shao, L. Dai, J. Li, and Q. He, "Macrophage Cell Membrane Camouflaged Au Nanoshells for in Vivo Prolonged Circulation Life and Enhanced Cancer Photothermal Therapy," *ACS Applied Materials & Interfaces*, vol. 8, no. 15, pp. 9610–9618, Apr. 2016. [Online]. Available: https://pubs.acs.org/doi/10.1021/acsami.6b00853

[88] P. R. Sankar, K. Prakash, P. Supraja, R. Rakesh Kumar, S. Mishra, and D. Haranath, "A triboelectric nanogenerator based on food packaging Aluminium foil and Parafilm for self-powered electronics," *Physica Scripta*, vol. 96, no. 12, p. 125005, Dec. 2021. [Online]. Available: https://iopscience.iop.org/article/10.1088/1402-4896/ac2086

[89] S. Lee, W. Ko, and J. Hong, "Enhanced performance of triboelectric nanogenerators integrated with zno nanowires," *Journal of Nanoscience and Nanotechnology*, vol. 14, no. 12, pp. 9319–9322, 2014.

[90] D. W. Kim, J. H. Lee, J. K. Kim, and U. Jeong, "Material aspects of triboelectric energy generation and sensors," *NPG Asia Materials*, vol. 12, no. 1, p. 6, Dec. 2020. [Online]. Available: https://www.nature.com/articles/s41427-019-0176-0

[91] J.-H. Zhang, Y. Li, J. Du, X. Hao, and H. Huang, "A high-power wearable triboelectric nanogenerator prepared from self-assembled electrospun poly(vinylidene fluoride) fibers with a heart-like structure," *Journal of Materials Chemistry A*, vol. 7, no. 19, pp. 11 724–11 733, 2019. [Online]. Available: http://xlink.rsc.org/?DOI=C9TA01956A

[92] J. Zhang, Z. Fang, C. Shu, J. Zhang, Q. Zhang, and C. Li, "A rotational piezoelectric energy harvester for efficient wind energy harvesting," *Sensors and Actuators A: Physical*, vol. 262, pp. 123–129, Aug. 2017. [Online]. Available: https://linkinghub.elsevier.com/retrieve/pii/S0924424717309196

[93] F. R. Fan, J. Luo, W. Tang, C. Li, C. Zhang, Z. Tian, and Z. L. Wang, "Highly transparent and flexible triboelectric nanogenerators: performance improvements and fundamental mechanisms," *J. Mater. Chem. A*, vol. 2, no. 33, pp. 13 219–13 225, Jul. 2014. [Online]. Available: http://xlink.rsc.org/?DOI=C4TA02747G

[94] Y. Han, Y. Han, X. Zhang, L. Li, C. Zhang, J. Liu, G. Lu, H.-D. Yu, and W. Huang, "Fish Gelatin Based Triboelectric Nanogenerator for Harvesting Biomechanical Energy and Self-Powered Sensing of Human Physiological Signals," *ACS Applied Materials & Interfaces*, vol. 12, no. 14, pp. 16 442–16 450, Apr. 2020. [Online]. Available: https://pubs.acs.org/doi/10.1021/acsami.0c01061

[95] K. Xia, Z. Zhu, H. Zhang, and Z. Xu, "A triboelectric nanogenerator as self-powered temperature sensor based on PVDF and PTFE," *Applied Physics A*, vol. 124, no. 8, p. 520, Aug. 2018. [Online]. Available: http://link.springer.com/10.1007/s00339-018-1942-5

[96] S. Wang, L. Lin, and Z. L. Wang, "Nanoscale Triboelectric-Effect-Enabled Energy Conversion for Sustainably Powering Portable Electronics," *Nano Letters*, vol. 12, no. 12, pp. 6339–6346, Dec. 2012. [Online]. Available: https://pubs.acs.org/doi/10.1021/nl303573d

[97] S. Ankanahalli Shankaregowda, R. F. Sagade Muktar Ahmed, C. B. Nanjegowda, J. Wang, S. Guan, M. Puttaswamy, A. Amini, Y. Zhang, D. Kong, K. Sannathammegowda, F. Wang, and C. Cheng, "Single-electrode triboelectric nanogenerator based on economical graphite coated paper for harvesting waste environmental energy," *Nano Energy*, vol. 66, p. 104141, Dec. 2019. [Online]. Available: https://linkinghub.elsevier.com/retrieve/pii/S2211285519308481

[98] S. R. K. Vanjari, "Flexible and ultra-fast bioresorbable nanofibers of silk fibroin-pva composite," 2021.

[99] L. Sarkar, M. V. Sushma, B. P. Yalagala, A. K. Rengan, S. G. Singh, and S. R. K. Vanjari, "ZnO nanoparticles embedded silk fibroin—a piezoelectric composite for nanogenerator applications," *Nanotechnology*, vol. 33, no. 26, p. 265403, Jun. 2022. [Online]. Available: https://iopscience.iop.org/article/10.1088/1361-6528/ac5d9f

[100] P. Ravi Sankar, P. Supraja, S. Mishra, K. Prakash, R. Rakesh Kumar, and D. Haranath, "A novel triboelectric nanogenerator based on only food packaging aluminium foils," *Materials Letters*, vol. 310, p. 131474, Mar. 2022. [Online]. Available: https://linkinghub.elsevier.com/retrieve/pii/S0167577X2102173X

[101] ——, "A novel triboelectric nanogenerator based on only food packaging aluminium foils," *Materials Letters*, vol. 310, p. 131474, Mar. 2022. [Online]. Available: https://linkinghub.elsevier.com/retrieve/pii/S0167577X2102173X

[102] B. P. Yalagala, P. Sahatiya, C. S. R. Kolli, S. Khandelwal, V. Mattela, and S. Badhulika, "V $_2$ O $_5$ Nanosheets for Flexible Memristors and Broadband Photodetectors," *ACS Applied Nano Materials*, vol. 2, no. 2, pp. 937–947, Feb. 2019. [Online]. Available: https://pubs.acs.org/doi/10.1021/acsanm.8b02233

[103] Z. Wang, L. He, X. Gu, S. Yang, S. Wang, P. Wang, and G. Cheng, "Rotational energy harvesting systems using piezoelectric materials: A review," *Review of Scientific Instruments*, vol. 92, no. 4, p. 041501, Apr. 2021. [Online]. Available: https://pubs.aip.org/rsi/article/92/4/041501/961163/Rotational-energy-harvesting-systems-using

[104] P. Owusu and S. Asumadu-Sarkodie, "A review of renewable energy sources, sustainability issues and climate change mitigation. cogent eng 3: 1167990," 2016.

[105] J. Luo and Z. L. Wang, "Recent advances in triboelectric nanogenerator based self-charging power systems," *Energy Storage Materials*, vol. 23, pp. 617–628, Dec. 2019. [Online]. Available: https://linkinghub.elsevier.com/retrieve/pii/S2405829718314065

[106] R. Pan, W. Xuan, J. Chen, S. Dong, H. Jin, X. Wang, H. Li, and J. Luo, "Fully biodegradable triboelectric nanogenerators based on electrospun polylactic acid and nanostructured gelatin films," *Nano Energy*, vol. 45, pp.

193–202, Mar. 2018. [Online]. Available: https://linkinghub.elsevier.com/retrieve/pii/S2211285517308248

[107] Y. Li, Z. Zhao, Y. Gao, S. Li, L. Zhou, J. Wang, and Z. L. Wang, "Low-Cost, Environmentally Friendly, and High-Performance Triboelectric Nanogenerator Based on a Common Waste Material," *ACS Applied Materials & Interfaces*, vol. 13, no. 26, pp. 30 776–30 784, Jul. 2021. [Online]. Available: https://pubs.acs.org/doi/10.1021/acsami.1c09192

[108] A. Gaur, S. Tiwari, C. Kumar, and P. Maiti, "Bio-waste orange peel and polymer hybrid for efficient energy harvesting," *Energy Reports*, vol. 6, pp. 490–496, Nov. 2020. [Online]. Available: https://linkinghub.elsevier.com/retrieve/pii/S2352484719311333

[109] S. K. Ghosh and D. Mandal, "High-performance bio-piezoelectric nanogenerator made with fish scale," *Applied Physics Letters*, vol. 109, no. 10, p. 103701, Sep. 2016. [Online]. Available: https://pubs.aip.org/apl/article/109/10/103701/31459/High-performance-bio-piezoelectric-nanogenerator

[110] H. Lu, W. Zhao, Z. L. Wang, and X. Cao, "Sugar-based triboelectric nanogenerators for effectively harvesting vibration energy and sugar quality assessment," *Nano Energy*, vol. 88, p. 106196, Oct. 2021. [Online]. Available: https://linkinghub.elsevier.com/retrieve/pii/S2211285521004523

[111] M.-K. Kim, M.-S. Kim, H.-B. Kwon, S.-E. Jo, and Y.-J. Kim, "Wearable triboelectric nanogenerator using a plasma-etched pdms–cnt composite for a physical activity sensor," *RSC advances*, vol. 7, no. 76, pp. 48 368–48 373, 2017.

[112] S. Niu, Y. Liu, X. Chen, S. Wang, Y. S. Zhou, L. Lin, Y. Xie, and Z. L. Wang, "Theory of freestanding triboelectric-layer-based nanogenerators," *Nano Energy*, vol. 12, pp. 760–774, Mar. 2015. [Online]. Available: https://linkinghub.elsevier.com/retrieve/pii/S2211285515000142

[113] Q. Wang, M. Chen, W. Li, Z. Li, Y. Chen, and Y. Zhai, "Size effect on the output of a miniaturized triboelectric nanogenerator based on superimposed electrode

layers," *Nano Energy*, vol. 41, pp. 128–138, Nov. 2017. [Online]. Available: https://linkinghub.elsevier.com/retrieve/pii/S2211285517305682

[114] A. A. Mathew, A. Chandrasekhar, and S. Vivekanandan, "A review on real-time implantable and wearable health monitoring sensors based on triboelectric nanogenerator approach," *Nano Energy*, vol. 80, p. 105566, 2021.

[115] W.-G. Kim, D.-W. Kim, I.-W. Tcho, J.-K. Kim, M.-S. Kim, and Y.-K. Choi, "Triboelectric nanogenerator: Structure, mechanism, and applications," *Acs Nano*, vol. 15, no. 1, pp. 258–287, 2021.

[116] C. Wu, A. C. Wang, W. Ding, H. Guo, and Z. L. Wang, "Triboelectric nanogenerator: a foundation of the energy for the new era," *Advanced Energy Materials*, vol. 9, no. 1, p. 1802906, 2019.

[117] J. Shao, T. Jiang, and Z. Wang, "Theoretical foundations of triboelectric nanogenerators (TENGs)," *Science China Technological Sciences*, vol. 63, no. 7, pp. 1087–1109, Jul. 2020. [Online]. Available: https://link.springer.com/10.1007/s11431-020-1604-9

[118] J. Luo and Z. L. Wang, "Recent progress of triboelectric nanogenerators: From fundamental theory to practical applications," *EcoMat*, vol. 2, no. 4, p. e12059, Dec. 2020. [Online]. Available: https://onlinelibrary.wiley.com/doi/10.1002/eom2.12059

[119] S. Chao, H. Ouyang, D. Jiang, Y. Fan, and Z. Li, "Triboelectric nanogenerator based on degradable materials," *EcoMat*, vol. 3, no. 1, p. e12072, Feb. 2021. [Online]. Available: https://onlinelibrary.wiley.com/doi/10.1002/eom2.12072

[120] D. Yu, Z. Zheng, J. Liu, H. Xiao, G. Huangfu, and Y. Guo, "Superflexible and Lead-Free Piezoelectric Nanogenerator as a Highly Sensitive Self-Powered Sensor for Human Motion Monitoring," *Nano-Micro Letters*, vol. 13, no. 1, p. 117, Dec. 2021. [Online]. Available: https://link.springer.com/10.1007/s40820-021-00649-9

[121] R. A. Shaukat, Q. M. Saqib, M. U. Khan, M. Y. Chougale, and J. Bae, "Bio-waste sunflower husks powder based recycled triboelectric nanogenerator for energy harvesting," *Energy Reports*, vol. 7, pp. 724–731, Nov. 2021. [Online]. Available: https://linkinghub.elsevier.com/retrieve/pii/S2352484721000378

[122] Z. Zhou, X. Li, Y. Wu, H. Zhang, Z. Lin, K. Meng, Z. Lin, Q. He, C. Sun, J. Yang, and Z. L. Wang, "Wireless self-powered sensor networks driven by triboelectric nanogenerator for in-situ real time survey of environmental monitoring," *Nano Energy*, vol. 53, pp. 501–507, Nov. 2018. [Online]. Available: https://linkinghub.elsevier.com/retrieve/pii/S2211285518306177

[123] G. Han, B. Wu, and Y. Pu, "A triboelectric nanogenerator based on waste plastic bags for flexible vertical interconnection system," *Microsystem Technologies*, vol. 26, pp. 3893–3899, 2020.

[124] S. Niu, Y. Liu, Y. S. Zhou, S. Wang, L. Lin, and Z. L. Wang, "Optimization of triboelectric nanogenerator charging systems for efficient energy harvesting and storage," *IEEE Transactions on Electron Devices*, vol. 62, no. 2, pp. 641–647, 2014.

[125] J. Bird, *Electrical Circuit Theory and Technology, 6th ed*, 0th ed. 6th ed. | New York : Routledge, [2017]: Routledge, Apr. 2017. [Online]. Available: https://www.taylorfrancis.com/books/9781317202813

[126] Z. Bai, Y. Xu, J. Li, J. Zhu, C. Gao, Y. Zhang, J. Wang, and J. Guo, "An Eco-friendly Porous Nanocomposite Fabric-Based Triboelectric Nanogenerator for Efficient Energy Harvesting and Motion Sensing," *ACS Applied Materials & Interfaces*, vol. 12, no. 38, pp. 42 880–42 890, Sep. 2020. [Online]. Available: https://pubs.acs.org/doi/10.1021/acsami.0c12709

[127] T. Kamilya, P. K. Sarkar, and S. Acharya, "Unveiling Peritoneum Membrane for a Robust Triboelectric Nanogenerator," *ACS Omega*, vol. 4, no. 18, pp. 17 684–17 690, Oct. 2019. [Online]. Available: https://pubs.acs.org/doi/10.1021/acsomega.9b01963

[128] Y. H. Ko, G. Nagaraju, S. H. Lee, and J. S. Yu, "PDMS-based Triboelectric and Transparent Nanogenerators with ZnO Nanorod Arrays," *ACS Applied Materials & Interfaces*, vol. 6, no. 9, pp. 6631–6637, May 2014. [Online]. Available: https://pubs.acs.org/doi/10.1021/am5018072

[129] W. Li, J. Sun, and M. Chen, "Triboelectric nanogenerator using nano-Ag ink

as electrode material," *Nano Energy*, vol. 3, pp. 95–101, Jan. 2014. [Online]. Available: https://linkinghub.elsevier.com/retrieve/pii/S2211285513001870

[130] S. Bhamre, S. Mali, and C. Mane, "Optimization of electric vehicle based on triboelectric nanogenerator," in *E3S Web of Conferences*, vol. 170. EDP Sciences, 2020, p. 01027.

[131] S. Bilgen, K. Kaygusuz, and A. Sari, "Renewable energy for a clean and sustainable future," *Energy sources*, vol. 26, no. 12, pp. 1119–1129, 2004.

[132] C. Qiu, F. Wu, C. Lee, and M. R. Yuce, "Self-powered control interface based on gray code with hybrid triboelectric and photovoltaics energy harvesting for iot smart home and access control applications," *Nano Energy*, vol. 70, p. 104456, 2020.

[133] B. Fatma, S. Gupta, C. Chatterjee, R. Bhunia, V. Verma, and A. Garg, "Triboelectric generators made of mechanically robust pvdf films as self-powered autonomous sensors for wireless transmission based remote security systems," *Journal of Materials Chemistry A*, vol. 8, no. 30, pp. 15 023–15 033, 2020.

[134] B. Mahapatra, K. K. Patel, P. K. Patel *et al.*, "A review on recent advancement in materials for piezoelectric/triboelectric nanogenerators," *Materials Today: Proceedings*, vol. 46, pp. 5523–5529, 2021.

[135] H. Askari, E. Hashemi, A. Khajepour, M. B. Khamesee, and Z. L. Wang, "Tire condition monitoring and intelligent tires using nanogenerators based on piezoelectric, electromagnetic, and triboelectric effects," *Advanced Materials Technologies*, vol. 4, no. 1, p. 1800105, 2019.

[136] X. Cheng, L. Miao, Y. Song, Z. Su, H. Chen, X. Chen, J. Zhang, and H. Zhang, "High efficiency power management and charge boosting strategy for a triboelectric nanogenerator," *Nano Energy*, vol. 38, pp. 438–446, 2017.

[137] K. Venugopal and V. Shanmugasundaram, "Effective modeling and numerical simulation of triboelectric nanogenerator for blood pressure measurement based on wrist pulse signal using comsol multiphysics software," *ACS omega*, vol. 7, no. 30, pp. 26 863–26 870, 2022.

[138] S. Shafeek and J. Luo, "Theoretical and numerical analysis of triboelectric nanogenerators for self-powered sensors," in *2016 5th International Conference on Electronic Devices, Systems and Applications (ICEDSA)*. IEEE, 2016, pp. 1–4.

[139] W. Wang, J. Zhang, Y. Zhang, F. Chen, H. Wang, M. Wu, H. Li, Q. Zhu, H. Zheng, and R. Zhang, "Remarkably enhanced hybrid piezo/triboelectric nanogenerator via rational modulation of piezoelectric and dielectric properties for self-powered electronics," *Applied Physics Letters*, vol. 116, no. 2, 2020.

[140] M. P. Mahmud, J. Lee, G. Kim, H. Lim, and K.-B. Choi, "Improving the surface charge density of a contact-separation-based triboelectric nanogenerator by modifying the surface morphology," *Microelectronic Engineering*, vol. 159, pp. 102–107, 2016.

[141] A. A. Ahmed, T. F. Qahtan, N. Afzal, M. Rashid, L. N. Thalluri, and M. S. M. Ali, "Low-pressure air plasma-treated polytetrafluoroethylene surface for efficient triboelectric nanogenerator," *Materials Today Sustainability*, vol. 21, p. 100330, 2023.

[142] D. L. Vu, C. D. Le, and K. K. Ahn, "Polyvinylidene fluoride surface polarization enhancement for liquid-solid triboelectric nanogenerator and its application," *Polymers*, vol. 14, no. 5, p. 960, 2022.

[143] J. Jeong, B. Yoo, E. Jang, I. Choi, and J. Lee, "Metal electrode polarization in triboelectric nanogenerator probed by surface charge neutralization," *Nanoscale Research Letters*, vol. 17, no. 1, p. 42, 2022.

[144] Q. Wang, M. Chen, W. Li, Z. Li, Y. Chen, and Y. Zhai, "Size effect on the output of a miniaturized triboelectric nanogenerator based on superimposed electrode layers," *Nano energy*, vol. 41, pp. 128–138, 2017.

[145] M. R. Sarker, S. Julai, M. F. M. Sabri, S. M. Said, M. M. Islam, and M. Tahir, "Review of piezoelectric energy harvesting system and application of optimization techniques to enhance the performance of the harvesting system," *Sensors and Actuators A: Physical*, vol. 300, p. 111634, Dec. 2019. [Online]. Available: https://linkinghub.elsevier.com/retrieve/pii/S0924424719312816

[146] S. Priya and D. J. Inman, *Energy harvesting technologies*. Springer, 2009, vol. 21.

[147] M. Lallart, S. Pruvost, and D. Guyomar, "Electrostatic energy harvesting enhancement using variable equivalent permittivity," *Physics Letters A*, vol. 375, no. 45, pp. 3921–3924, Oct. 2011. [Online]. Available: https://linkinghub.elsevier.com/retrieve/pii/S0375960111011704

[148] K. Guo, Z. Yang, C.-H. Yu, and M. J. Buehler, "Artificial intelligence and machine learning in design of mechanical materials," *Materials Horizons*, vol. 8, no. 4, pp. 1153–1172, 2021. [Online]. Available: http://xlink.rsc.org/?DOI=D0MH01451F

[149] M. Khorsand, J. Tavakoli, K. Kamanya, and Y. Tang, "Simulation of high-output and lightweight sliding-mode triboelectric nanogenerators," *Nano Energy*, vol. 66, p. 104115, Dec. 2019. [Online]. Available: https://linkinghub.elsevier.com/retrieve/pii/S2211285519308225

[150] H. Zunair and A. Ben Hamza, "Sharp U-Net: Depthwise convolutional network for biomedical image segmentation," *Computers in Biology and Medicine*, vol. 136, p. 104699, Sep. 2021. [Online]. Available: https://linkinghub.elsevier.com/retrieve/pii/S0010482521004935

[151] J. Vamathevan, D. Clark, P. Czodrowski, I. Dunham, E. Ferran, G. Lee, B. Li, A. Madabhushi, P. Shah, M. Spitzer, and S. Zhao, "Applications of machine learning in drug discovery and development," *Nature Reviews Drug Discovery*, vol. 18, no. 6, pp. 463–477, Jun. 2019. [Online]. Available: https://www.nature.com/articles/s41573-019-0024-5

[152] L. Wang, J. Liu, and S. Z. Li, "Texture classification using wavelet decomposition with markov random field models," in *Proceedings. Fourteenth International Conference on Pattern Recognition (Cat. No. 98EX170)*, vol. 2. IEEE, 1998, pp. 1613–1615.

[153] Y. Zhou, M. Shen, X. Cui, Y. Shao, L. Li, and Y. Zhang, "Triboelectric nanogenerator based self-powered sensor for artificial intelligence," *Nano Energy*, vol. 84, p. 105887, Jun. 2021. [Online]. Available: https://linkinghub.elsevier.com/retrieve/pii/S2211285521001452

[154] R. A. Kishore and S. Priya, "A review on design and performance of thermomagnetic devices," *Renewable and Sustainable Energy Reviews*, vol. 81, pp. 33–44, Jan. 2018. [Online]. Available: https://linkinghub.elsevier.com/retrieve/pii/S1364032117311036

[155] J. K. Kaldellis and D. Zafirakis, "The wind energy (r)evolution: A short review of a long history," *Renewable Energy*, vol. 36, no. 7, pp. 1887–1901, Jul. 2011. [Online]. Available: https://linkinghub.elsevier.com/retrieve/pii/S0960148111000085

[156] F. Invernizzi, S. Dulio, M. Patrini, G. Guizzetti, and P. Mustarelli, "Energy harvesting from human motion: materials and techniques," *Chemical Society Reviews*, vol. 45, no. 20, pp. 5455–5473, 2016. [Online]. Available: http://xlink.rsc.org/?DOI=C5CS00812C

[157] W. Kim, D. Bhatia, S. Jeong, and D. Choi, "Mechanical energy conversion systems for triboelectric nanogenerators: Kinematic and vibrational designs," *Nano Energy*, vol. 56, pp. 307–321, Feb. 2019. [Online]. Available: https://linkinghub.elsevier.com/retrieve/pii/S2211285518308607

[158] L. Atzori, A. Iera, and G. Morabito, "The Internet of Things: A survey," *Computer Networks*, vol. 54, no. 15, pp. 2787–2805, Oct. 2010. [Online]. Available: https://linkinghub.elsevier.com/retrieve/pii/S1389128610001568

[159] M. Ha, J. Park, Y. Lee, and H. Ko, "Triboelectric Generators and Sensors for Self-Powered Wearable Electronics," *ACS Nano*, vol. 9, no. 4, pp. 3421–3427, Apr. 2015. [Online]. Available: https://pubs.acs.org/doi/10.1021/acsnano.5b01478

[160] A. Yu, X. Pu, R. Wen, M. Liu, T. Zhou, K. Zhang, Y. Zhang, J. Zhai, W. Hu, and Z. L. Wang, "Core–Shell-Yarn-Based Triboelectric Nanogenerator Textiles as Power Cloths," *ACS Nano*, vol. 11, no. 12, pp. 12 764–12 771, Dec. 2017. [Online]. Available: https://pubs.acs.org/doi/10.1021/acsnano.7b07534

[161] N. J. Vickers, "Animal Communication: When I'm Calling You, Will You Answer Too?" *Current Biology*, vol. 27, no. 14, pp. R713–R715, Jul. 2017. [Online]. Available: https://linkinghub.elsevier.com/retrieve/pii/S0960982217306309

[162] Z. LináWang, "Triboelectric nanogenerators as new energy technology and self-powered sensors–principles, problems and perspectives," *Faraday discussions*, vol. 176, pp. 447–458, 2014.

[163] G. Zhu, Z.-H. Lin, Q. Jing, P. Bai, C. Pan, Y. Yang, Y. Zhou, and Z. L. Wang, "Toward Large-Scale Energy Harvesting by a Nanoparticle-Enhanced Triboelectric Nanogenerator," *Nano Letters*, vol. 13, no. 2, pp. 847–853, Feb. 2013. [Online]. Available: https://pubs.acs.org/doi/10.1021/nl4001053

[164] S. Zhang, M. Bick, X. Xiao, G. Chen, A. Nashalian, and J. Chen, "Leveraging triboelectric nanogenerators for bioengineering," *Matter*, vol. 4, no. 3, pp. 845–887, Mar. 2021. [Online]. Available: https://linkinghub.elsevier.com/retrieve/pii/S2590238521000060

[165] S. J. Shah, M. P. Anand, A. R. Billimoria, and B. K. Goyal, "Cardiovascular effects of beta-receptor stimulants in healthy volunteers," *Indian Heart Journal*, vol. 27, no. 3, pp. 206–212, Jul. 1975.

[166] Y. Li, Z. Zhao, Y. Gao, S. Li, L. Zhou, J. Wang, and Z. L. Wang, "Low-cost, environmentally friendly, and high-performance triboelectric nanogenerator based on a common waste material," *ACS Applied Materials & Interfaces*, vol. 13, no. 26, pp. 30 776–30 784, 2021.

[167] A. W. Senior, R. Evans, J. Jumper, J. Kirkpatrick, L. Sifre, T. Green, C. Qin, A. Žídek, A. W. R. Nelson, A. Bridgland, H. Penedones, S. Petersen, K. Simonyan, S. Crossan, P. Kohli, D. T. Jones, D. Silver, K. Kavukcuoglu, and D. Hassabis, "Improved protein structure prediction using potentials from deep learning," *Nature*, vol. 577, no. 7792, pp. 706–710, Jan. 2020. [Online]. Available: https://www.nature.com/articles/s41586-019-1923-7

[168] J. Vamathevan, D. Clark, P. Czodrowski, I. Dunham, E. Ferran, G. Lee, B. Li, A. Madabhushi, P. Shah, M. Spitzer *et al.*, "Applications of machine learning in drug discovery and development," *Nature reviews Drug discovery*, vol. 18, no. 6, pp. 463–477, 2019.

[169] M. Jiang, B. Li, W. Jia, and Z. Zhu, "Predicting output performance of triboelectric nanogenerators using deep learning model," *Nano Energy*, vol. 93, p. 106830, Mar. 2022. [Online]. Available: https://linkinghub.elsevier.com/retrieve/pii/S221128552101079X

[170] M. Jiang, Y. Lu, Z. Zhu, and W. Jia, "Advances in Smart Sensing and Medical Electronics by Self-Powered Sensors Based on Triboelectric Nanogenerators," *Micromachines*, vol. 12, no. 6, p. 698, Jun. 2021. [Online]. Available: https://www.mdpi.com/2072-666X/12/6/698

[171] C.-H. Yu and M. J. Buehler, "Sonification based *de novo* protein design using artificial intelligence, structure prediction, and analysis using molecular modeling," *APL Bioengineering*, vol. 4, no. 1, p. 016108, Mar. 2020. [Online]. Available: https://pubs.aip.org/apb/article/4/1/016108/23083/Sonification-based-de-novo-protein-design-using

[172] W. Mei, L. Jiang, C. Liang, J. Sun, and Q. Wang, "Understanding of Li-plating on graphite electrode: detection, quantification and mechanism revelation," *Energy Storage Materials*, vol. 41, pp. 209–221, Oct. 2021. [Online]. Available: https://linkinghub.elsevier.com/retrieve/pii/S2405829721002749

[173] P. Jiao, "Emerging artificial intelligence in piezoelectric and triboelectric nanogenerators," *Nano Energy*, vol. 88, p. 106227, Oct. 2021. [Online]. Available: https://linkinghub.elsevier.com/retrieve/pii/S2211285521004833

[174] X. Lu, H. Zhang, X. Zhao, H. Yang, L. Zheng, W. Wang, and C. Sun, "Triboelectric nanogenerator based self-powered sensor with a turnable sector structure for monitoring driving behavior," *Nano Energy*, vol. 89, p. 106352, 2021.